NASA-CR-167922

CR167922

DESIGN DOCUMENTATION REPORT
COUNTERFLOW FILM-COOLED COMBUSTOR PROGRAM
NASA LEWIS RESEARCH CENTER
CONTRACT NAS3-22116

21-4007-A

JUNE 21, 1982

GARRETT TURBINE ENGINE COMPANY
A DIVISION OF THE GARRETT CORPORATION
PHOENIX, ARIZONA

(NASA-CR-167922) DESIGN DOCUMENTATION REPORT: COUNTERFLOW FILM-COOLED COMBUSTOR PROGRAM (Garrett Turbine Engine Co.) 126 p

N89-70827

Unclas

00/25 0197126

CR167922

DESIGN DOCUMENTATION REPORT
COUNTERFLOW FILM-COOLED COMBUSTOR PROGRAM
NASA LEWIS RESEARCH CENTER
CONTRACT NAS3-22116

21-4007-A

June 21, 1982

Prepared by: Engineering Staff/DHC

Approved by: H C Mongia

H. C. Mongia, Principal Investigator
Combustors, Aircraft Propulsion
Engines

D. J. Brandes, Program Manager
Advanced Technology, Aircraft
Propulsion

GARRETT TURBINE ENGINE COMPANY
A DIVISION OF THE GARRETT CORPORATION
PHOENIX, ARIZONA

REPORT NO. 21-4007

TOTAL PAGES 106

ATTACHMENTS:

Appendix I (8 Pages)
Appendix II (3 Pages)

REV	BY	APPROVED	DATE	PAGES AND/OR PARAGRAPHS AFFECTED
A	TWA	GJS	6-21-82	Added 2 Figures to Appendix I

GARRETT TURBINE ENGINE COMPANY
A DIVISION OF THE GARRETT CORPORATION
PHOENIX, ARIZONA

TABLE OF CONTENTS

		Page
1.0	INTRODUCTION	1
2.0	TECHNICAL DISCUSSION	3
2.1	Original Combustor Flow and Temperature Distribution	3
2.1.1	Combustor Internal-Flow Distribution	3
2.1.2	Liner-Wall Temperature Prediction	5
2.1.3	3-D Combustor Internal-Flow Analysis	6
2.2	Analysis and Optimization of the Cooling Air Distribution	38
2.2.1	Cylindrical Liners	38
2.2.2	Transition Liner	71
2.2.3	Detailed Analysis of Combustor Layout	88
2.3	Technical Summary	95
3.0	CONCLUSION	102

APPENDICES

I Airflow Distribution - Cylindrical Liners (8 Pages)

II Airflow Distribution - Transition Liners (3 Pages)

GARRETT TURBINE ENGINE COMPANY
A DIVISION OF THE GARRETT CORPORATION
PHOENIX, ARIZONA

DESIGN DOCUMENTATION REPORT
COUNTERFLOW FILM-COOLED COMBUSTOR PROGRAM
NASA LEWIS RESEARCH CENTER
CONTRACT NAS3-22116

1.0 INTRODUCTION

This document, submitted by the Garrett Turbine Engine Company, a division of The Garrett Corporation, presents the Design Documentation Report (Task III) for the Counterflow Film-Cooled Combustor Program in compliance with Item A of Reports of Work, NASA Contract NAS3-22116.

This report documents the technical efforts undertaken during the design of the Counterflow Film-Cooled Combustor (CFFC) and consists of the following tasks.

- Brief analysis of the combustor-flow and wall-temperature distribution in its original configuration that included:
  - A one-dimensional (1-D) analysis of the airflow distribution around the combustor.
  - A three-dimensional (3-D) prediction of the combustor internal flow.
  - A one-dimensional analytical evaluation of the combustor liner wall distribution.
- Analysis and optimization of the cooling air distribution to achieve acceptable wall temperature distribution through
  - Selection of optimal cooling scheme combinations for the cylindrical liner sections — conventional forced convection-film cooling and extended surface-film cooling.

- Thermal analysis of the inner- and outer-transition liners (torus) to optimize of the geometrical configuration for maximum wall temperature reduction and minimum stress distribution.

- Detailed analysis of combustor film-cooling skirts.

2.0 TECHNICAL DISCUSSION

2.1 Original Combustor Flow and Temperature Distribution

2.1.1 Combustor Internal-Flow Distribution

A one-dimensional annulus-flow model was used to predict the airflow distribution around the combustor liner. This was based on the airflow rates through the outer-transition liners, part of the inner-transition liner and the fuel nozzles as specified in the program Statement of Work. The one-dimensional (1-D) model computed the pressure losses, annulus Mach number and associated air velocity and flow distribution around the combustor liner. The analysis considered the effect of area change, wall-friction, injection and extraction of air from the annulus, and drag introduced by inserted obstacles such as fuel nozzles and service struts. It predicted the airflow distribution presented in Figure 1 for the following sea level take-off point:

P_3 = 235 psi (15.98 atm.)
T_3 = 1290°R (716°K)
W_{a3} = 8 pps (3.628 kg/sec)

The combustor empirical parameters at the design points were:

Combustor volume = 0.2179 ft^3 ($6.2 \times 10^{-3} m^3$)

Combustor reference area = 0.5811 ft^2 ($54 \times 10^{-3} m^2$)

Air loading parameter =

$$\frac{W_{a3}}{1.75\ V_{comb}\ e\ T_3/540} = 0.0265\ pps/ft^3\ (0.4244\ kg/m^3/\$)$$

Heat-release rate = 3.86×10^6 Btu/hr/ft^3/atm (39.92 MJ/s/m^3/atm)

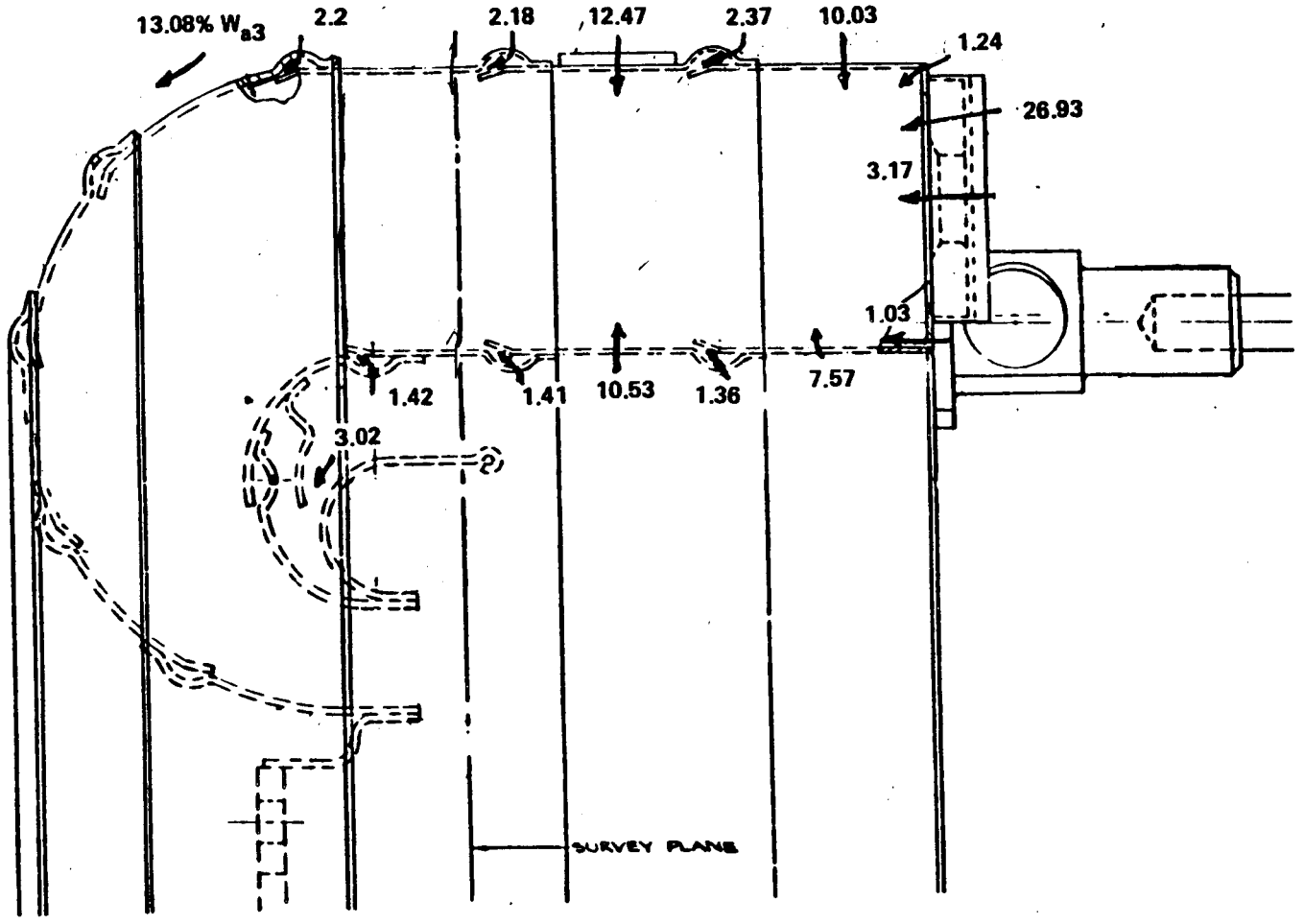

Figure 1. Air-Flow Distribution as Predicted by a One-Dimensional Annulus-Flow Model.

Reference velocity = 28.2 ft/sec (8.59 m/sec)

Combustor residence time = 13.3 ms

Combustor liner corrected flow W_c = 0.662 lb/sec (0.3 kg/sec)

2.1.2 Liner-Wall Temperature Prediction

The combustor liner-wall temperature analysis was performed using a one-dimensional computational scheme. The first case to be examined dealt with the airflow distribution shown in Figure 1. The analysis included convection and radiation heat-transfer contributions from the hot gas and the annulus sides, film cooling efficiency along the wall, and the change of area, wall thickness, and materials.

For computational purposes, the liner wall was divided into independent sections. The outer liner was divided into three panels:

(a) The primary panel, extending from the combustor dome (from which all the lengths "x" were measured) up to the second cooling injection slot at x = 1.5 inches.

(b) The first-dilution panel from x = 1.5 inches to x = 3 inches which included the second dilution jets at x = 2.25 inches.

(c) The second-dilution panel covers the third cooling slot at x = 3 inches up to the fourth slot at x = 4.5 inches.

The inner liner was divided into the same corresponding panels as on the outer liner, although the second-dilution section extended to x = 4 inches only. The transition liners, beyond x = 4.5 inches, will be discussed separately, due to their complex flow.

For each section, a fuel-air ratio (f/a) was computed from the total amount of air and fuel present at the section. Only the effect of the cooling film was excluded for the panel being evaluated, since the cooling film serves to cool the liner and does not interact with the burning process; however, the cooling film's flow rate was taken into account on the next downstream panel, where the flow was assumed to be mixed completely with the hot gases. The flame temperatures were estimated from the adiabatic flame temperature corresponding to the known f/a and a combustion efficiency, η_c.

In the primary section, η_c was assumed to be 90 percent; for the other panels, η_c was assumed to be 100 percent. Based upon the result from the annular flow distribution, the simple counterflow film-cooled combustor displayed a temperature profile along the liners as shown in Figures 2A and 2B. Note that the coolant-mass flow is indicated and corresponded to the annular-flow prediction.

The highest temperatures calculated by the 1-D program were located along the primary panels and first dilution sections.

2.1.3 3-D Combustor Internal-Flow Analysis

In parallel with the use of the 1-D liner cooling model, work was initiated for predicting the combustor internal-flow field to accomplish the following objectives:

- Provide thermal-boundary conditions for analyzing stresses in the combustor walls and the transition liners.

- Predict the trajectory of the fuel spray to define a liner configuration which would minimize near-wall burning and thus reduce thermally-induced liner stresses.

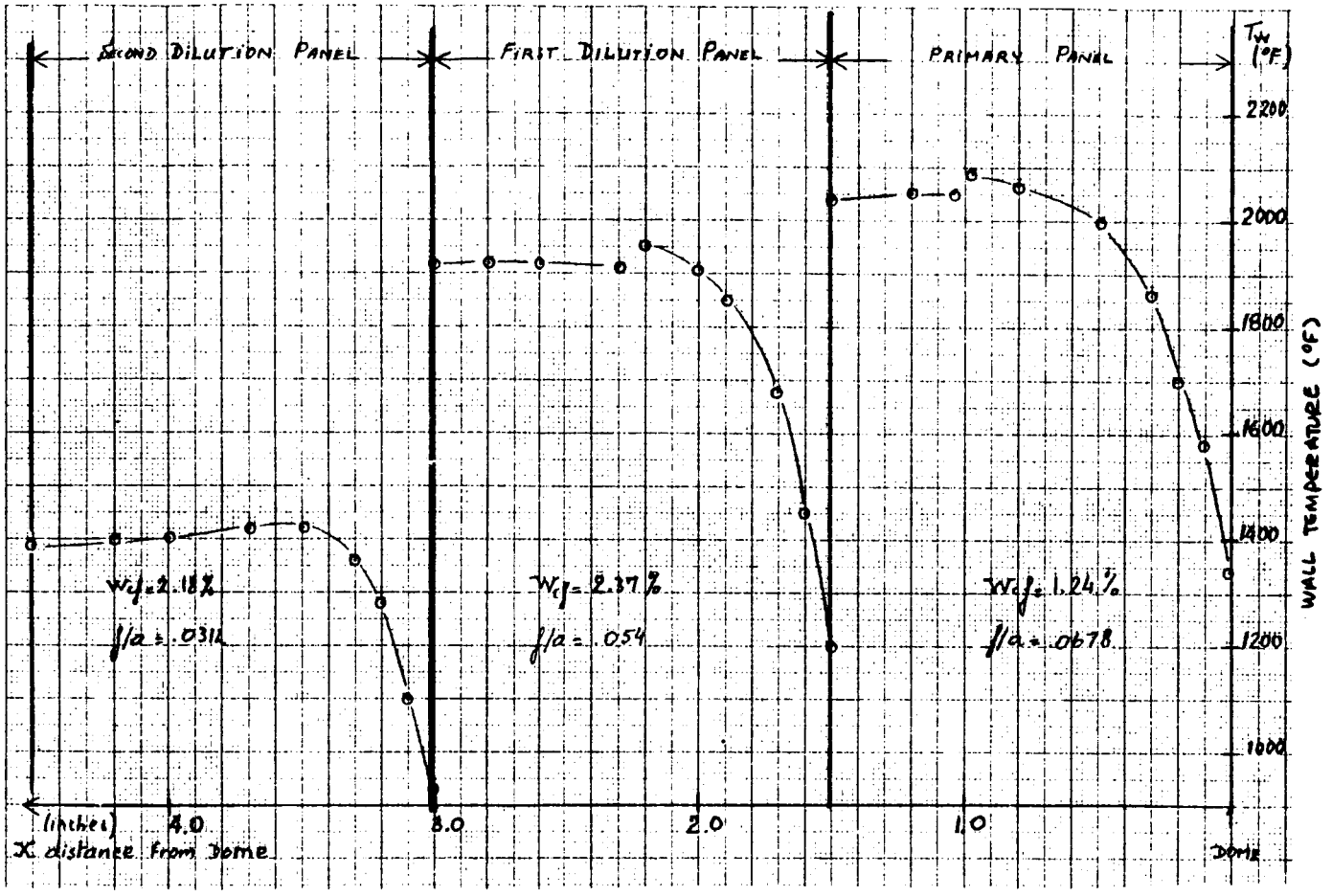

Figure 2 A. Temperature Distribution Outer Liner - Original Combustor.

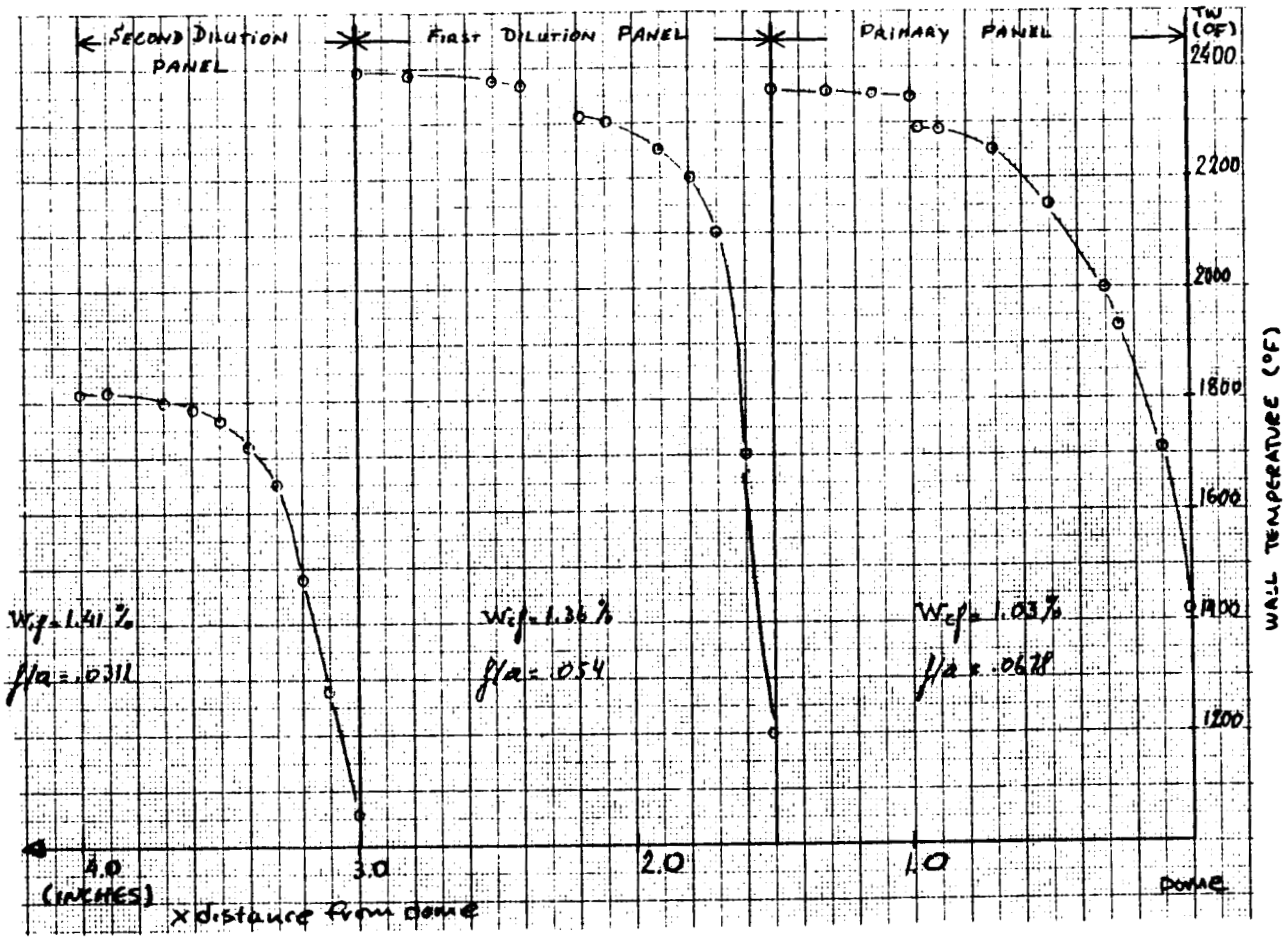

Figure 2 B. Temperature Distribution Inner Liner - Original Combustor.

A 20-degree sector of the combustor 11.89 cm long was analyzed by the 3-D model. The sector was divided into 32 x 18 x 13 nodes the center of the fuel nozzle spray being at $\theta = 10$ degrees. A total of three runs were made using the 3-D computer program for the following cases:

Run Number 1 - Baseline run with airflow distribution as predicted by the annulus flow program (Figure 1) with the predicted jet velocities.

Run Number 2 - Rerun of the above with 54 radial orifices per row for both inner- and outer-liner walls, to determine the effect of the number of primary/secondary orifices per nozzle.

Run Number 3 - Rerun of Run Number 2 with a 75-degree spray cone instead of the 90-degree spray cone assumed in Runs 1 and 2.

All three cases were run using a simplex-pressure atomizer with 365 psid fuel-pressure drop and a SMD (Sauter Mean Diameter) of 30 microns.

Figures 3 and 4 present computed axial velocity isopleths for Runs 1 and 2, respectively, for an "x-y" plane in line with the nozzle spray centerline. There were two distinct recirculation zones (denoted by the zero velocity lines) for Run Number 1, whereas a single elongated recirculation zone was predicted for Run Number 2.

Predicted fuel-air ratio profiles for an "x-y" plane between the fuel nozzles are shown in Figures 5 through 7 for Runs 1 through 3, respectively. For Run Number 1 (Figure 5), a 0.8 equivalence ratio pocket extended in the axial direction up to a distance of x = 7.5 cm. However, the model did not predict any stoichiometric pocket. The

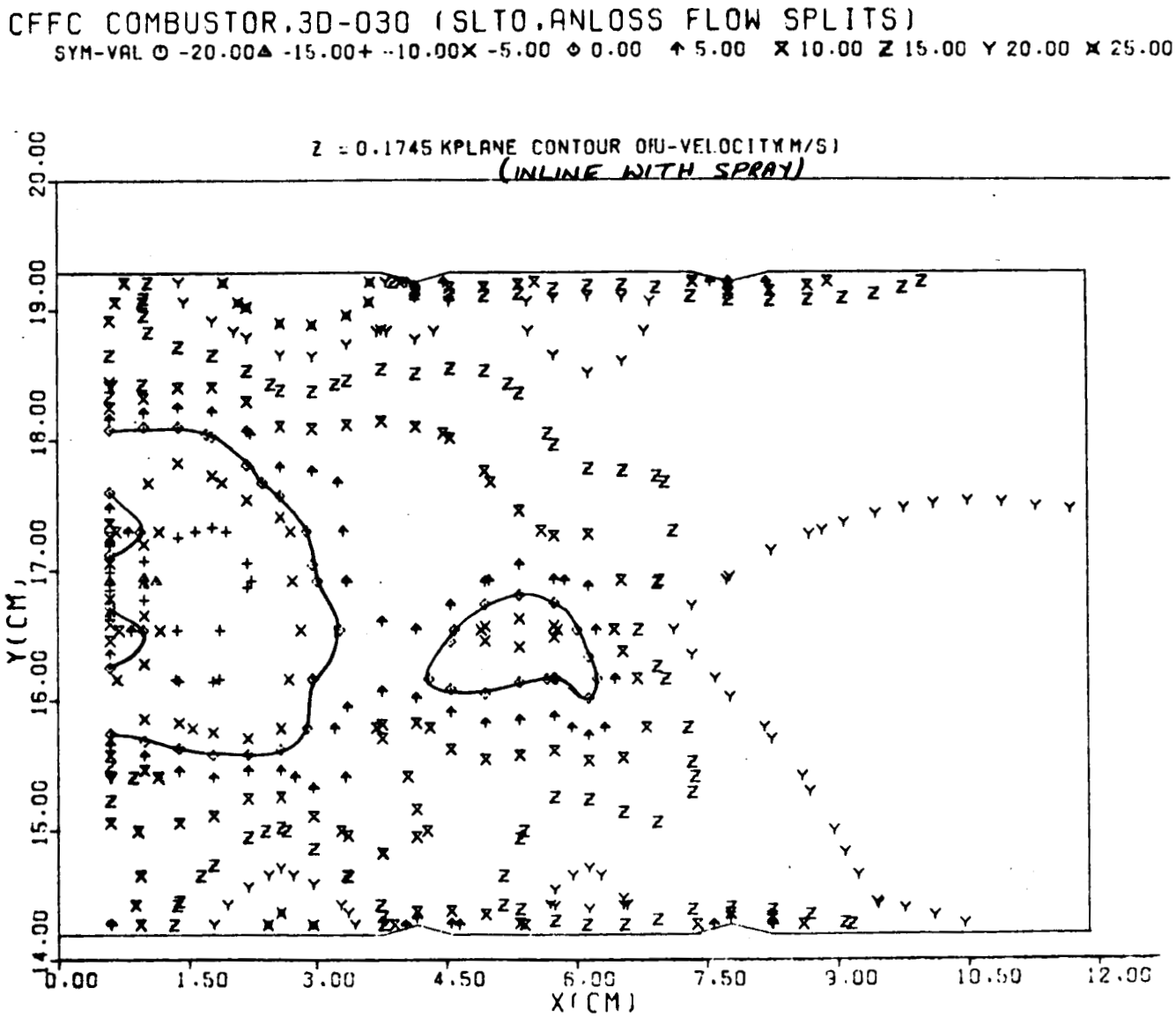

Figure 3. Axial Velocity Distribution (Run No. 1).

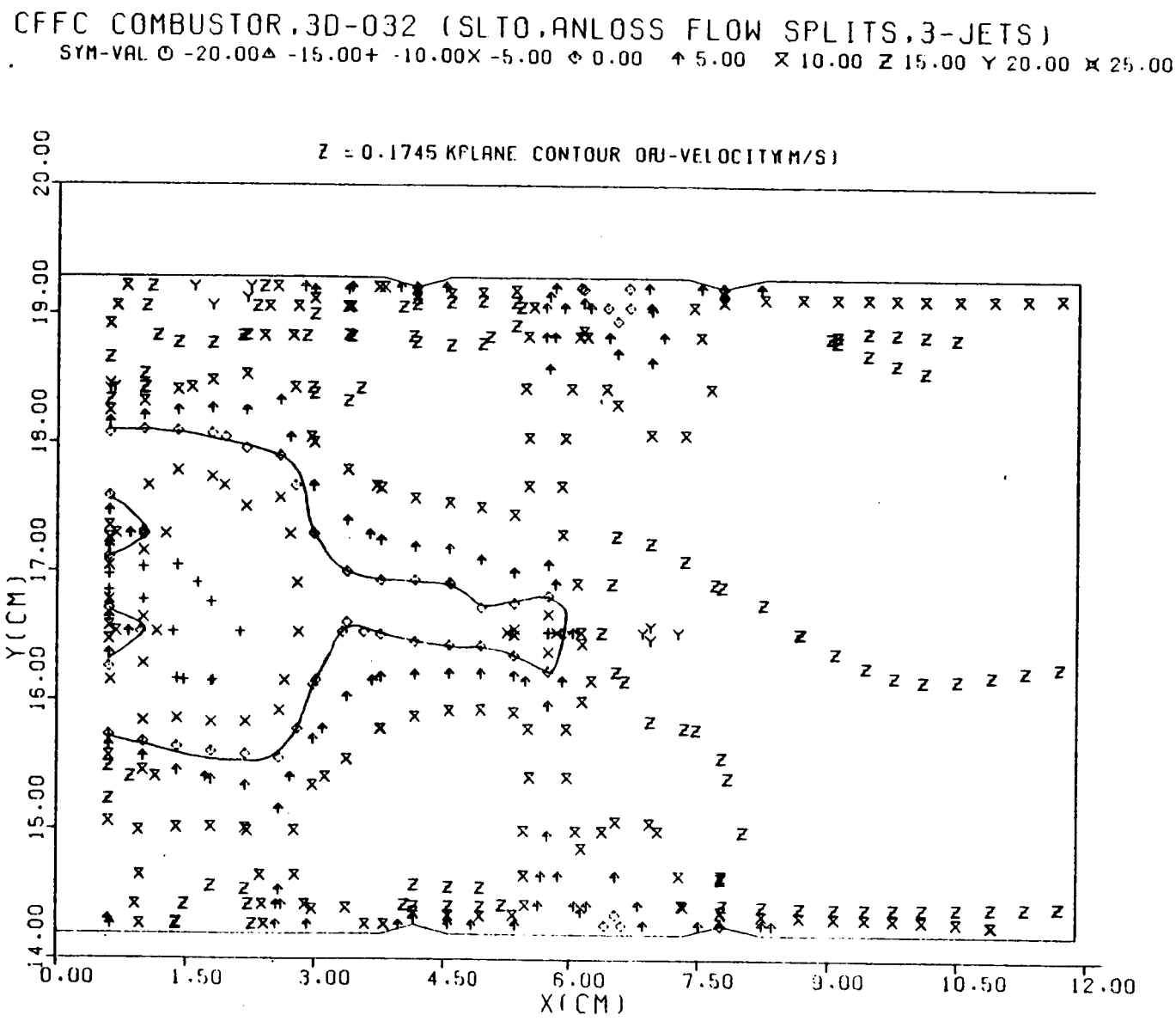

Figure 4. Axial Velocity Distribution (Run No. 2).

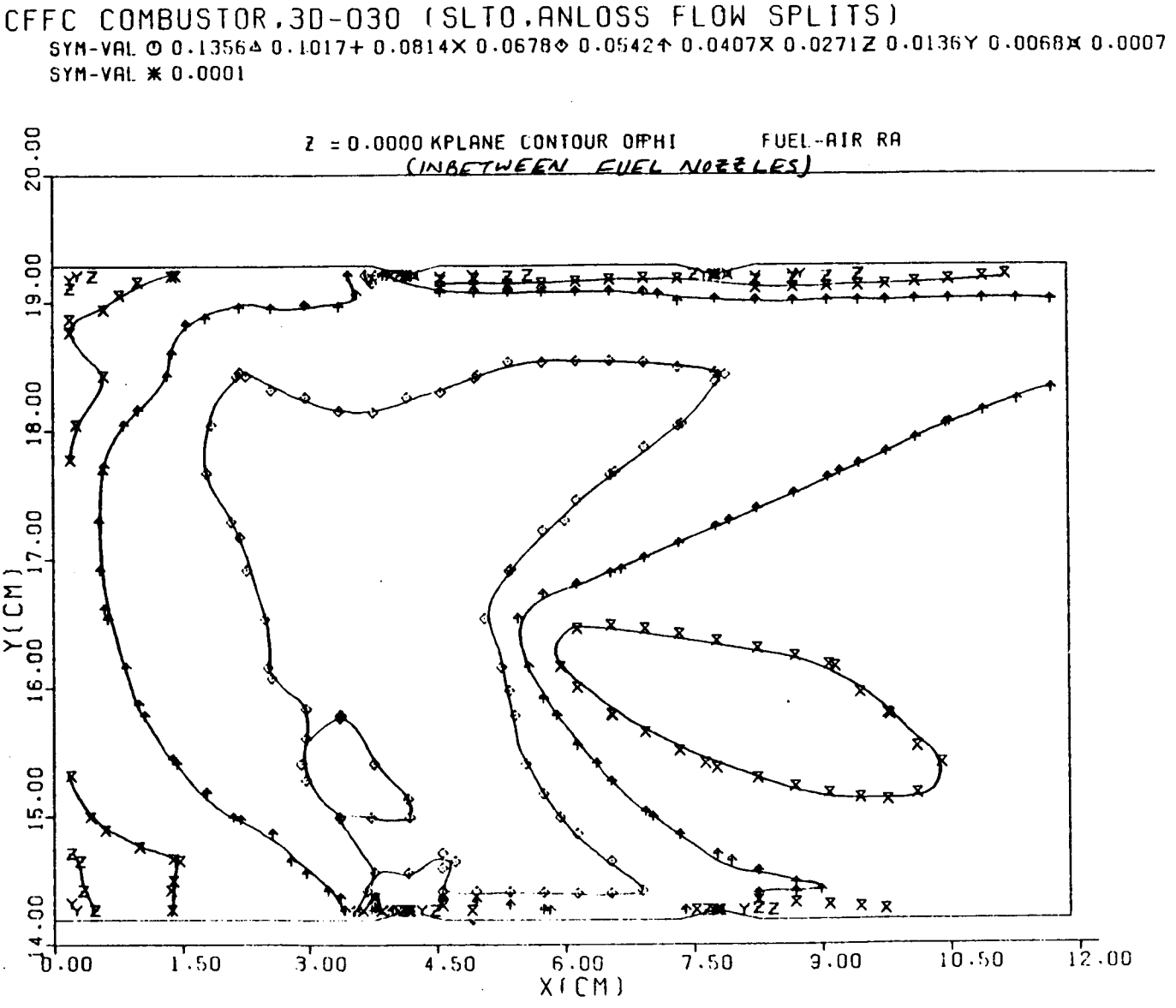

Figure 5. Fuel-Air Ratio Distribution (Run No. 1)
Plane in Between Fuel Nozzle.

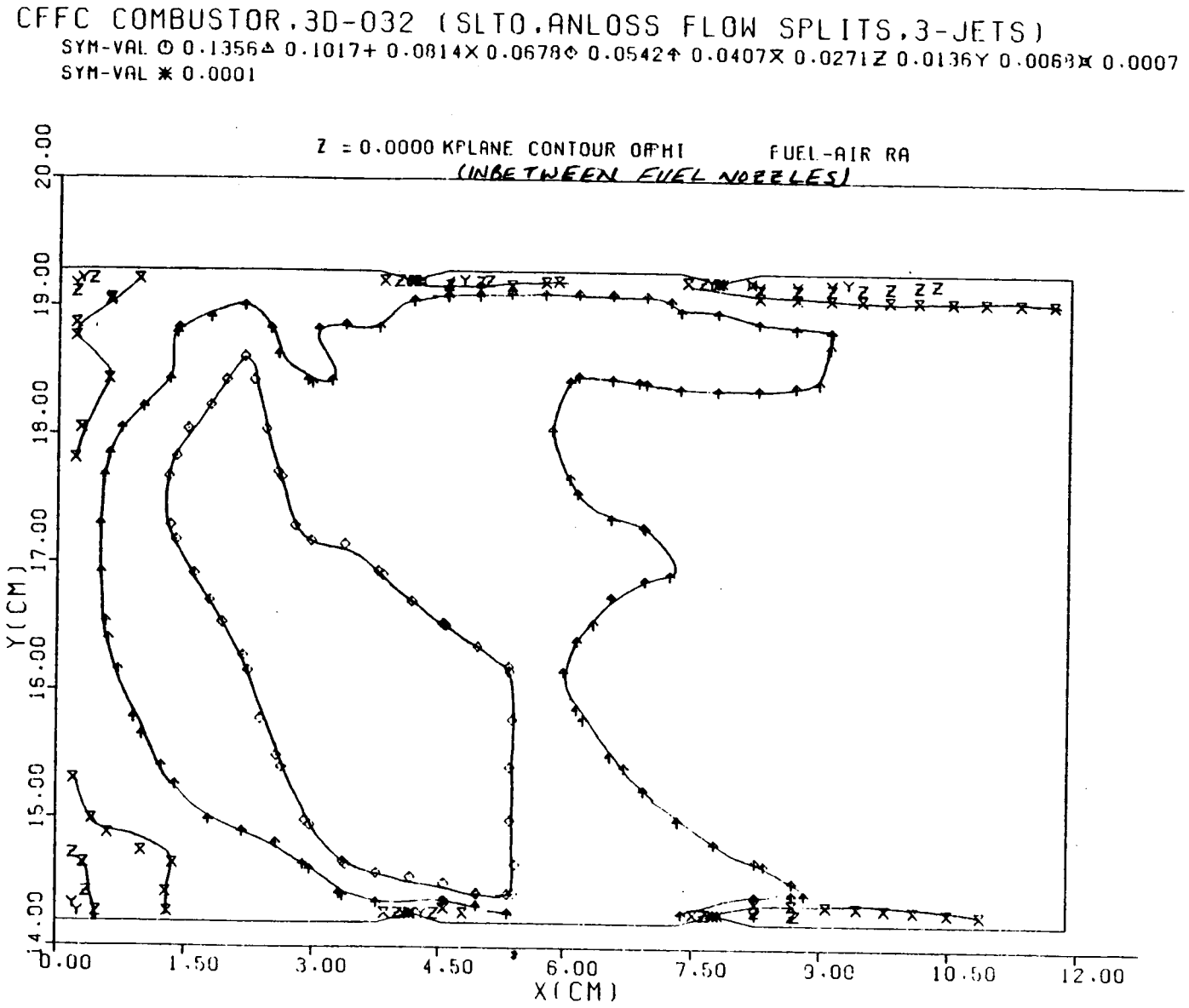

Figure 6. Fuel-Air Ratio Distribution (Run No. 2) Plane in Between Fuel Nozzle.

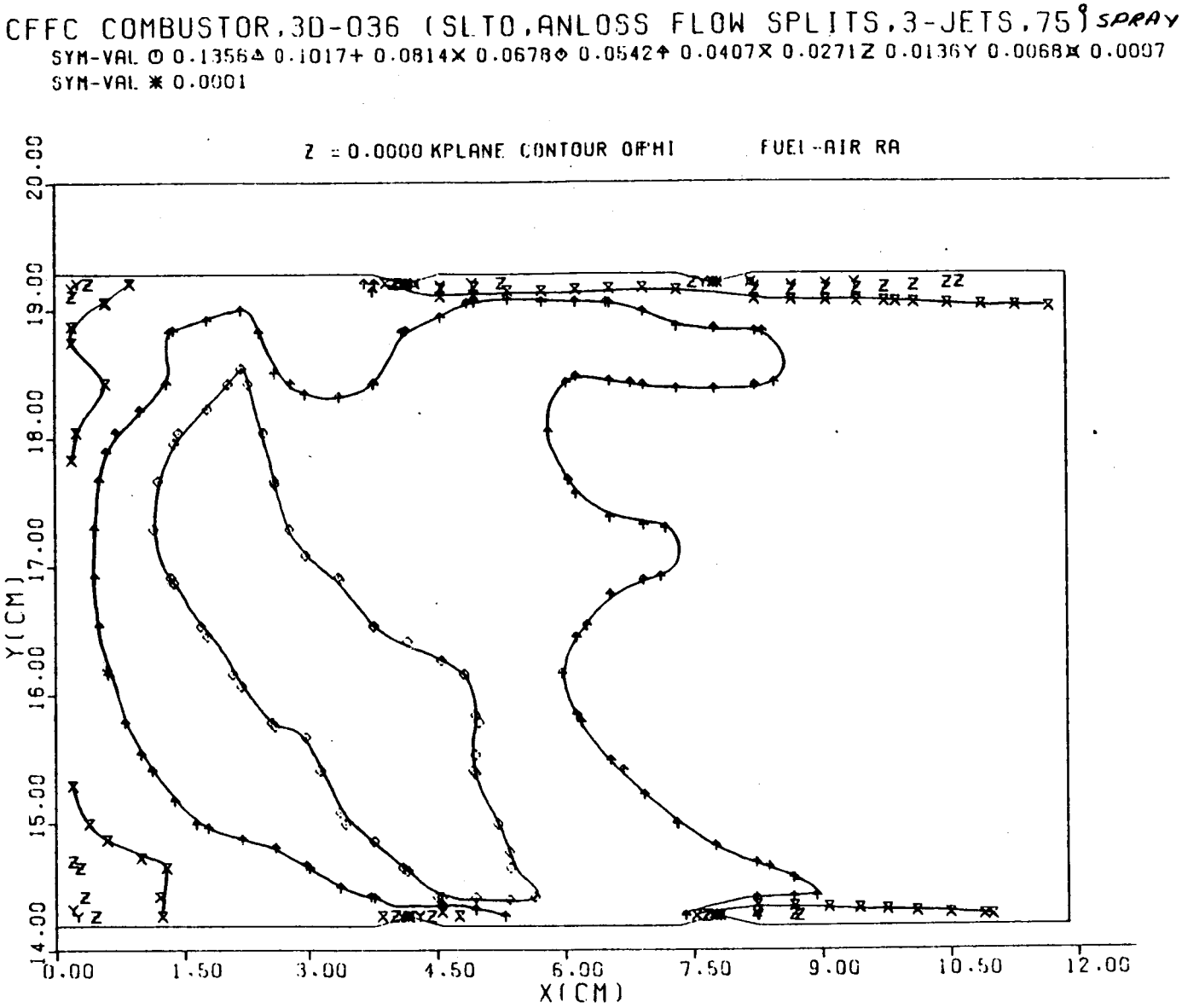

Figure 7. Fuel-Air Ratio Distribution (Run No. 3)
Plane in Between Fuel Nozzle.

extension of the 0.8 equivalence-ratio pocket beyond the dilution orifices was stopped by increasing the number of primary and dilution orifices, as was studied in Run Number 2. The predicted profiles shown in Figure 6 indicated that the pocket has now been contained because of the three primary jets. The effect of the smaller spray-core angle (75 degrees versus 90 degrees) is presented in Figure 7. The 0.8 equivalence-ratio pocket was slightly smaller with the 75-degree spray.

Figure 8 presents predicted fuel-air ratio profiles for a plane in line with the first primary jet that was located upstream of the nozzle in the direction of swirl; the results are for Run 1. Due to increased dome flow for Run Number 1, the fuel-rich pocket of equivalence ratio 2.0 was reduced considerably. Increasing the number of jets (Run Number 2) further reduced the fuel-rich pocket size as shown in Figure 9. A decrease in spray-included-angle slightly reduced the fuel-rich pocket size, as shown in Figure 10.

Figures 11 through 13 present the predicted profiles along the θ = 17-degree spray centerline for Runs 1 through 3, respectively. The extent of fuel impingement on the liner walls was reduced because of the increased dome flow, as shown in Figure 11. Also, increasing the number of orifices, as in Run 2, reduced fuel impingement (Figure 12). Reducing spray-included-angle did not reduce fuel impingement (Figure 13 versus Figure 12).

Figures 14 through 16 show predicted profiles along a θ = 17-degree plane for Runs 1 through 3, respectively. Only a slight improvement in liner-fuel impingement was achieved in Runs 2 and 3, as indicated in Figures 15 and 16. Figures 17 through 29 present predicted isothermal lines for the planes for fuel-air ratio profiles that were discussed in the preceeding paragraphs. An important conclusion was reached from these plots, in that the hot-gas streak was

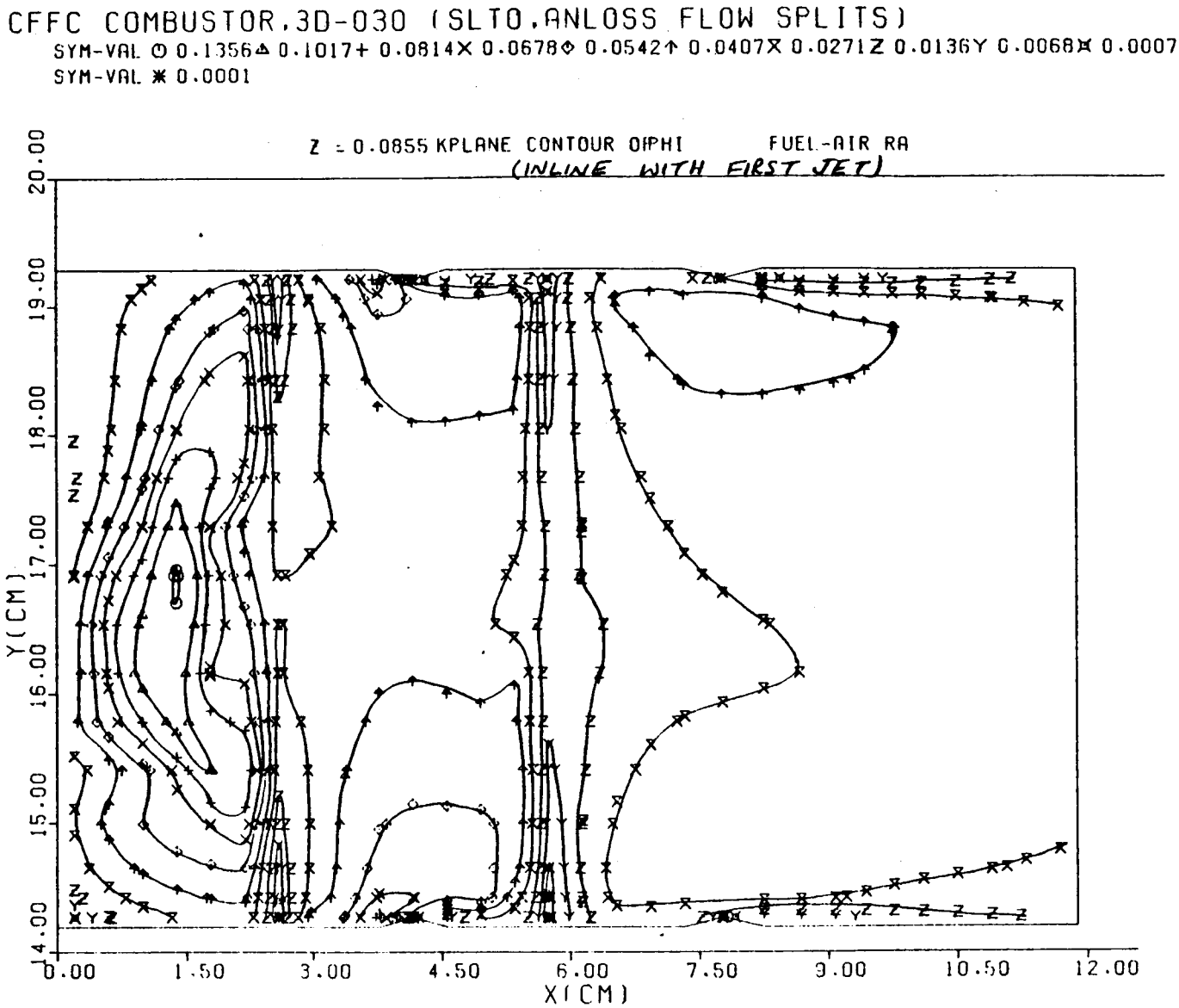

Figure 8. Fuel-Air Ratio Distribution (Run No. 1)
Plane in Line with Primary Jet.

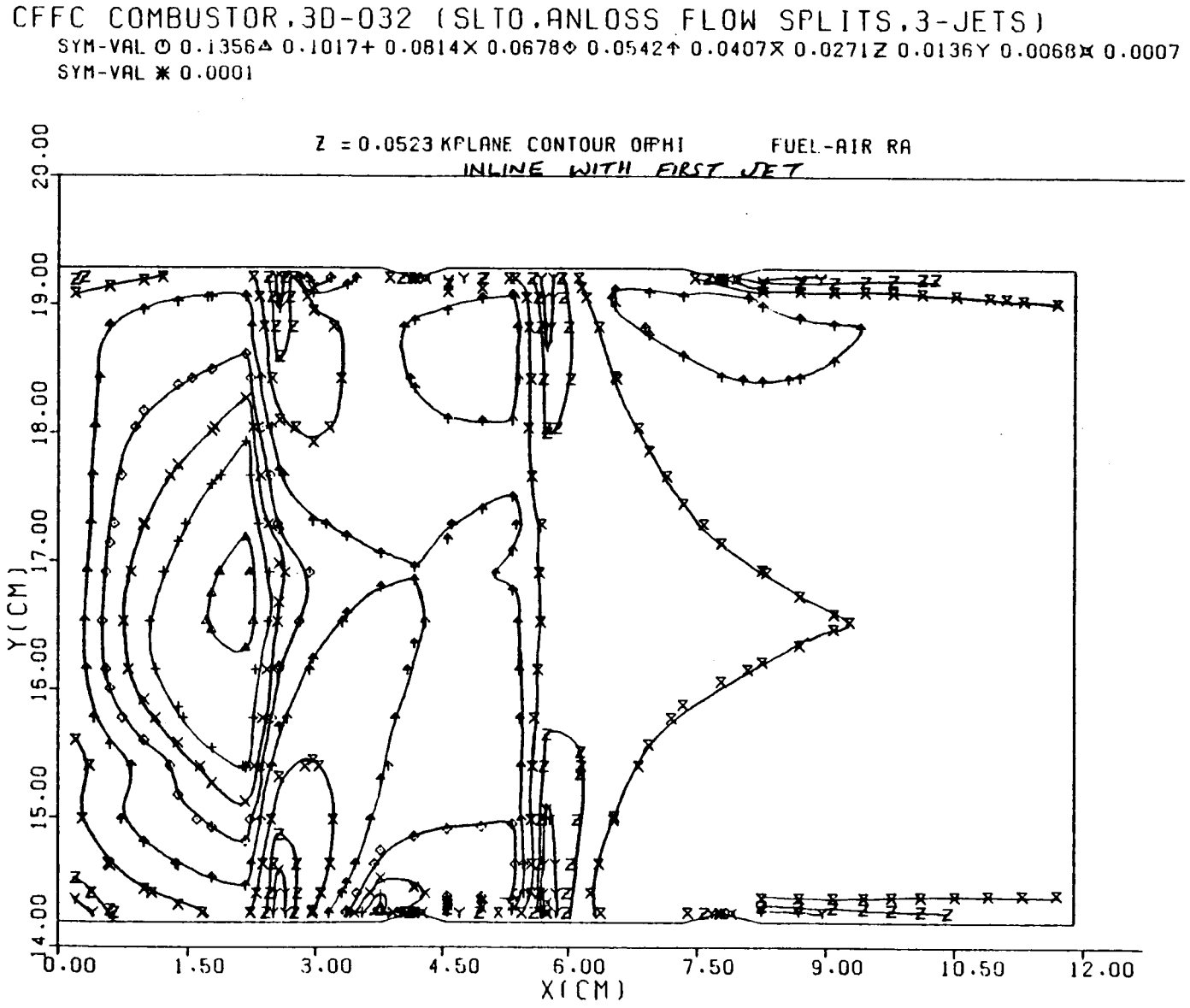

Figure 9. Fuel-Air RAtio Distribution (Run No. 2)
Plane in Line with Primary Jet.

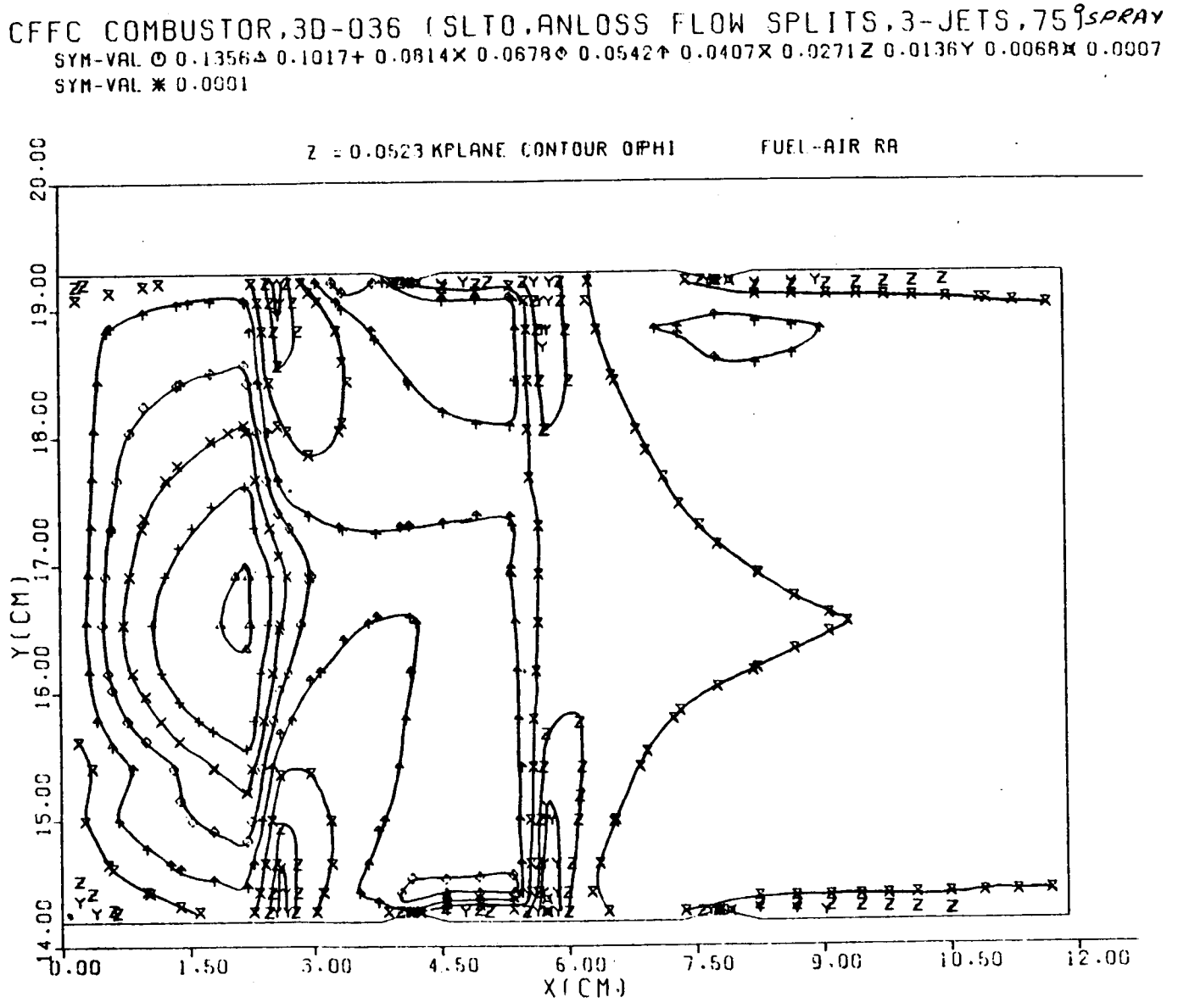

Figure 10. Fuel-Air Ratio Distribution (Run No. 3) Plane in Line with Primary Jet.

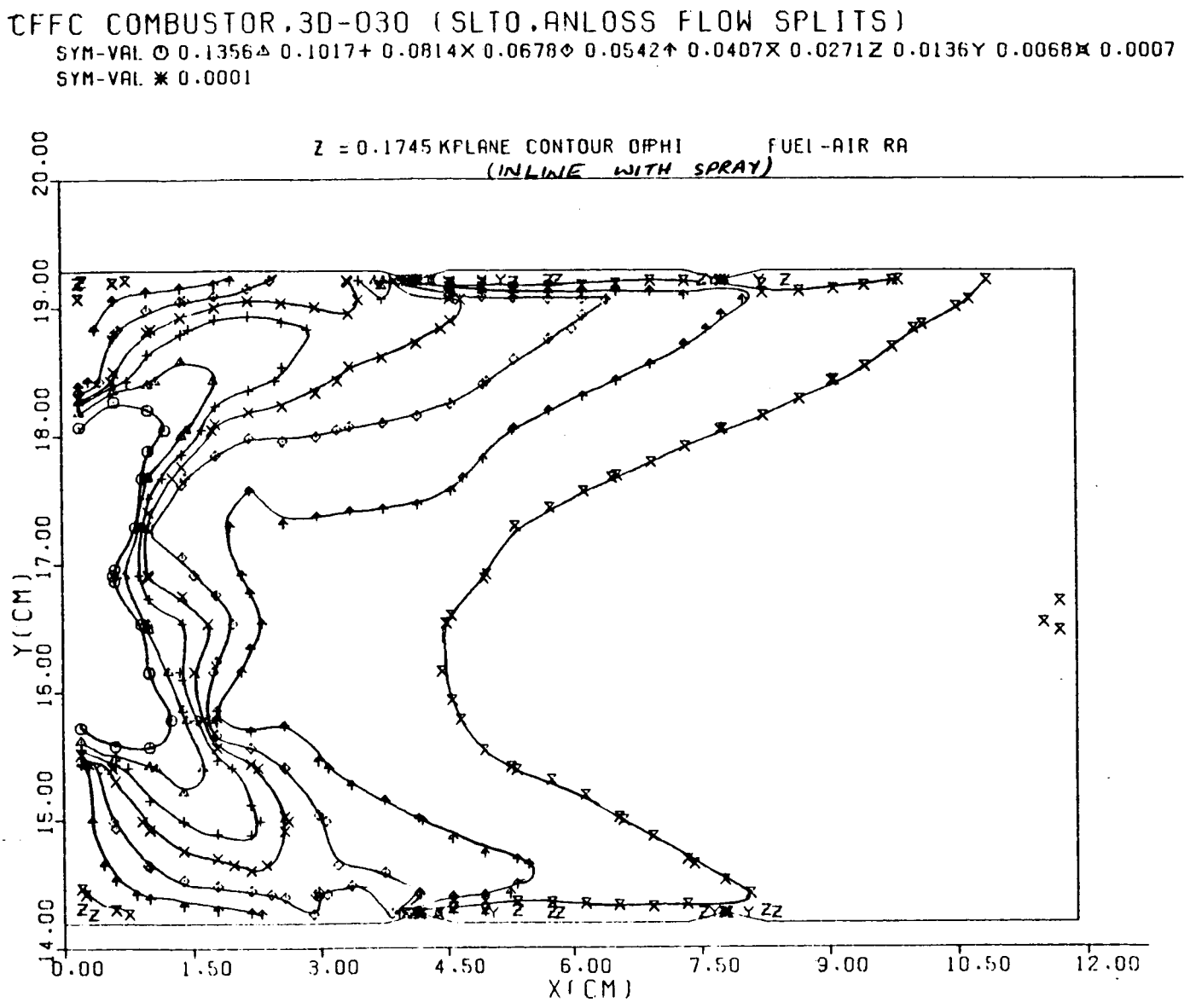

Figure 11. Fuel-Air Ratio Distribution (Run No. 1) Plane in Line with Spray.

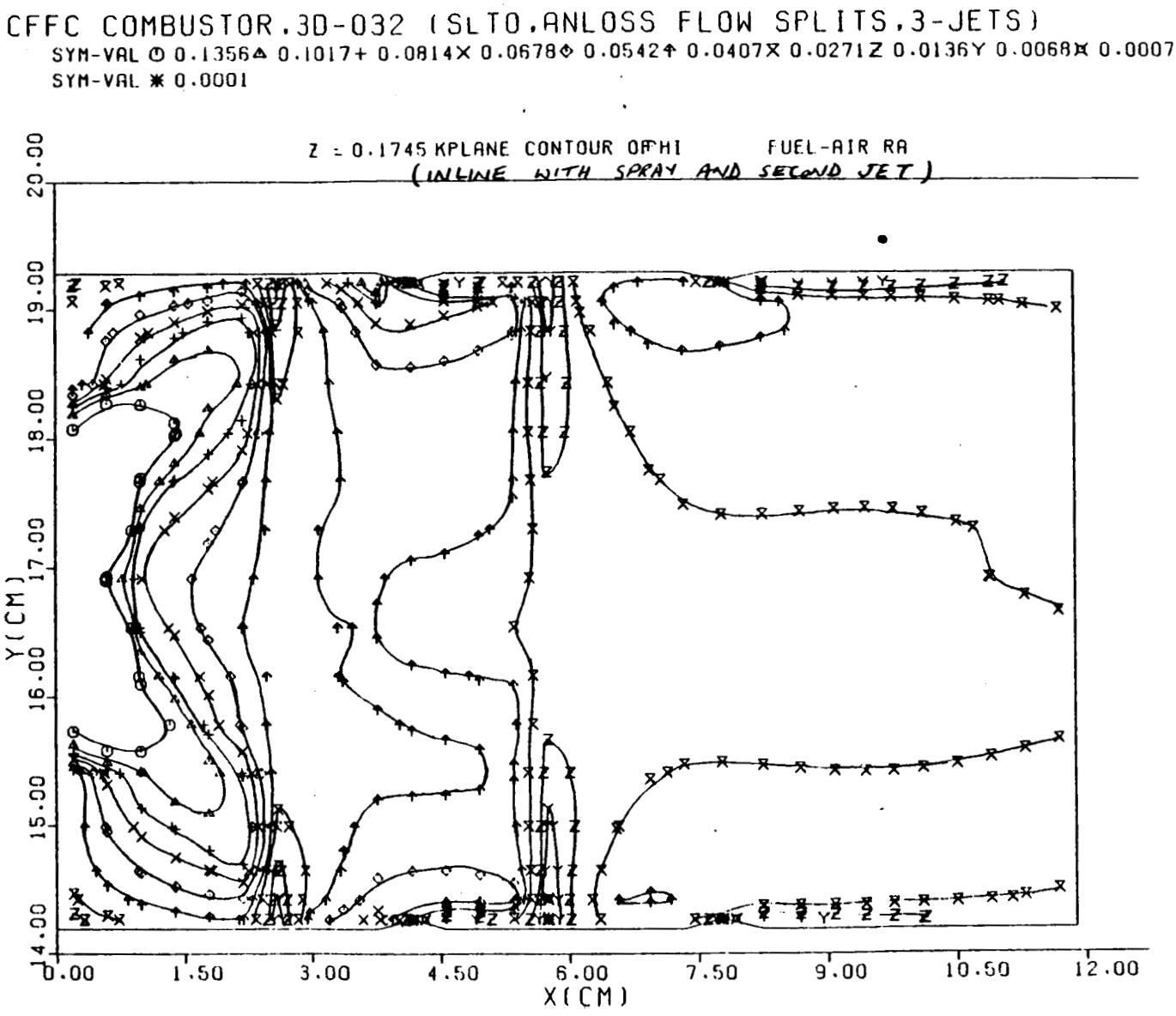

Figure 12. Fuel-Air Ratio Distribution (Run No. 2) Plane in Line with Spray.

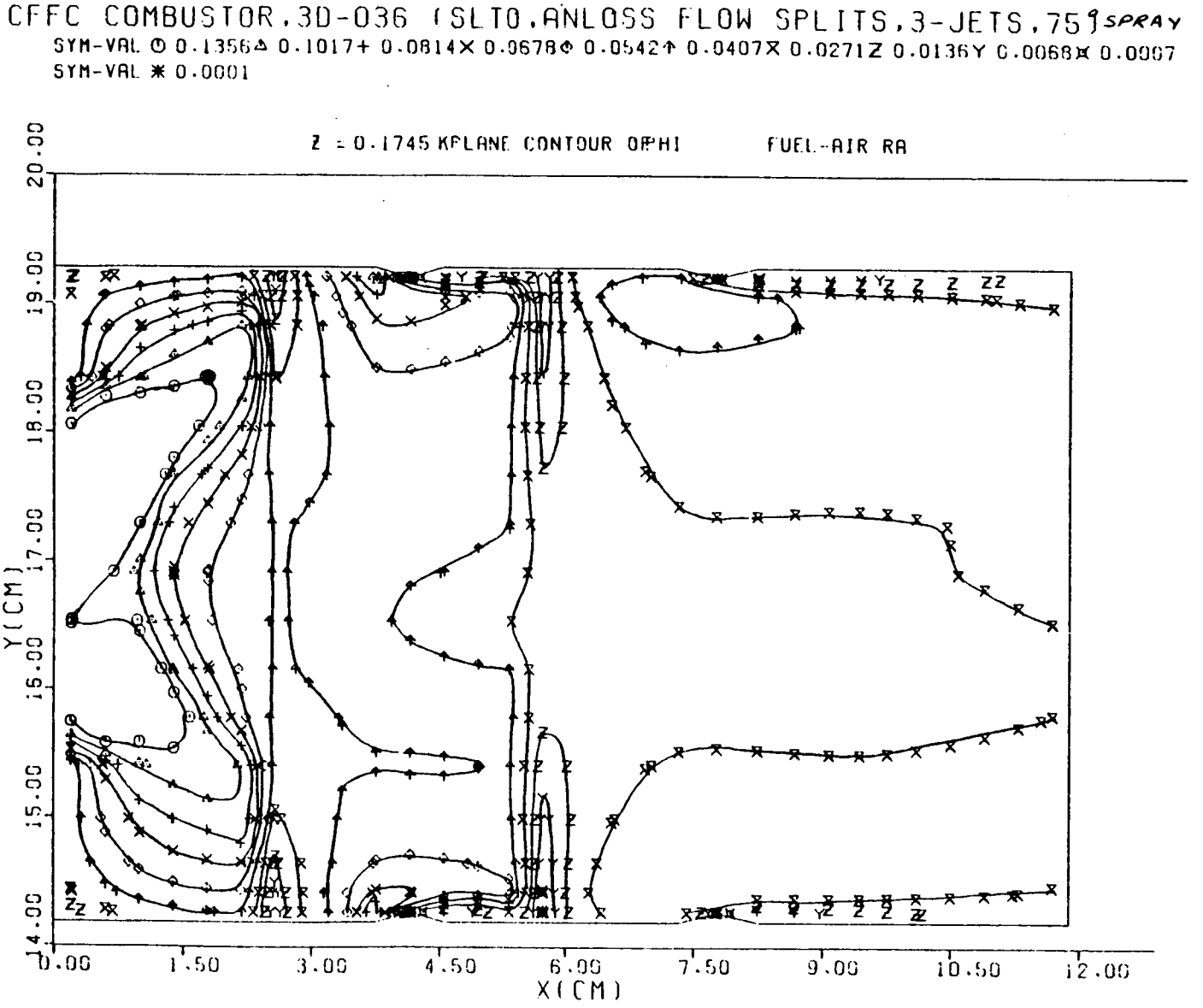

Figure 13. Fuel-Air Ratio Distribution (Run No. 3) Plane in Line with Spray.

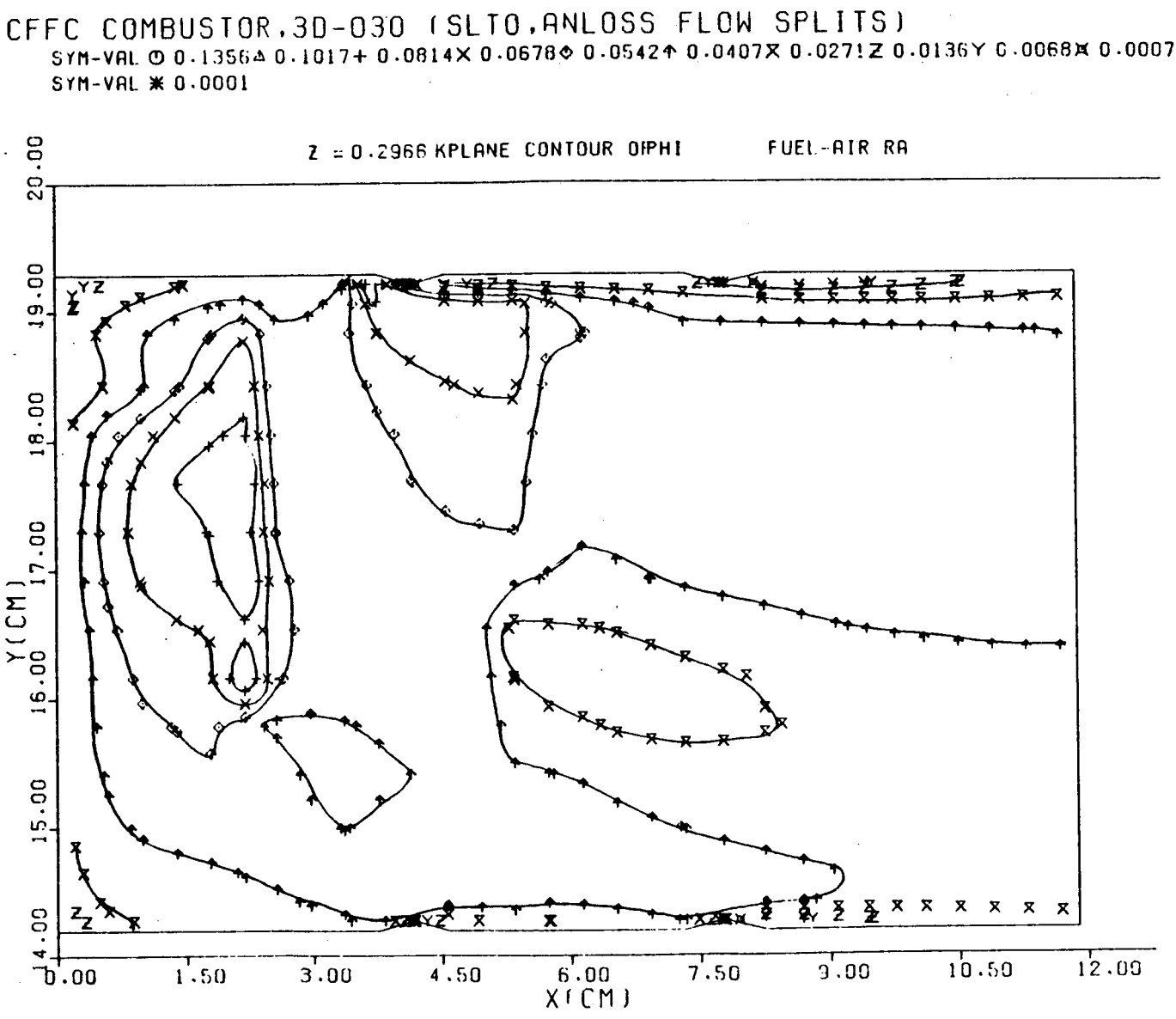

Figure 14. Fuel-Air Ratio Distribution (Run No. 1)
Plane θ = 17-Degree.

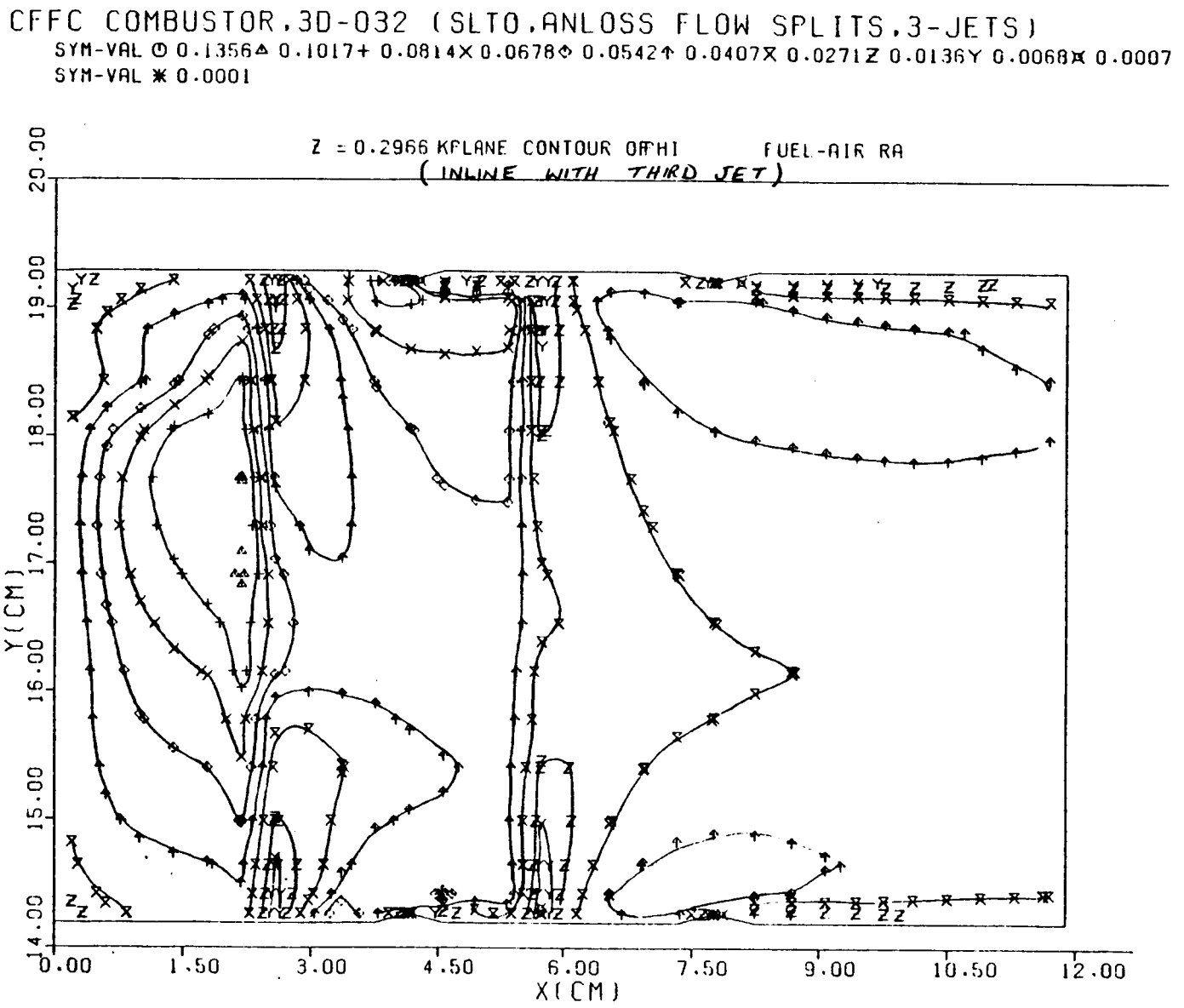

Figure 15. Fuel-Air Ratio Distribution (Run No. 2)
Plane θ = 17-Degree.

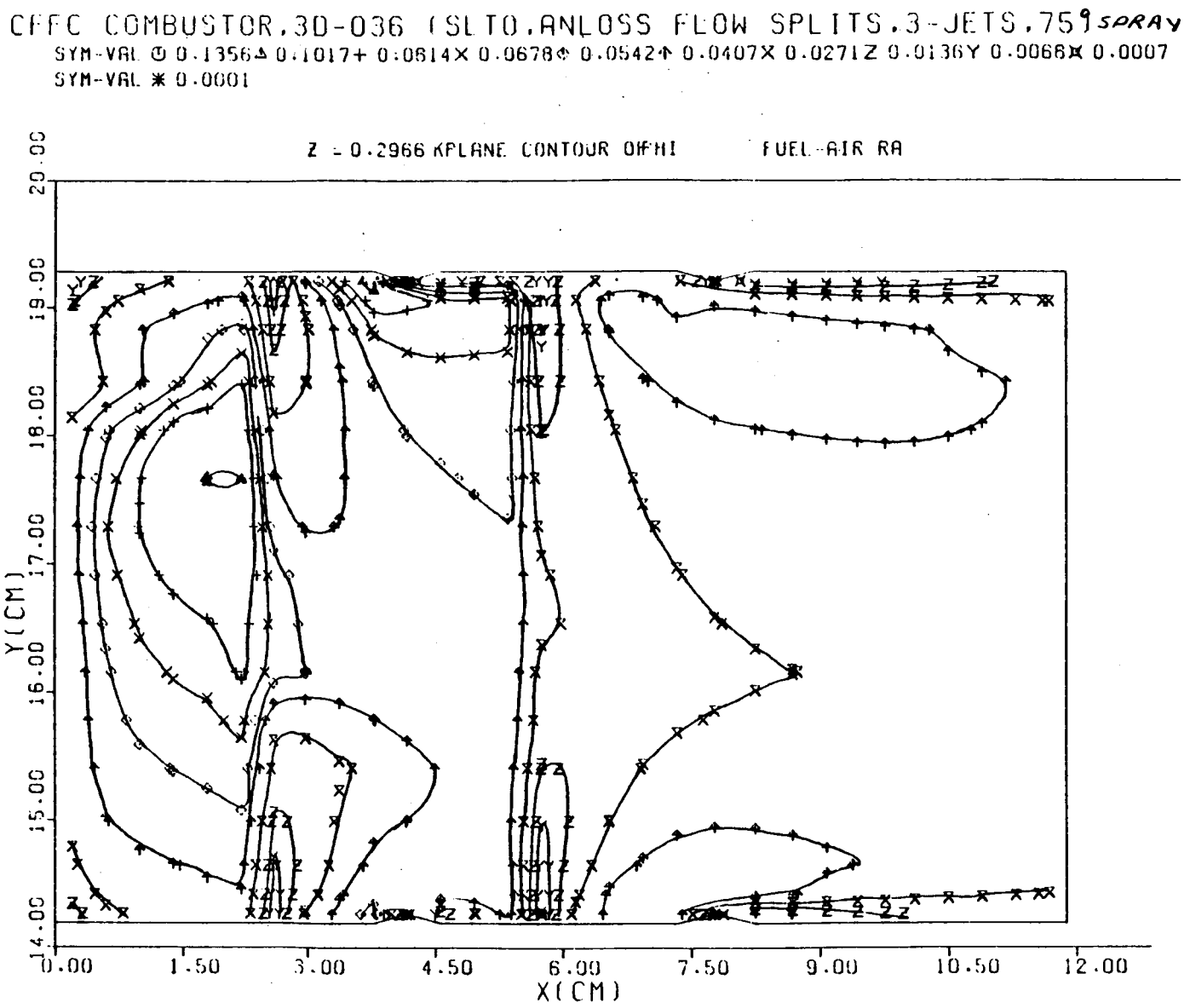

Figure 16. Fuel-Air Ratio Distribution (Run No. 3)
Plane θ = 17-Degree.

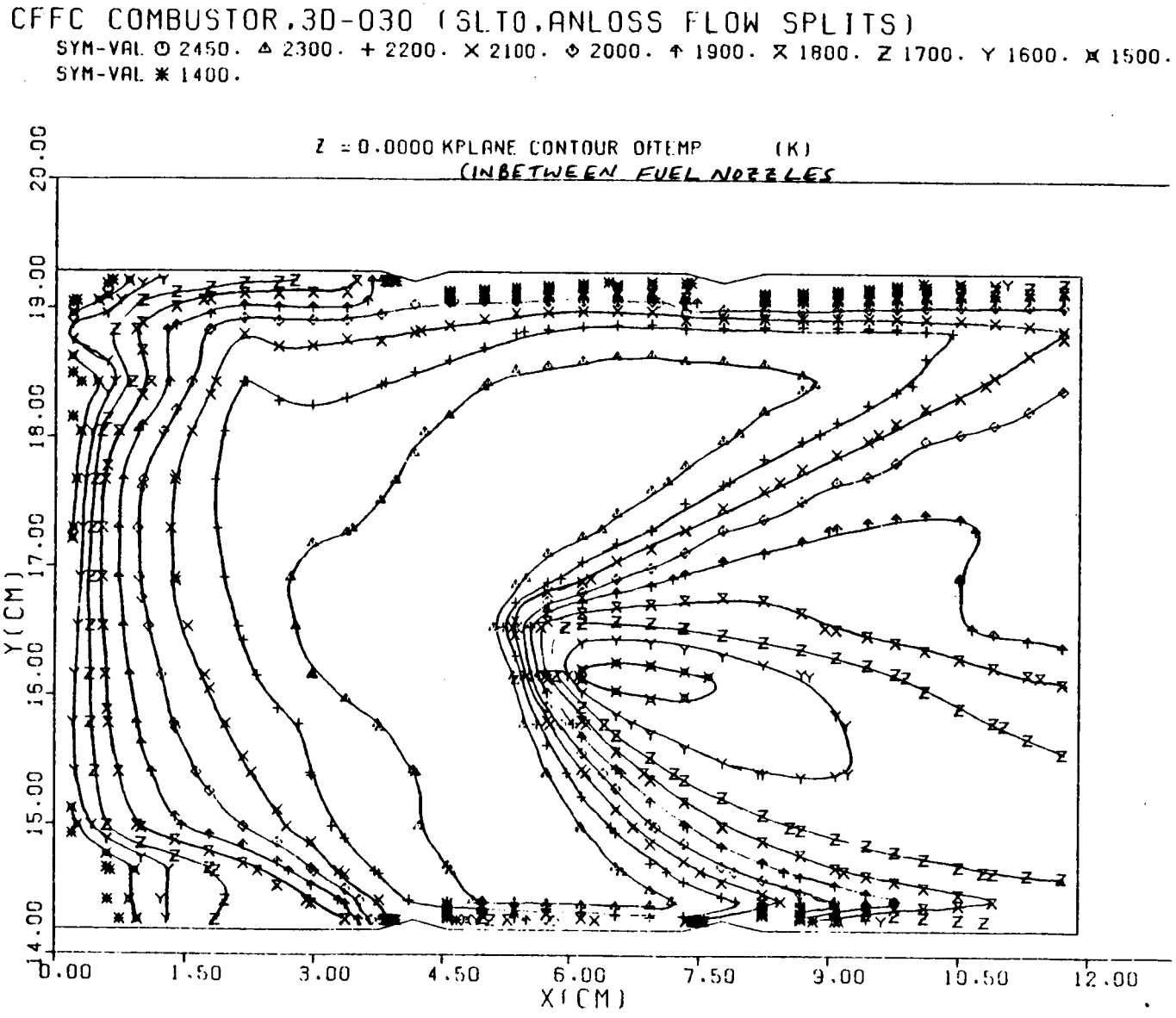

Figure 17. Temperature Distribution (Run No. 1)
Plane in Between Nozzle.

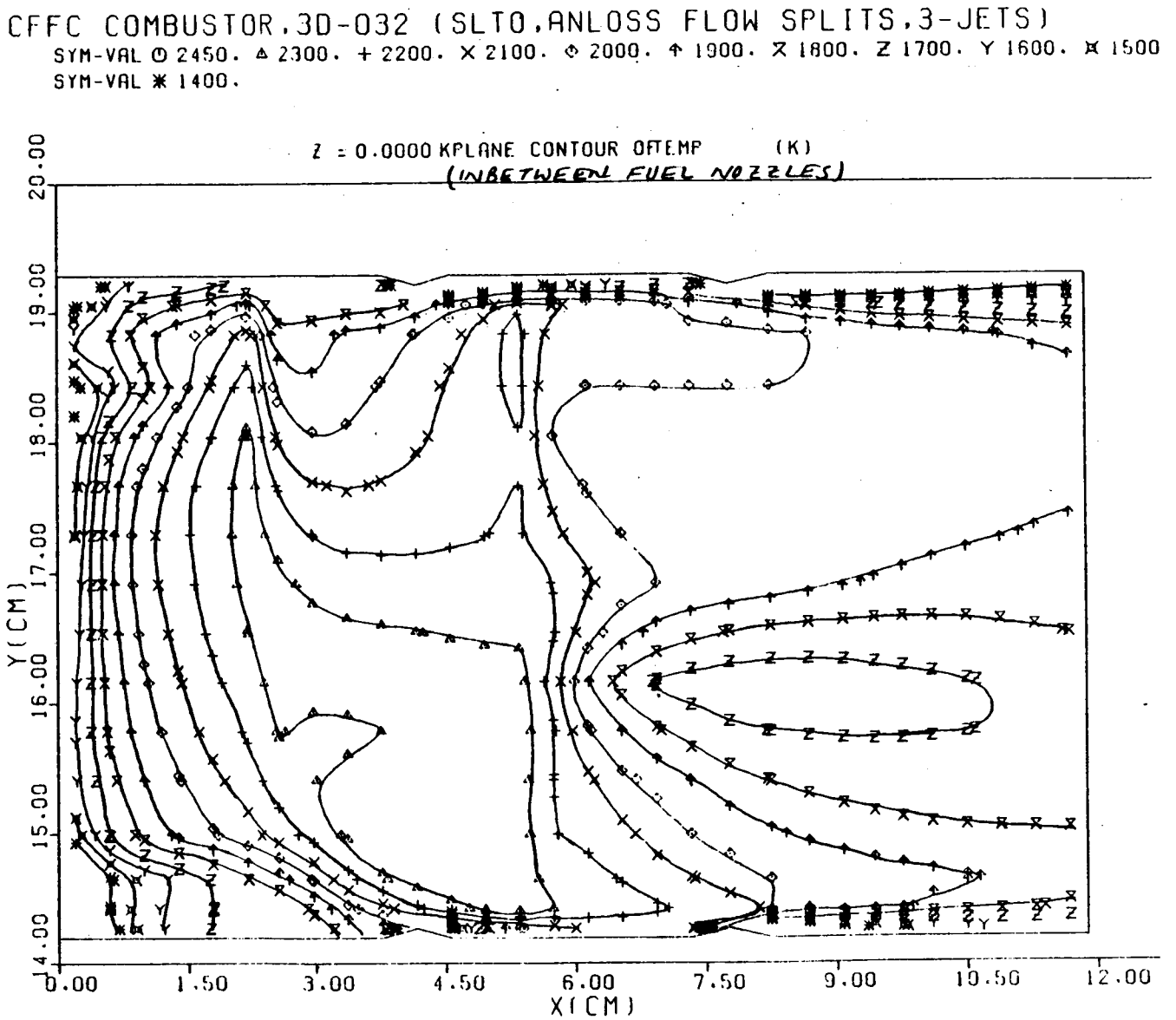

Figure 18. Temperature Distribution (Run No. 2) Plane in Between Fuel Nozzle.

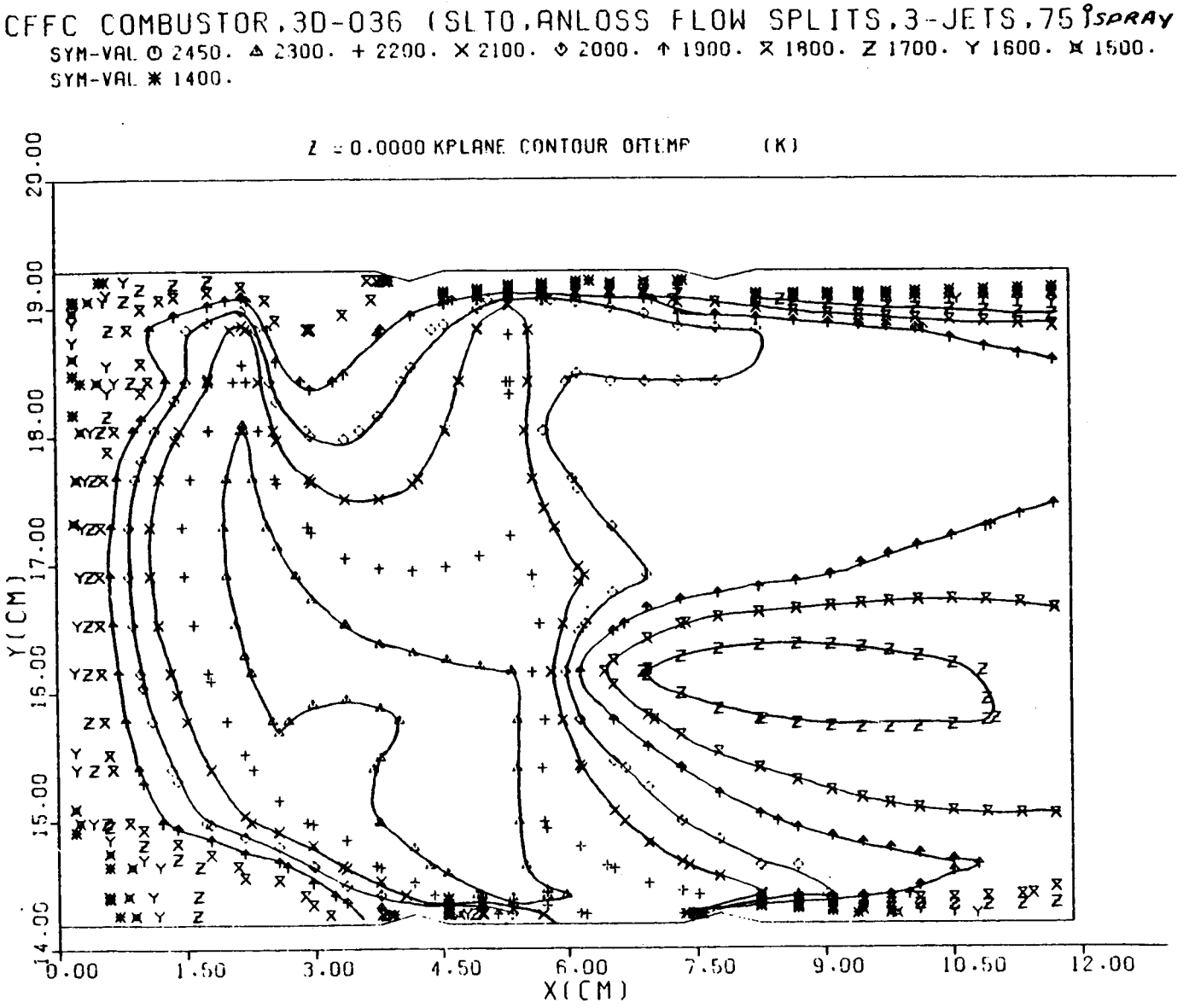

Figure 19. Temperature Distribution (Run No. 3) Plane in Between Nozzle.

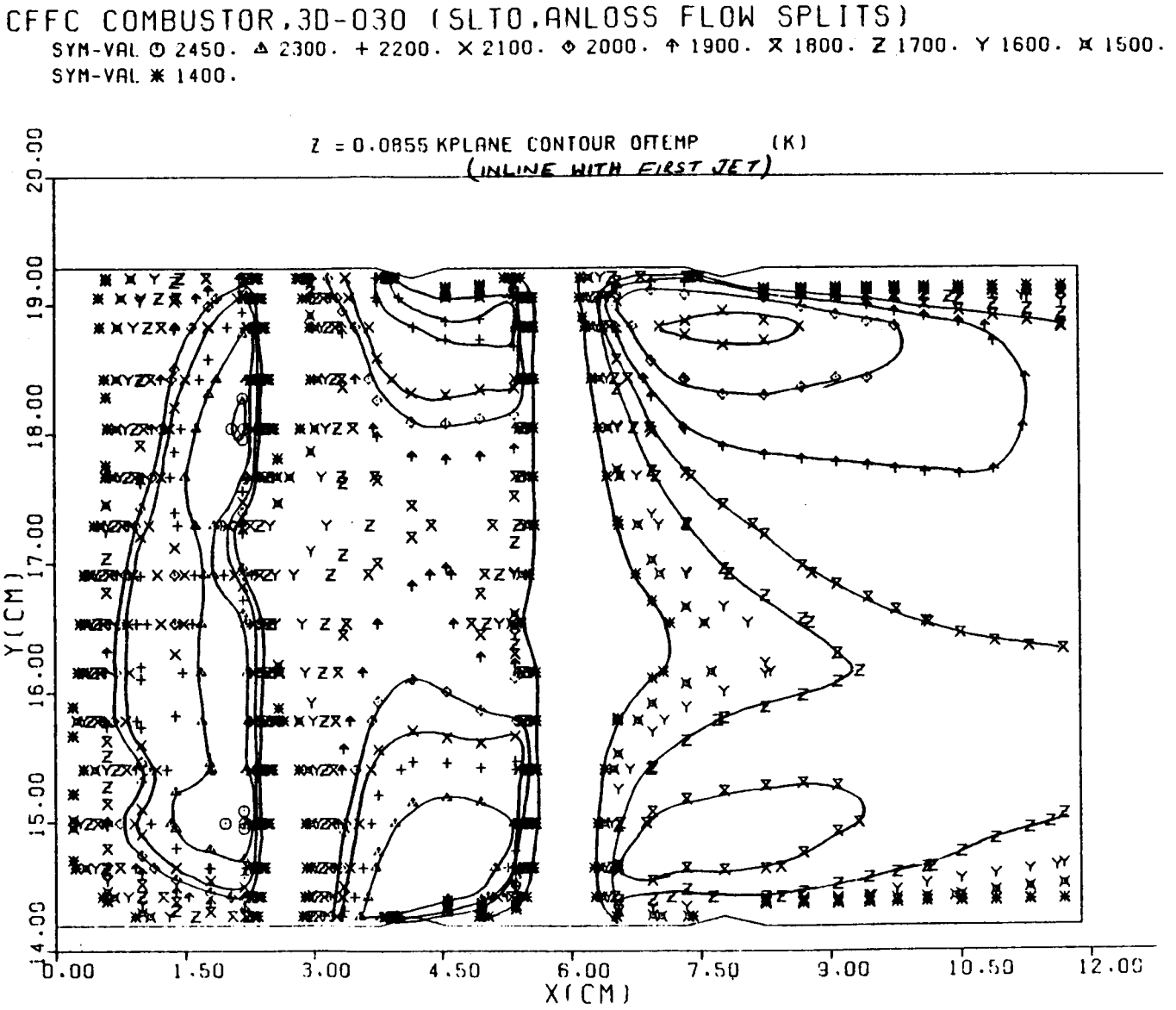

Figure 20. Temperature Distribution (Run No. 1)
Plane in Line with Primary Jet.

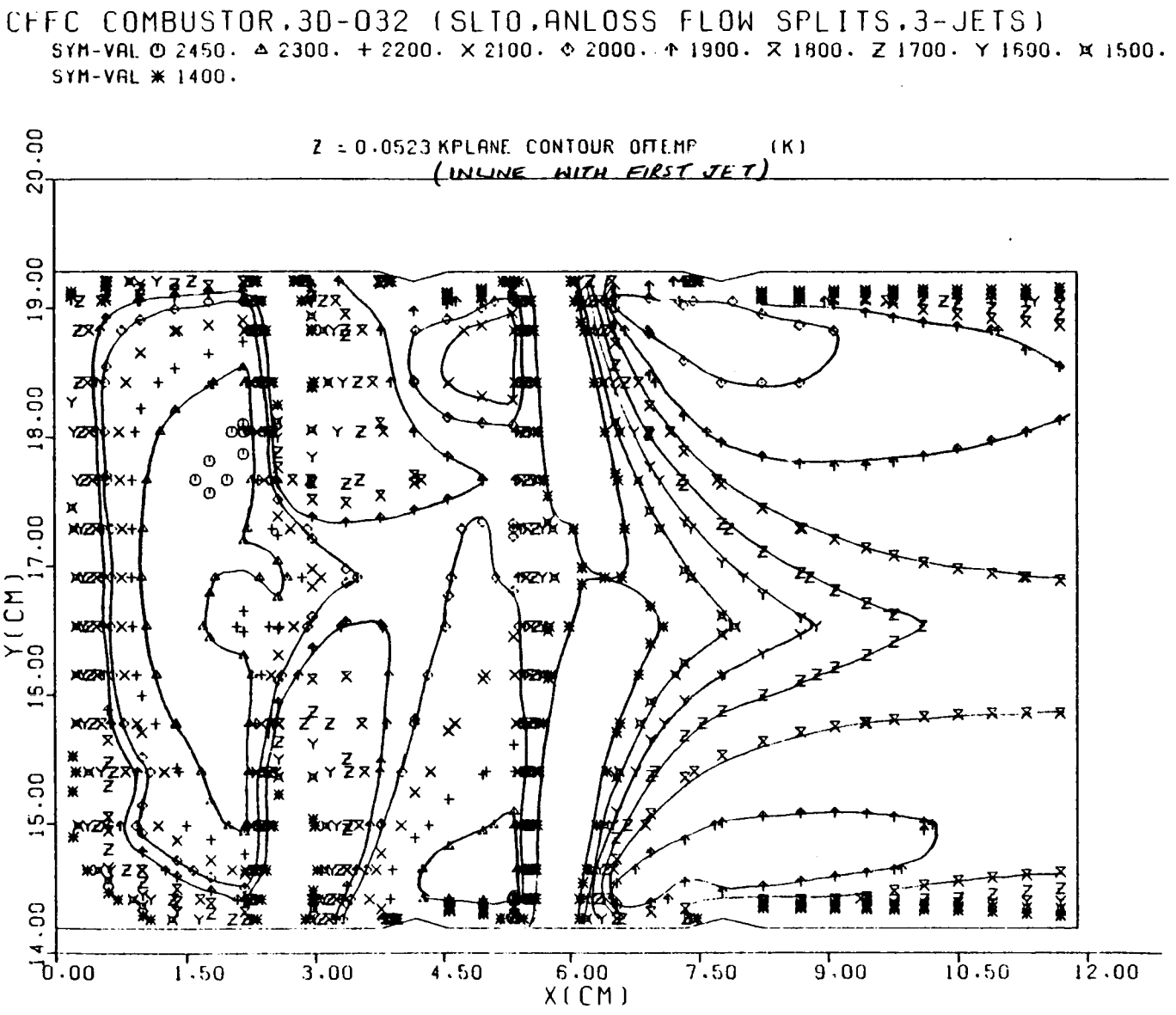

Figure 21. Temperature Distribution (Run No. 2) Plane in Line with Primary Jet.

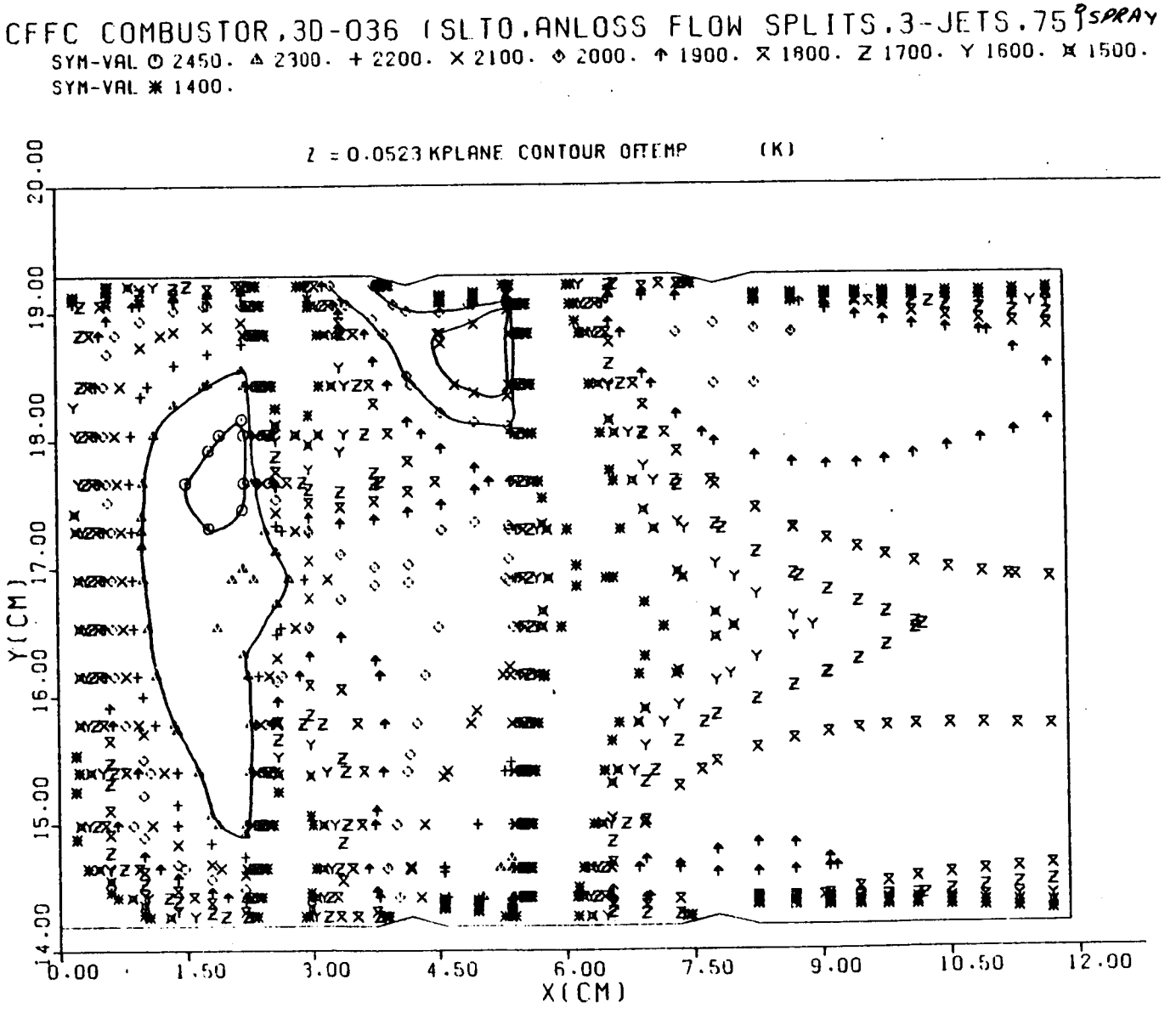

Figure 22. Temperature Distribution (Run No. 3)
Plane in Line with Primary Jet.

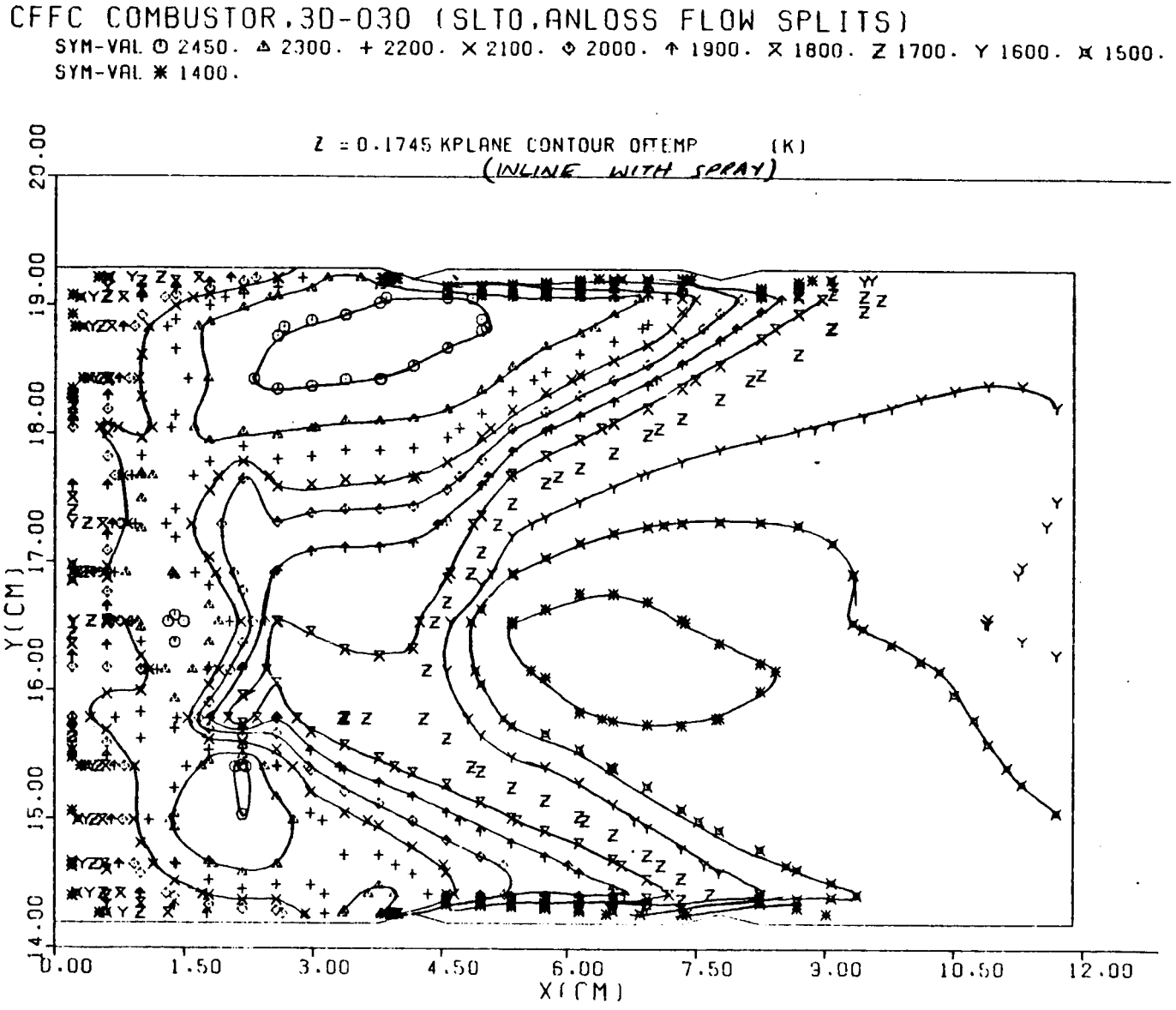

Figure 23. Temperature Distribution (Run No. 1) Plane in Line with Spray.

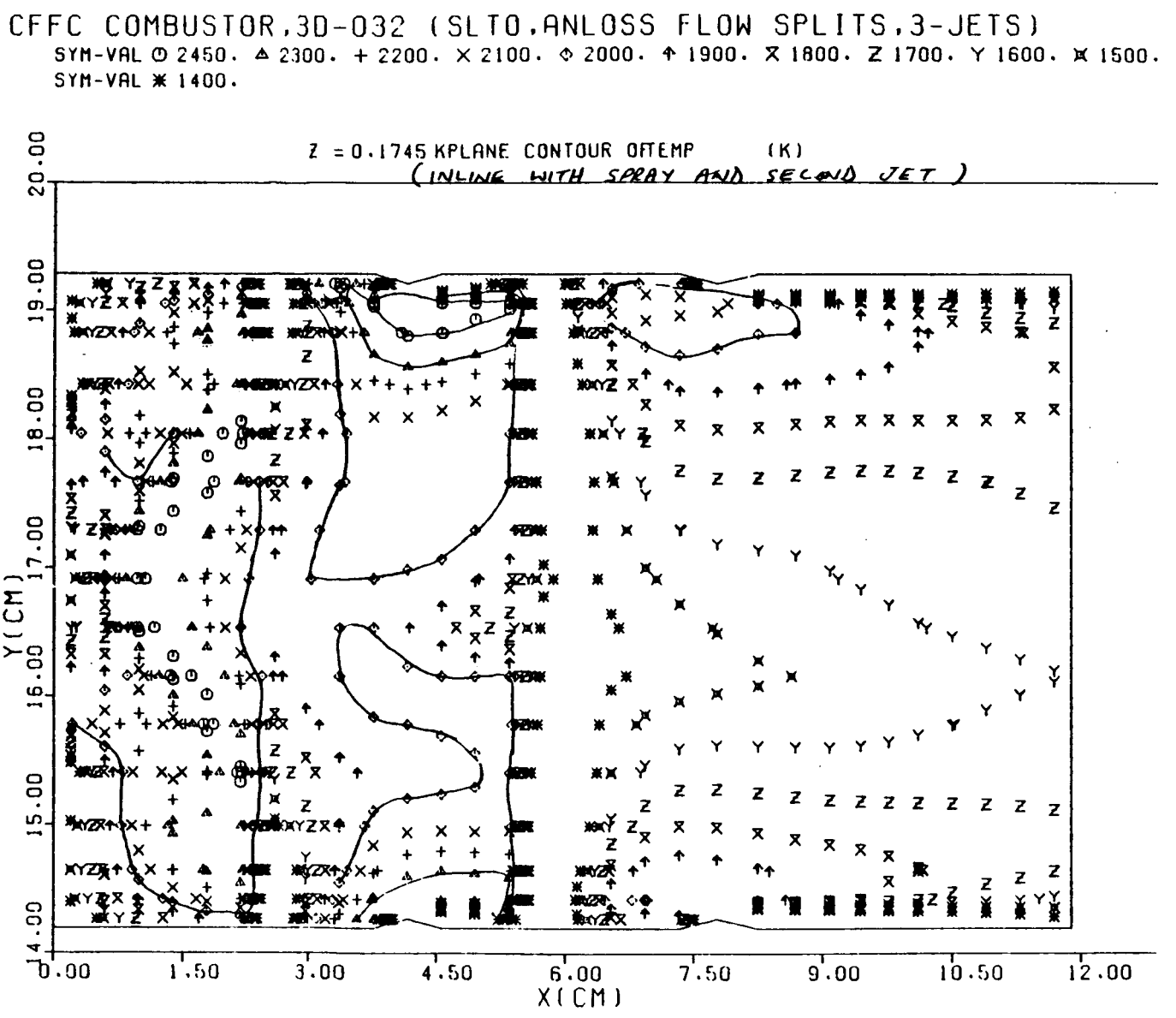

Figure 24. Temperature Distribution (Run No. 2) Plane in Line with Spray.

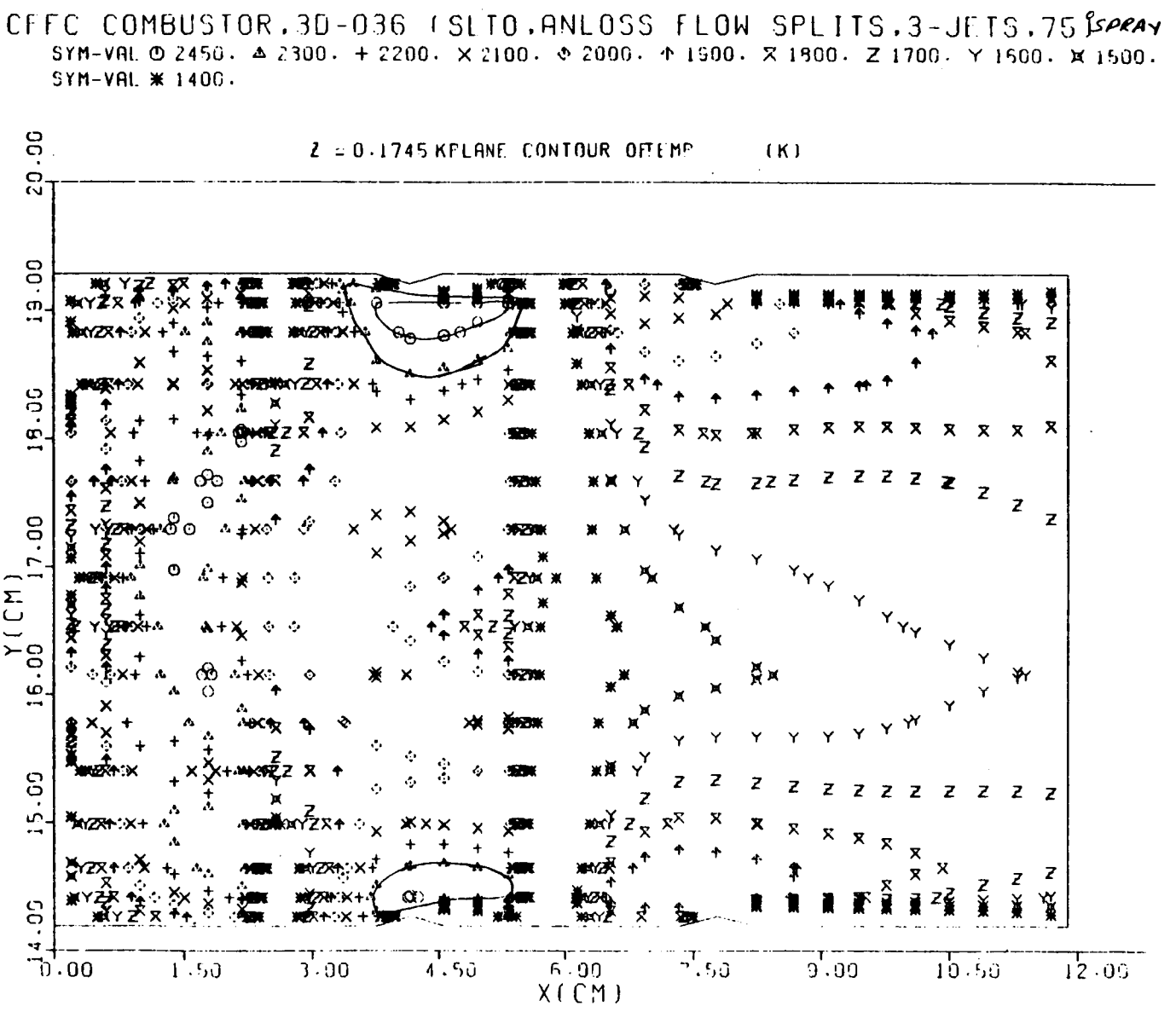

Figure 25. Temperature Distribution (Run No. 3) Plane in Line with Spray.

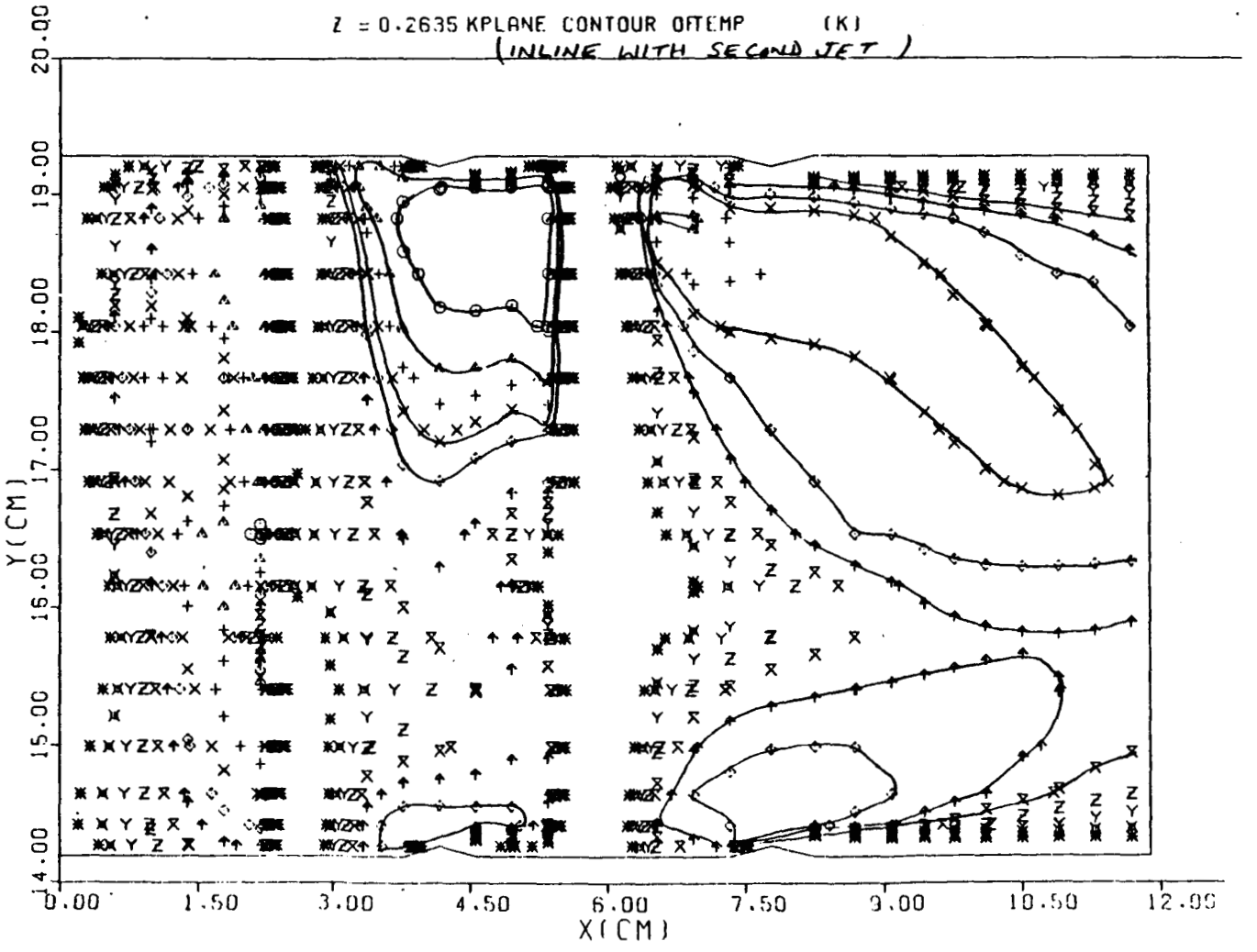

Figure 26. Temperature Distribution (Run No. 1) Plane θ = 17-Degree.

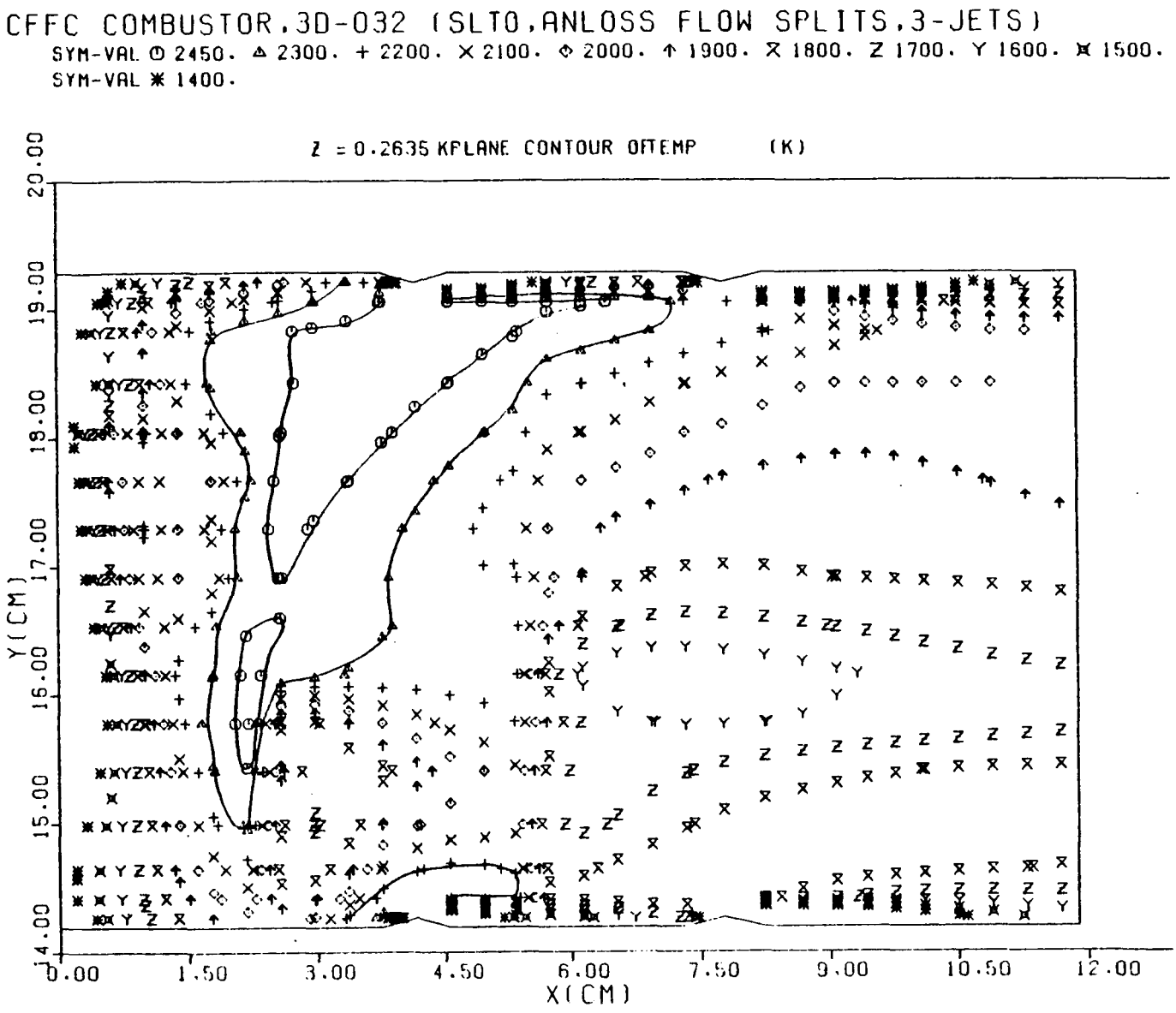

Figure 27. Temperature Distribution (Run No. 2) Plane θ = 17-Degree.

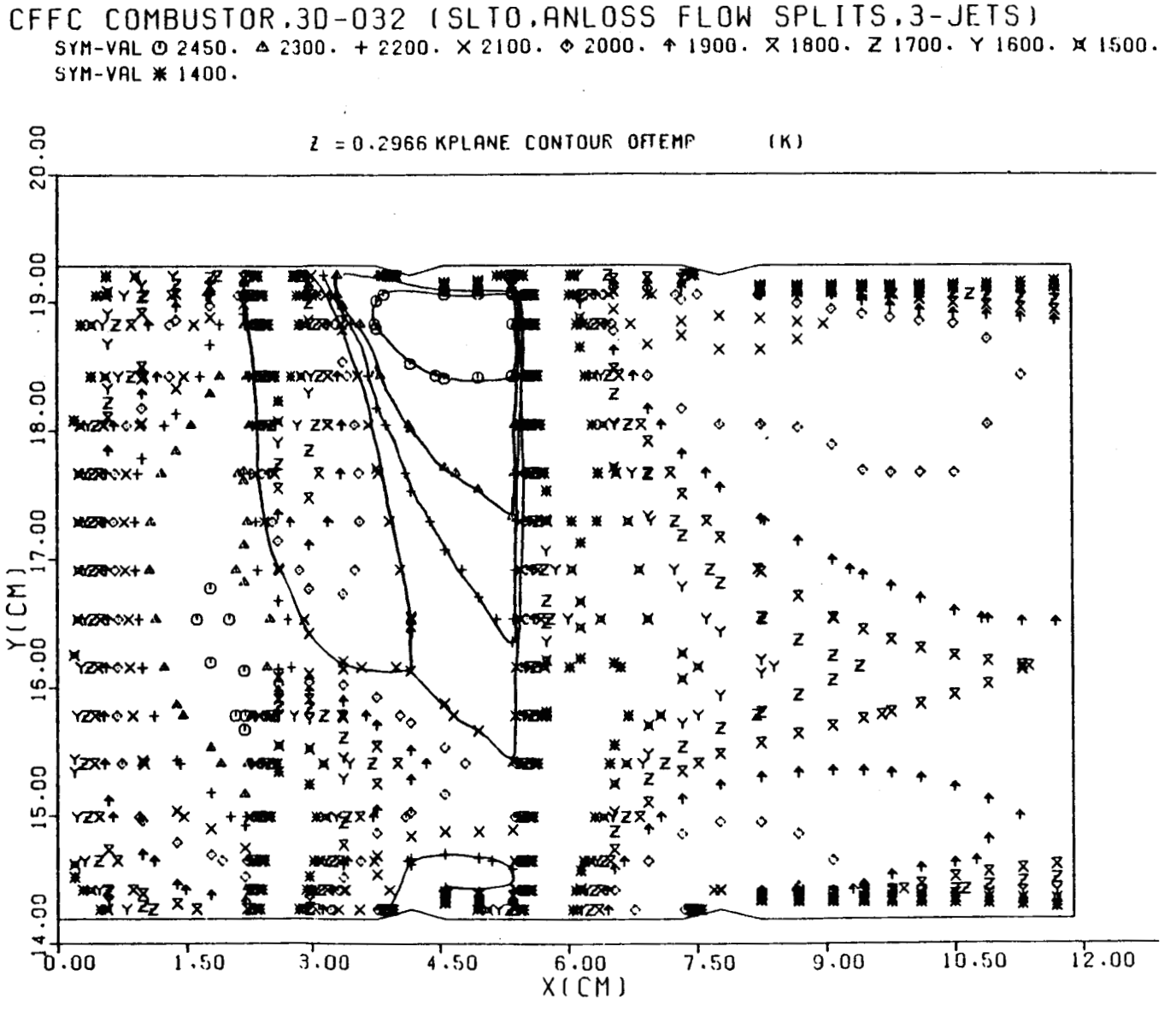

Figure 28. Temperature Distribution (Run No. 2) Plane θ = 17-Degree.

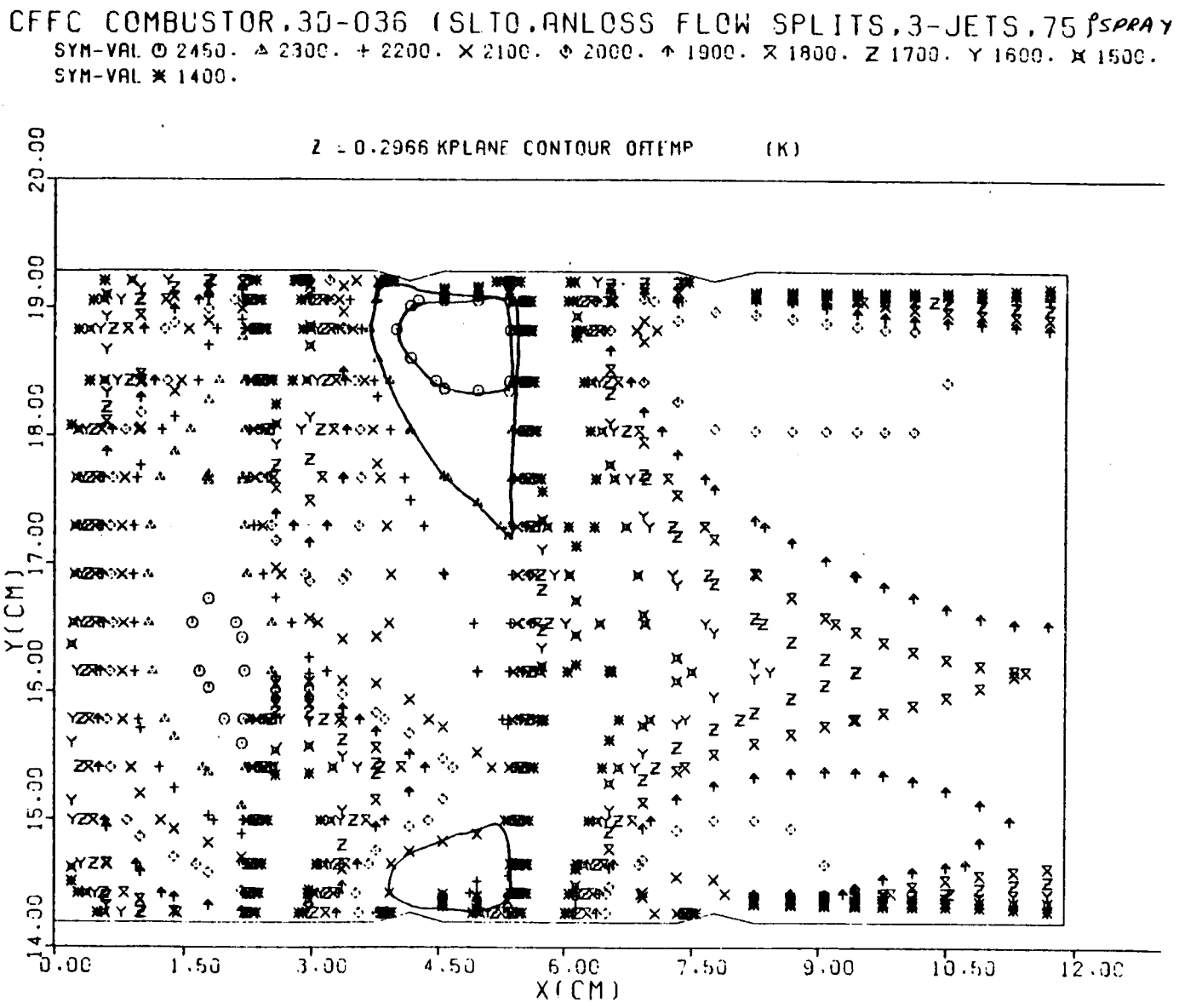

Figure 29. Temperature Distribution (Run No. 3) Plane θ = 17-Degree.

contained better with a three-jet configuration, as shown by comparing Figures 17 and 18.

After the analysis of the original combustor characteristics, the efforts were concentrated on reducing the excessive liner wall temperature below a liner peak of 1700°F (927°C). The approach that was used is discussed in the following paragraphs.

2.2 Analysis and Optimization of the Cooling Air Distribution

2.2.1 Cylindrical Liners

The goal for this task was to reduce the liner-wall temperature by a significant magnitude without modifying the combustion process. The overall geometric envelope of the combustor was preserved, as were the locations and airflow rates of the primary and dilution-zone orifices and of the dome swirlers. The wall temperatures predicted indicated very severe liner conditions; consequently, three techniques were employed to reduce the wall temperatures to an acceptable level:

- Convective counterflow-film cooling
- Rectangular offset-fin plate cooling
- Extended surface-film cooling

For each technique, the coolant flowed through the convective or fin passages before it was injected into the hot-combustion gases.

The second cooling scheme was evaluated only on the cylindrical section of the combustor. The transition-liner geometry prohibited the use of the offset-fin plates in this area. The temperature reductions obtained (from the three cooling techniques) for each section of the combustor are presented in the following paragraphs.

Technique 1 - Convective Counterflow-Film Cooling

Since the coolant film flows through the annulus channel before being injected in the hot-combustion gases, an increase in heat transfer was expected if the velocity of the coolant was significantly increased. This was achieved by forcing the air to flow through confining channels. The ratio (F) of these convective passages' cross section to the coolant metering holes effective area was varied from F = 1.5 to F = 3. A fully developed flow-in-a-pipe approach allowed the computation of the frictional pressure drop in the coolant channel.

On the outer liner, Figures 30 through 32, significant improvements in cooling were achieved; however, the temperature levels remained unacceptably high. Although the pressure drop increased to 1 psi, the primary-panel wall temperature was reduced to 1800°F only when coolant-film flow was increased to 4 percent of the total airflow.

On the inner liner (Figures 33 through 35), the wall temperature profiles were greatly improved due to the increased flow velocity along the liner-wall cold side. The primary and the first-dilution panel required more coolant flow to limit the temperature rise. The second-dilution panel displayed a satisfactory temperature profile but also resulted in a relatively large pressure drop. In order to increase the heat transfer and reduce the pressure drop of the coolant, a set of fins with higher heat-transfer coefficients and larger channel area were investigated.

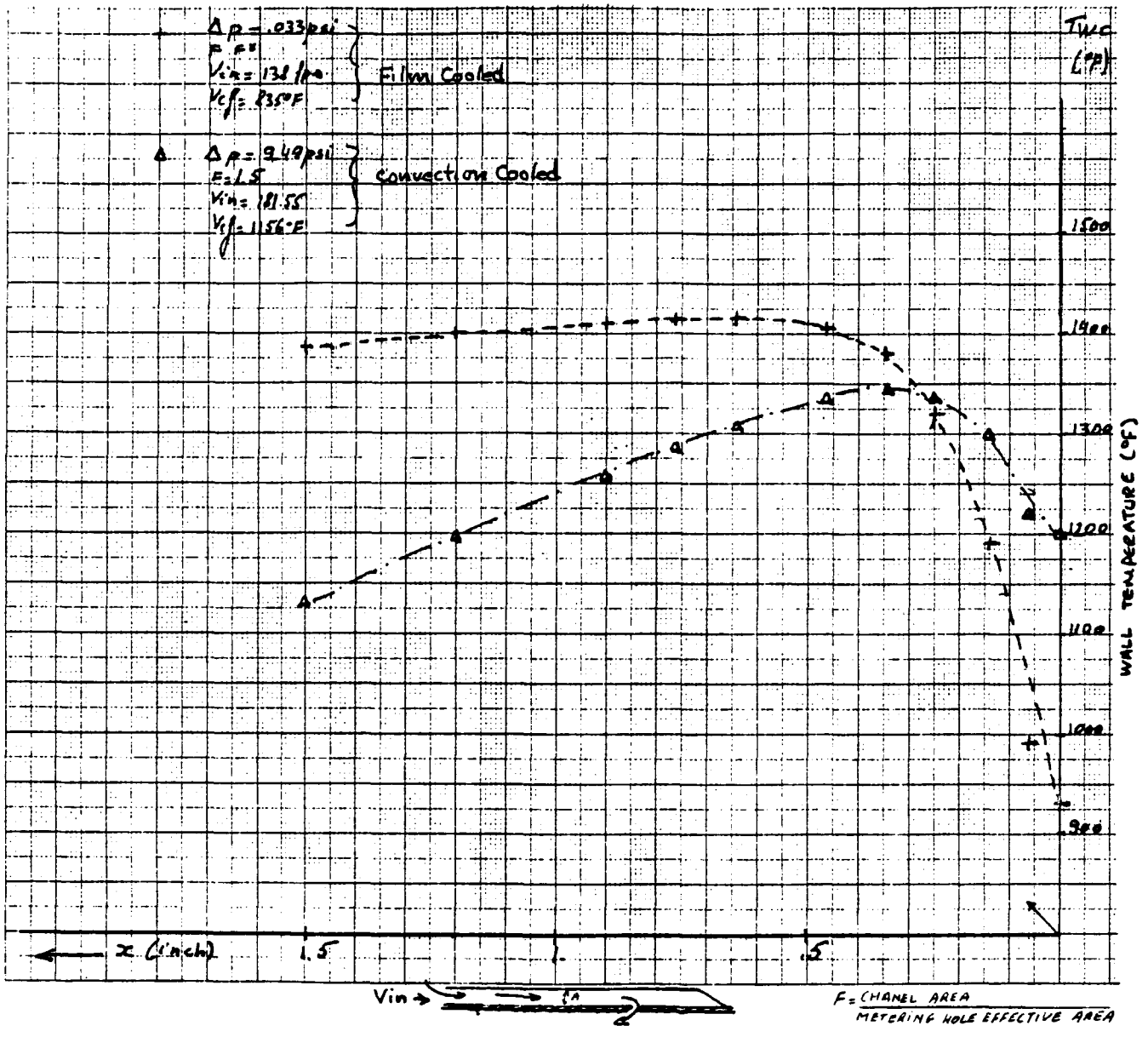

Figure 30. Second-Dilution Panel Outer Liner Temperature Distribution (X = 3 inches to 4.5 inches).

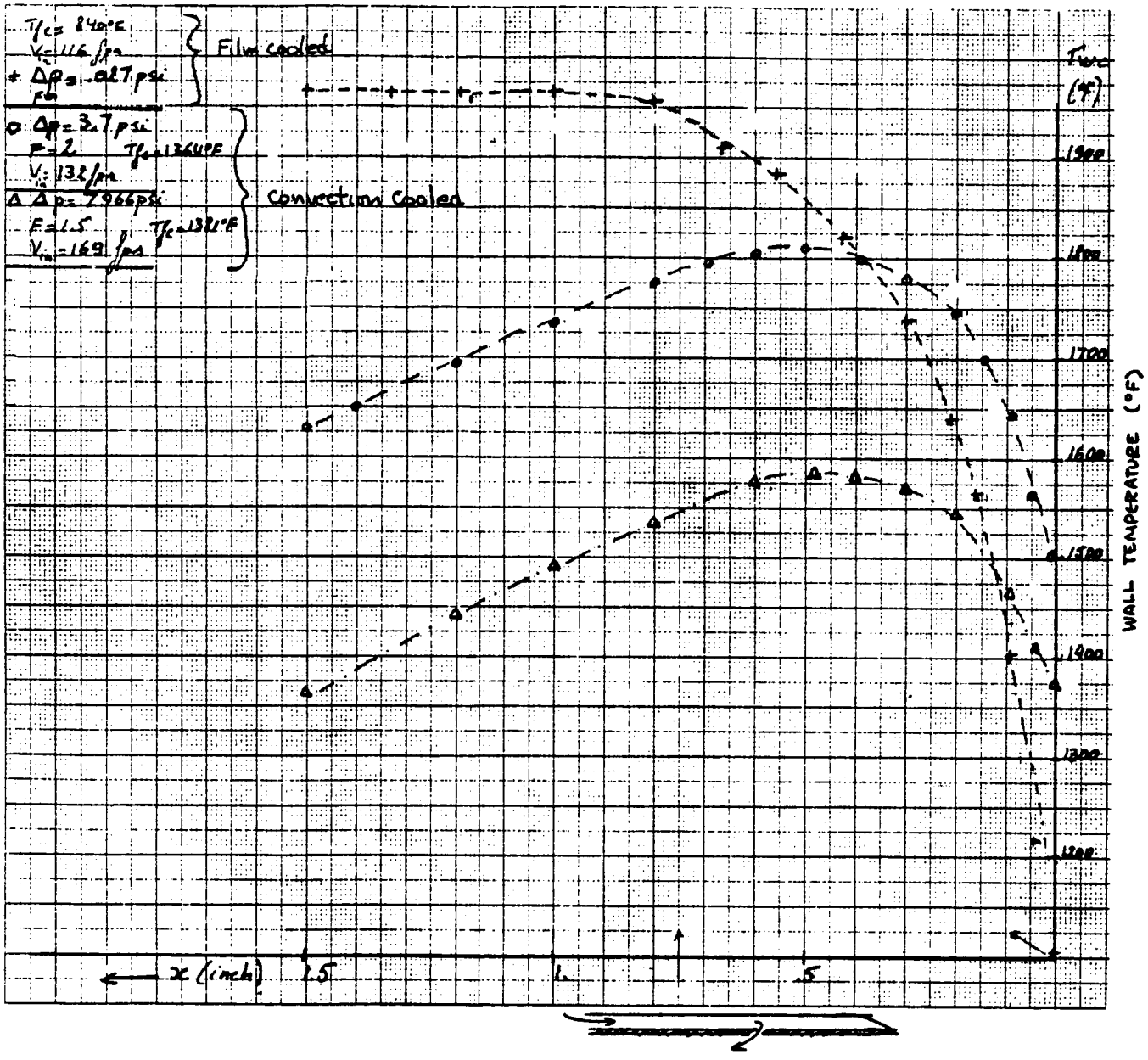

Figure 31. First-Dilution Panel Outer Liner Temperature Distribution (X = 1.5 inches to 3 inches).

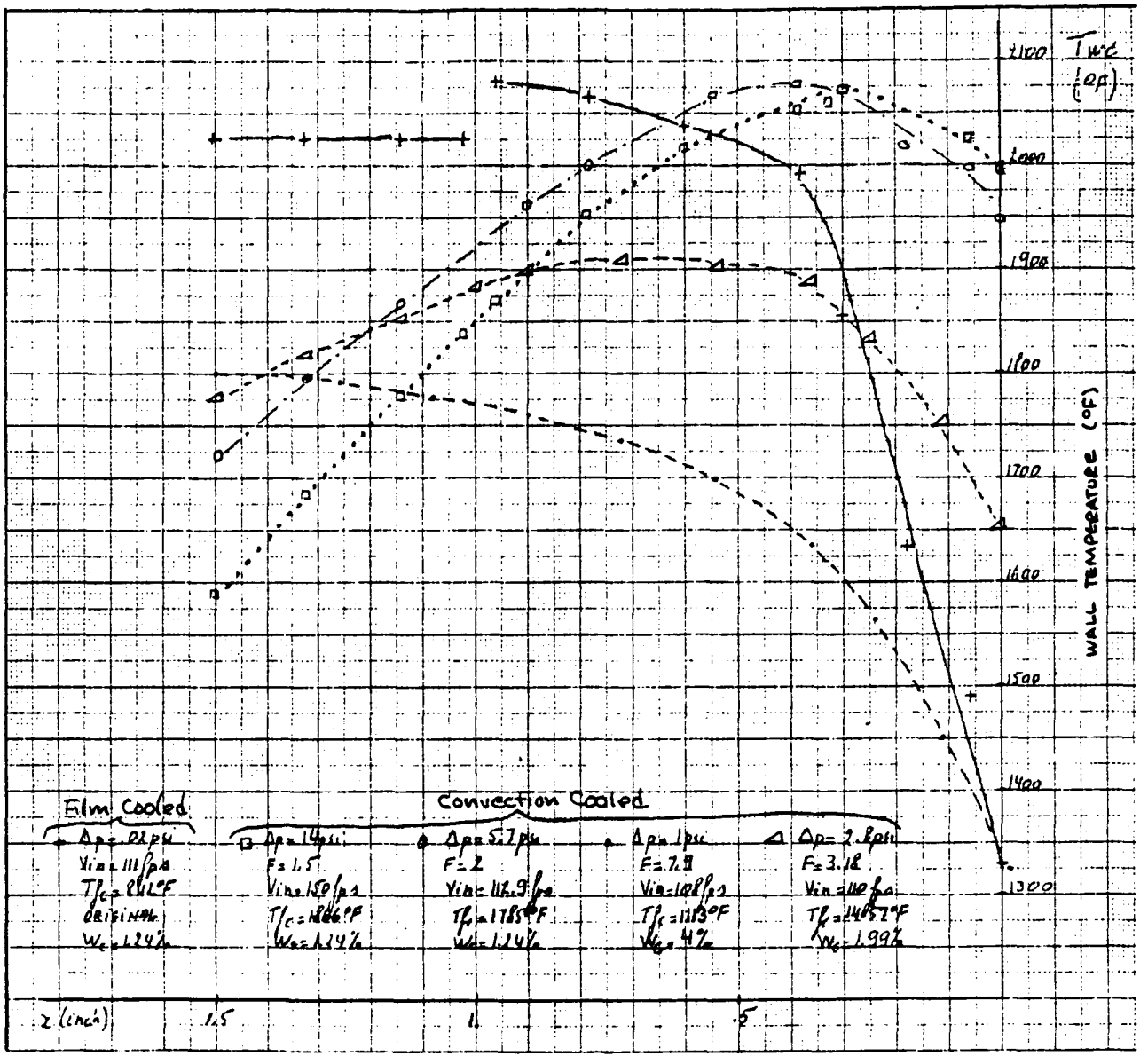

Figure 32. Primary Panel Outer Liner Temperature Distribution (X = 0 inches to 1.5 inches).

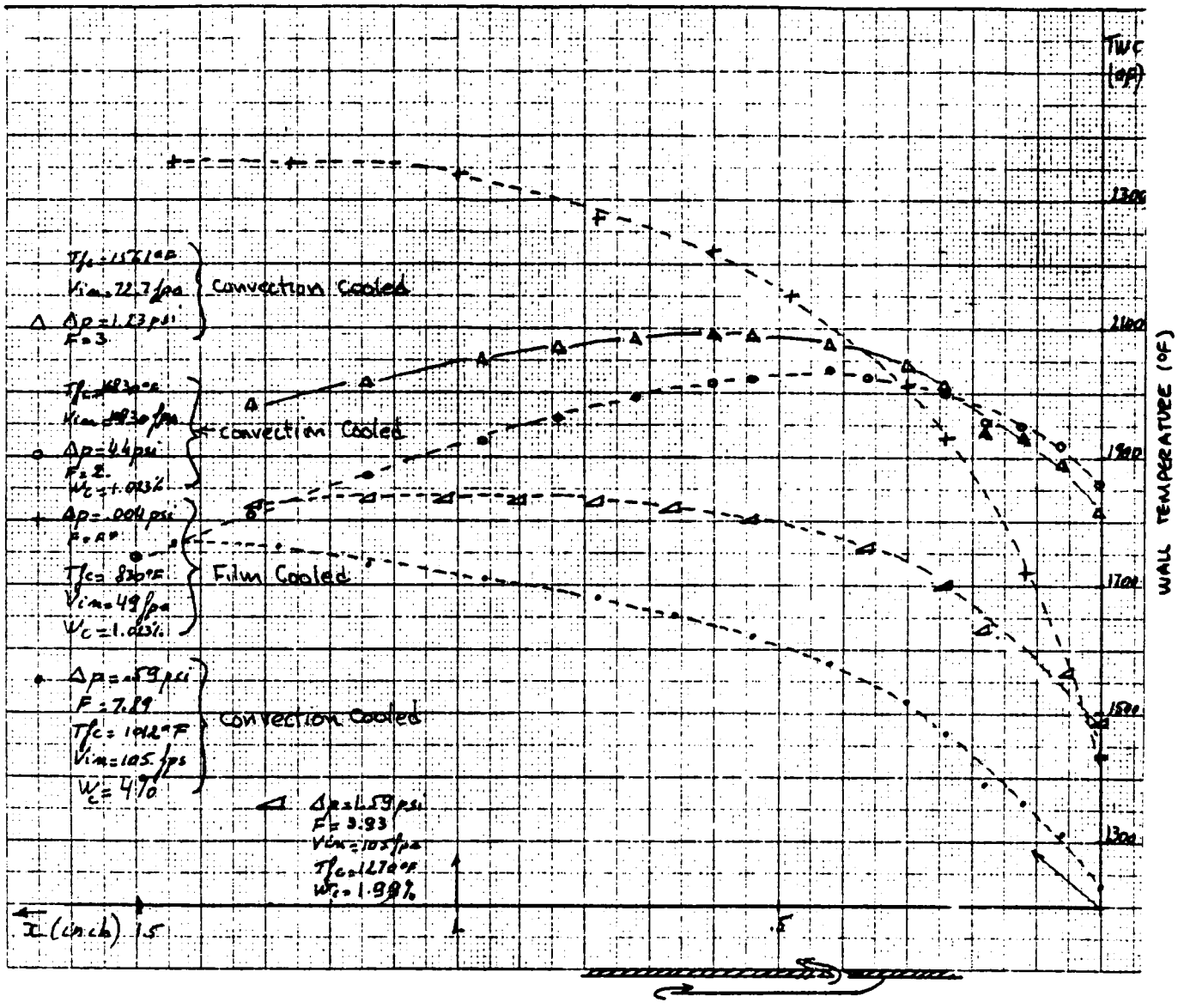

Figure 33. Primary Panel Inner Liner Temperature Distribution (X = 0 Inch to 1.5 Inches).

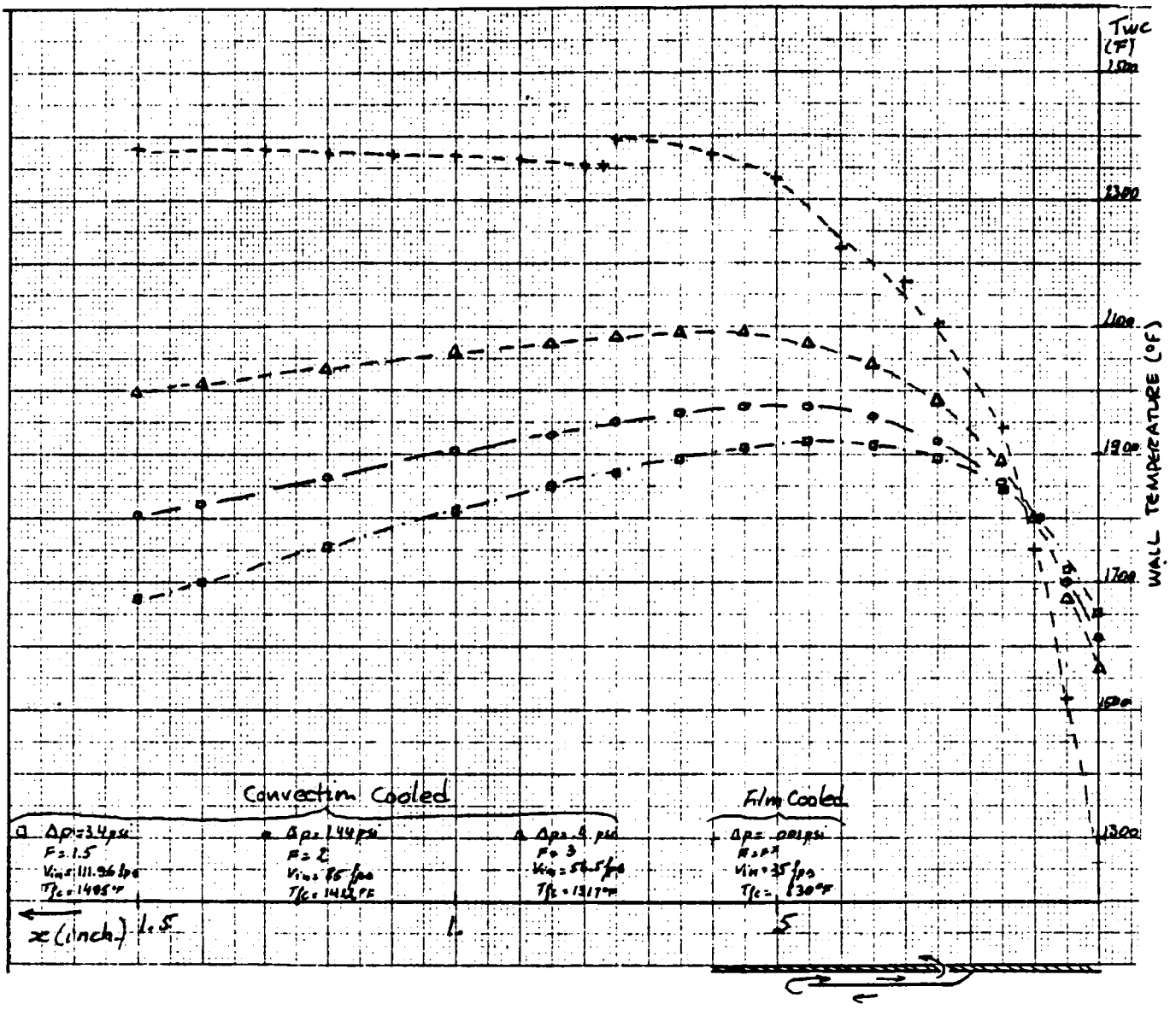

Figure 34. First-Dilution Panel Inner Liner Temperature Distribution (X = 1.5 Inches to 3 Inches).

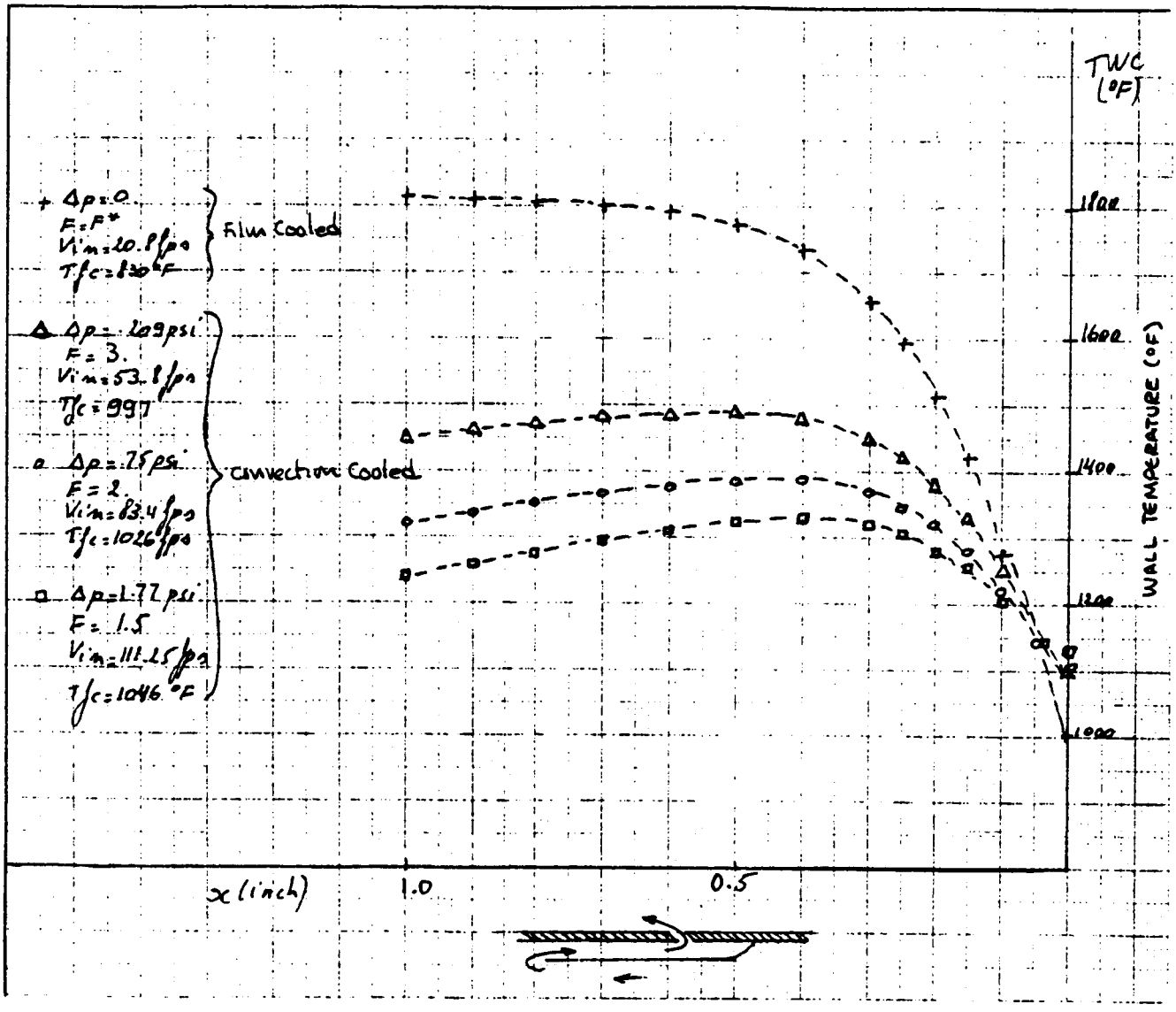

Figure 35. Second-Dilution Panel Inner Liner Temperature Distribution (X = 3 Inches to 4 Inches).

Technique 2 - Rectangular Offset-Fin Plate

The need for small size, lightweight, high performance heat-exchangers in an energy-saving era has resulted in the development of plate-fin heat-exchangers for a multitude of applications. The Garrett rectangular offset-fin plates, as shown in Figure 36, are extremely promising. The fins are staggered in consecutive rows of short length. The fins are offset to prevent a fully developed flow and, thereby, take advantage of the increased heat-transfer rate of the continuously interrupted boundary layer. This effect is translated into higher heat transfer coefficients. Empirical heat transfer and flow-friction data was available for several rectangular offset-fin configurations; the nondimensional Collburn coefficient and the ratio of the friction factor to the Colburn coefficient versus the Reynolds number based on the fin hydraulic diameter, allowed computation of the heat-transfer and pressure-loss coefficients.

The offset fins are geometrically characterized by their density, shape, height, wall thickness, and fin length:

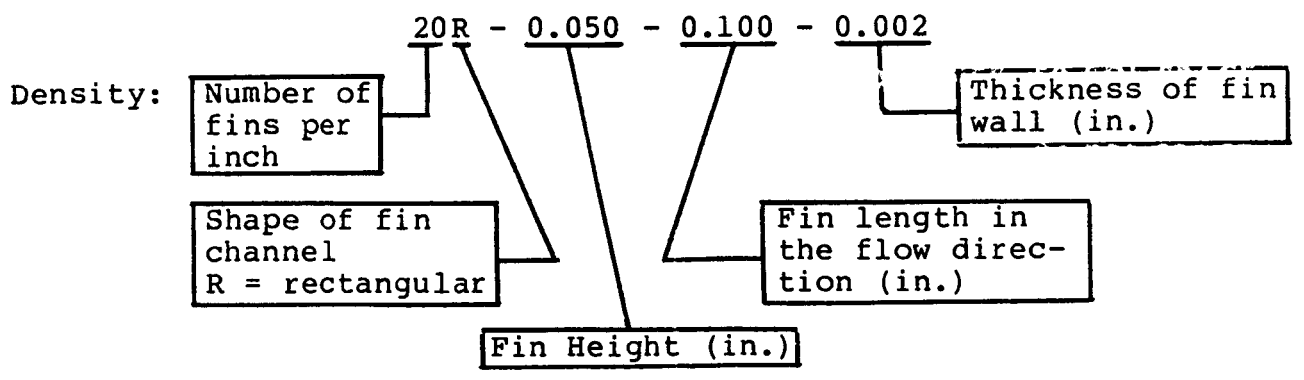

The monthly technical progress reports gave an extensive comparison of each available fins performance within the frame of the present application. An iterative process was established to match air-flow distribution with fin performances, temperature reduction, and pressure drop penalties.

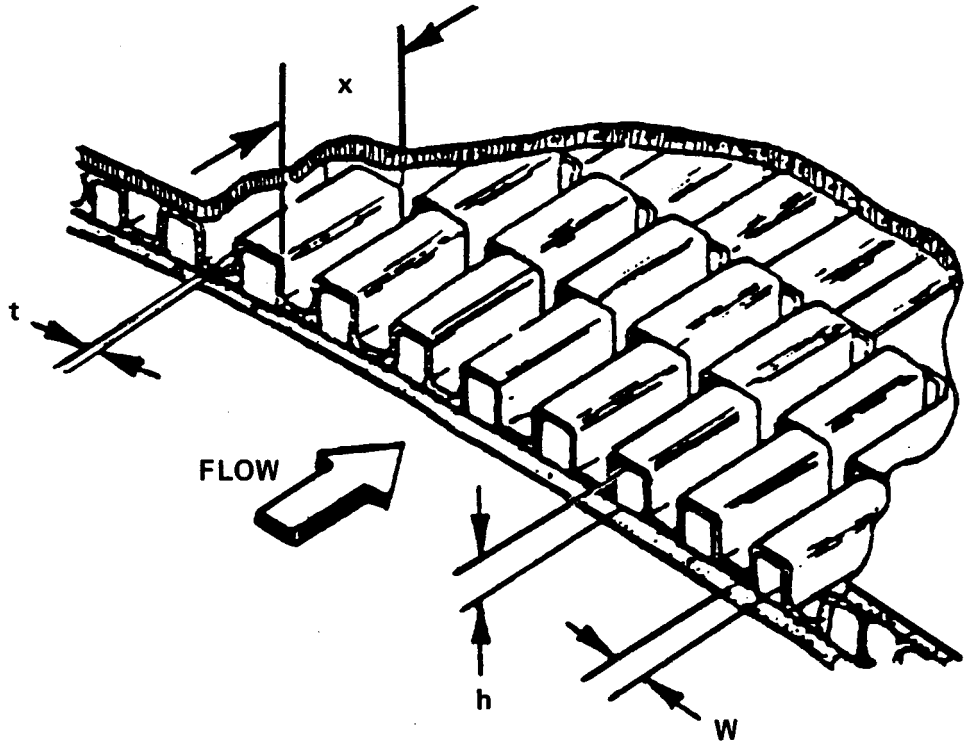

Figure 36. Typical Rectangular Offset-Fin-Plate-Fin Heat Exchanger.

The original combustor airflow predictions were characterized by a large amount of air (13 percent of the total mass flow) towards the transition-liner region (refer to Figure 1). A more appropriate distribution would favor the overall reduction of combustor-transition liner wall temperatures.

The prime objective was to determine among the existing and available offset-fin tooling, a configuration that would ensure acceptable wall temperatures and minimum friction losses. Also taken into account was severe tool manufacturing restrictions in the choice of the shape, ratios of wall thickness to fin height, and maximum fin density (due to the difficulty of forming the Hastelloy X fin material).

The location of the primary and dilutions jets were examined carefully from the point of view of both fluid mechanics and manufacturing cost (Figure 37). The complex flow distribution around the large jet holes and the unidirectional flow feature of the fins created flow nonuniformities and the result was a lack of coolant downstream of the jet holes.

Different geometrical configurations were investigated to minimize the wall temperature for the least flow penalty . Among these, the original cooling configuration was modified to incorporate the dilution and primary jets, by incorporating a convective annular channel extending upstream from their injection location (see Figure 38). Hence, the surface area covered by the fin coolant was reduced greatly. The large amount of jet-airflow (of the order of 10 to 12 percent) would have allowed a reduction of the coolant temperature at the entrance of the fin section (at L = 1.0 inch). Hence, an improved wall-temperature distribution would have been obtained further downstream. The convective channel height chosen to match the fin height resulted in a high velocity in the passage; consequently, the rate of heat transfer increased along the first part of the panel (L = 0.5 inch), along, unfortunately, with the coolant temperature. This was contrary to the desired effect.

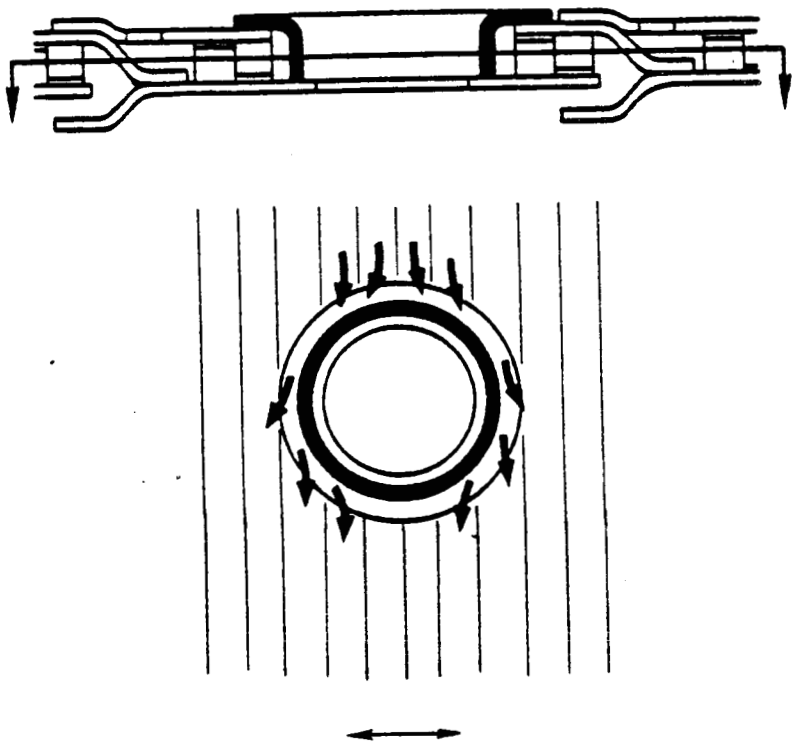

Figure 37. Lack of Coolant Due to Jets Holes Obstruction.

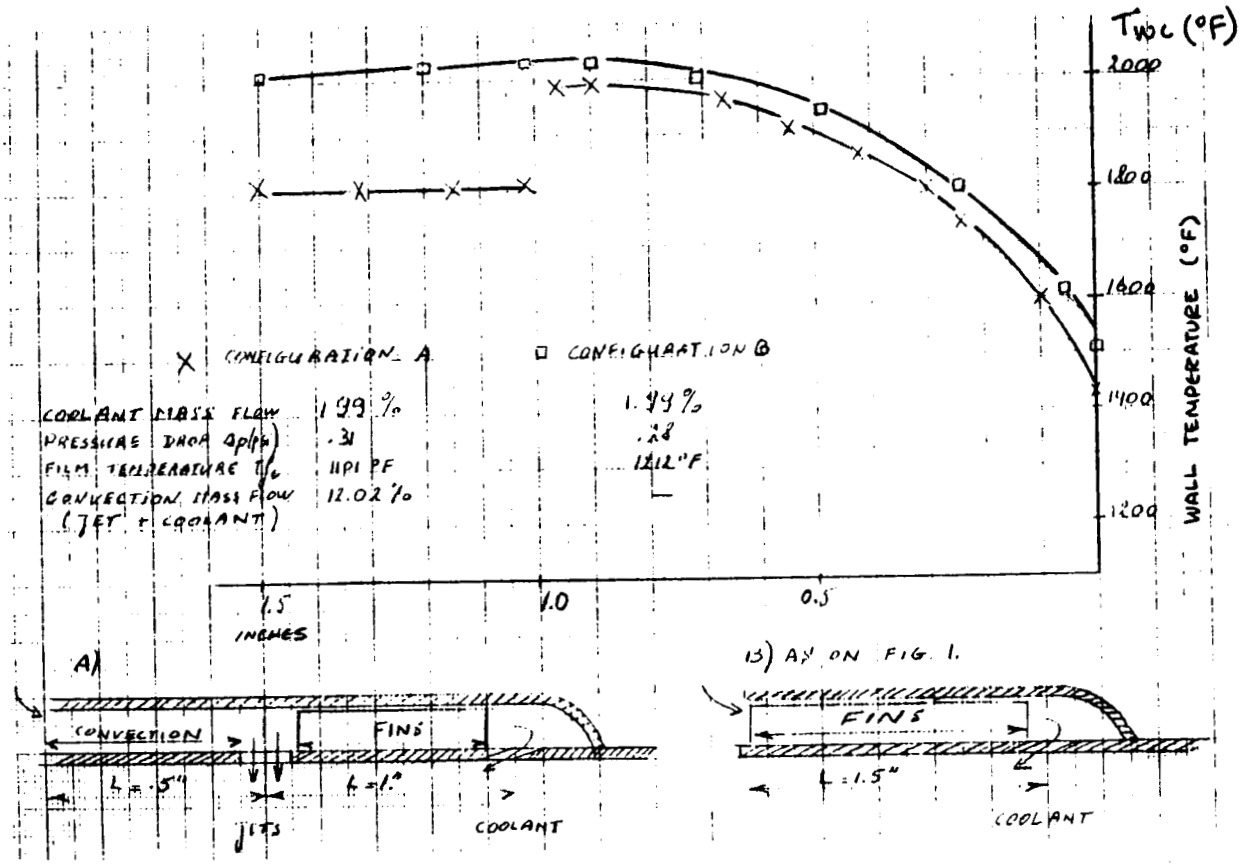

Figure 38. Primary Zone (Outer-Liner).

One configuration (Figure 39) led to significant wall temperature reductions.

On the inner liner, a coflow cooling configuration along the primary and first-dilution panels took advantage of the free-stream dynamic head. In order to increase heat-transfer along the outer wall without affecting the flow distribution, the results of the thermal and stress analysis showed that the series of 20 fins per inch provided satisfactory wall temperatures. Figure 40 shows the temperature profile for the primary panel. A reduction mainly in fin height (from fin type 20R-075-0.100-0.004 to fin type 20R-0.050- 0.100-0.002) led to an appreciable coolant flow reduction (from 4 percent to 1 percent). An acceptable temperature (1540°F) was predicted at the exit of the fin passage (at X = 1, where the primary jets were located), even at a cooling film flow as low as 1 percent. However, around X = 0.9, the predictions showed a film cooling effectiveness of $\eta = 0.13$. Increasing the coolant flow to 2 percent increased the effectiveness to $\eta = 0.27$, all other conditions being constant. These were more realistic, considering the need to provide a cooling means downstream, between the primary jet holes and the cooling slot of the next panel. Hence, 2 percent of film coolant flow is planned for the primary zone.

Along the dilution panel (Figure 41), taller fins were used to allow for the larger mass flow. Again, a significant reduction in coolant flow was obtained. The film effectiveness dropped to $\eta = 0.045$ at x = 1.2 inch at the lowest flow rate. Hence, a coolant flow of 2 percent, for which the film effectiveness is $\eta = 0.18$, has been chosen to provide an effective film protection further downstream.

In the second dilution panel (Figure 42), acceptable wall temperatures were obtained with a counterflow cooling scheme (fins 20R-0.050-0.100- 0.002 and cooling flow of 1.4 percent). Protection of the double wall was fully achieved.

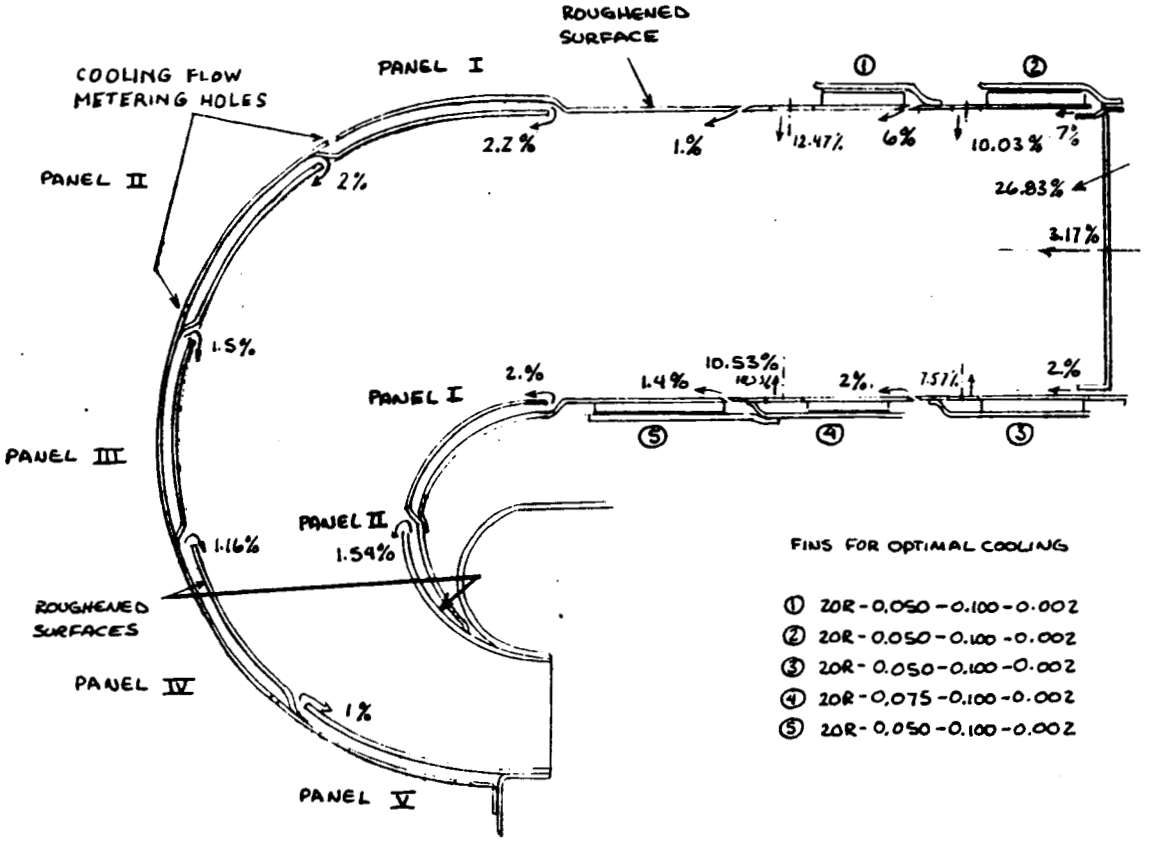

Figure 39. Flow Distribution.

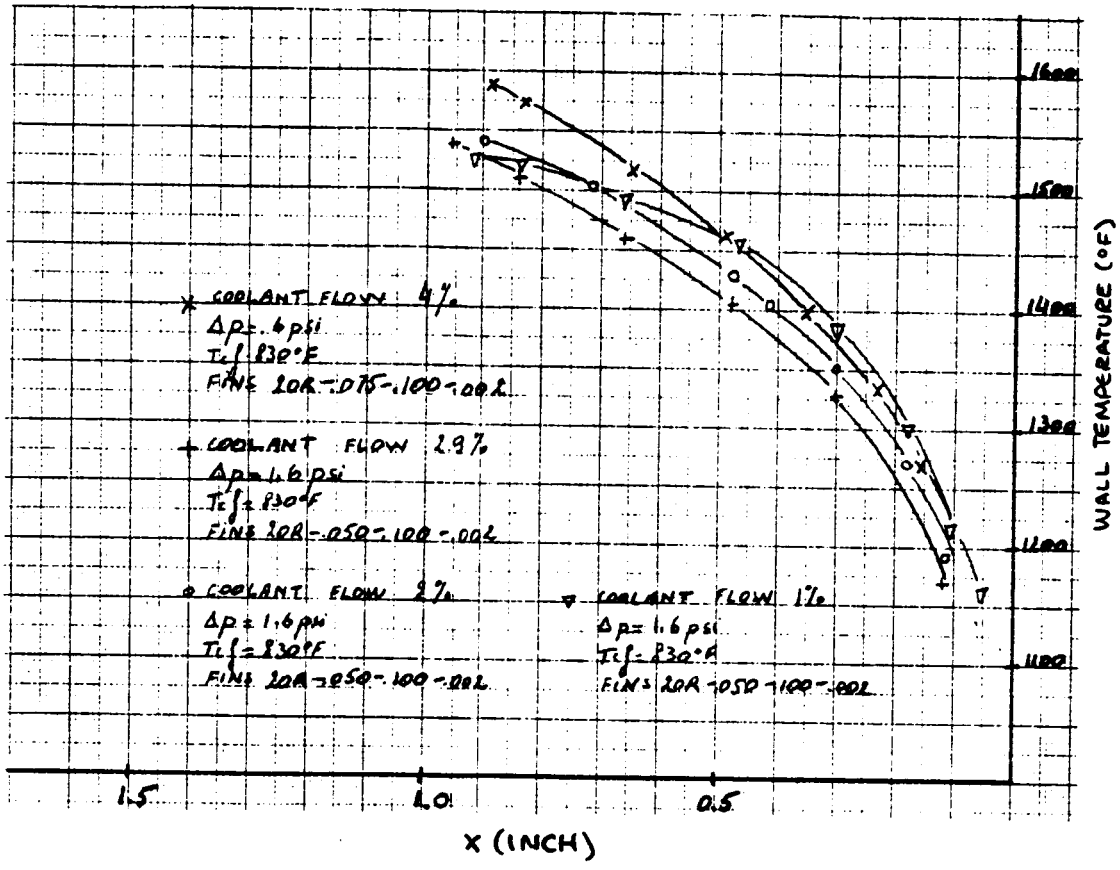

Figure 40. Inner Liner (Primary Zone).

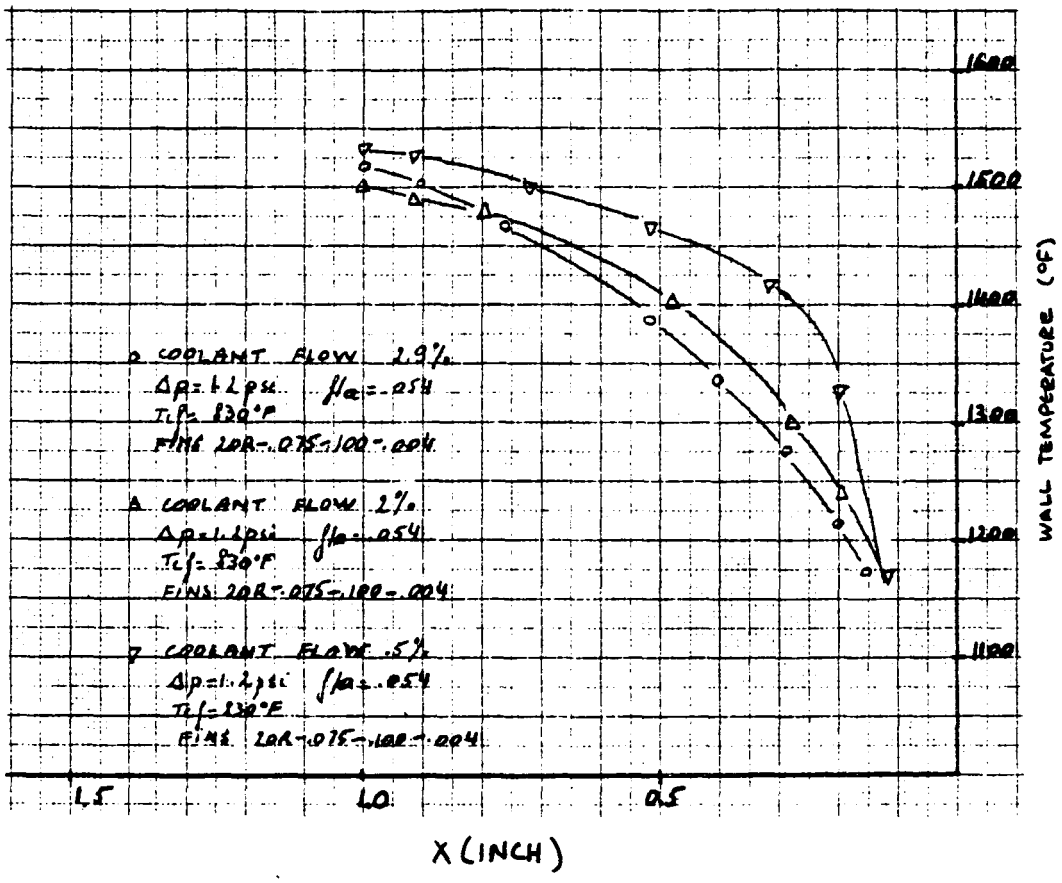

Figure 41. Inner Liner (First-Dilution Zone).

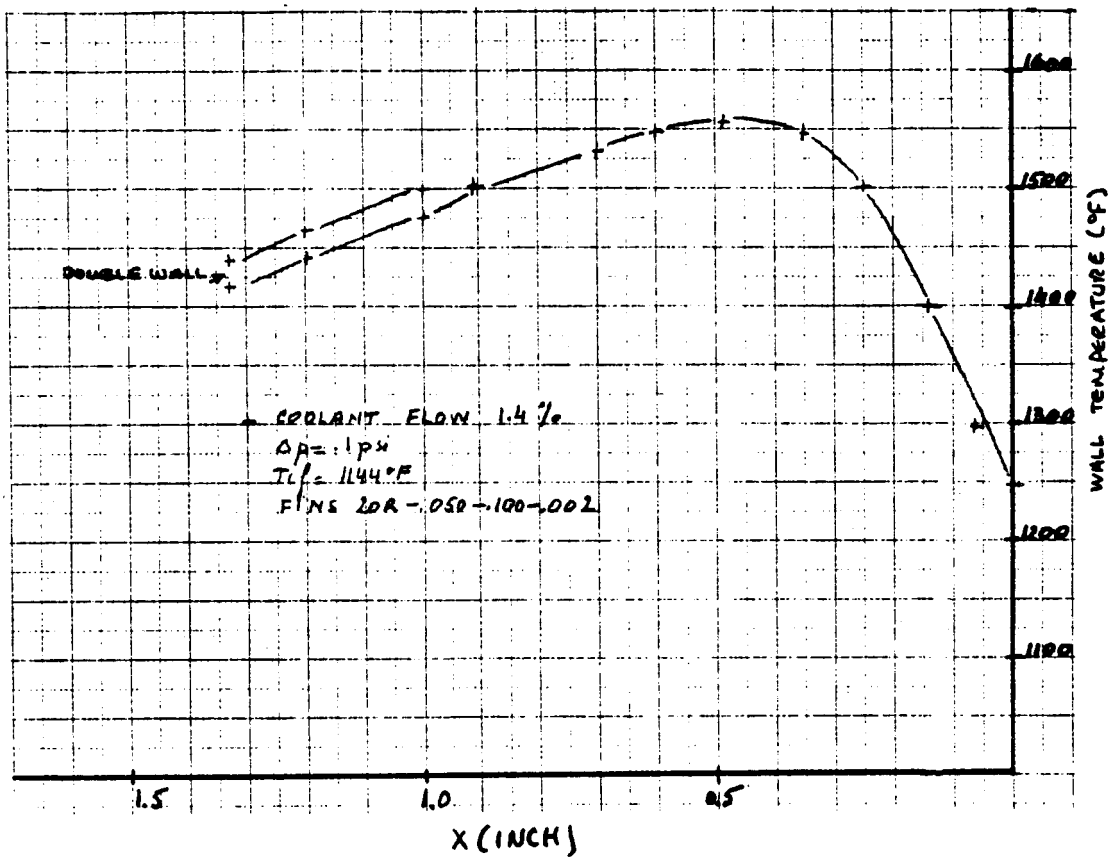

Figure 42. Inner Liner (Second-Dilution Zone).

On the outer liner, the primary and first-dilution panel were cooled in a counter-flow manner using 20R-050-0.100-0.002 fins with 7 percent and 6 percent, respectively, of the total airflow. The second-dilution panel benefitted from the high velocity in the annulus to reduce the temperature to an acceptable level. A roughening treatment was used on the outside wall to enhance the heat-transfer rate which permitted a reduction of the coolant amount to one percent of the combustor airflow (refer to Step 3 "Extended Surface Film-Cooling" and Figure 45).

Along the primary zone of the outer liner (Figure 43), a coolant flow of 7 percent was required to ensure significant temperature reductions. The film temperature at the injection was 1200°F. The higher temperature of the coolant at the injection slot called for a greater coolant amount than on the inner liners. A similar conclusion was deduced from the dilution panel (Figure 44) where two wall temperature profiles were plotted. They corresponded to a fuel-air ratio (f/a) based on a predicted equivalence ratio (0.67) for one, and on the usual experimentally-observed equivalence ratio of 0.8 for the other. The f/a are 0.0458 and 0.054 respectively. A coolant flow of 6 percent was selected.

It should be noted that the fin type 28R-0.050-0.100-0.004, unfortunately not available in hard material, would have allowed a significant reduction in the amount of air spent for cooling (5 percent instead of 7 percent), at a relatively similar pressure drop (1.5 psi), see Figure 43. High-density fins may provide further coolant decrease, if they are developed in the future. The Stanton number is 30 percent higher for the denser fins. This demonstrates their high potential.

The selection of the fins as an optimal cooling scheme required a slight change in the amount of air flowing through the swirler, 25.43 percent instead of 26.93 percent.

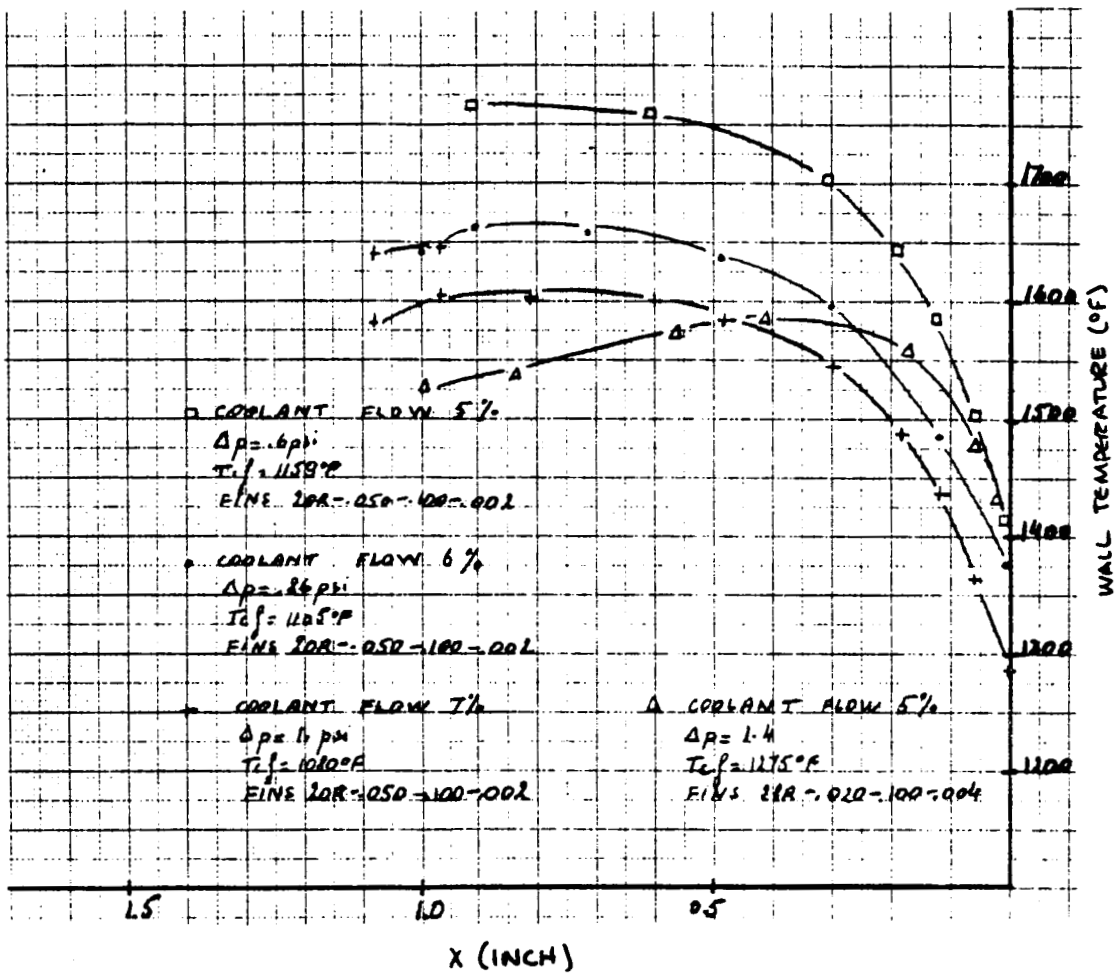

Figure 43. Outer Liner (Primary Zone).

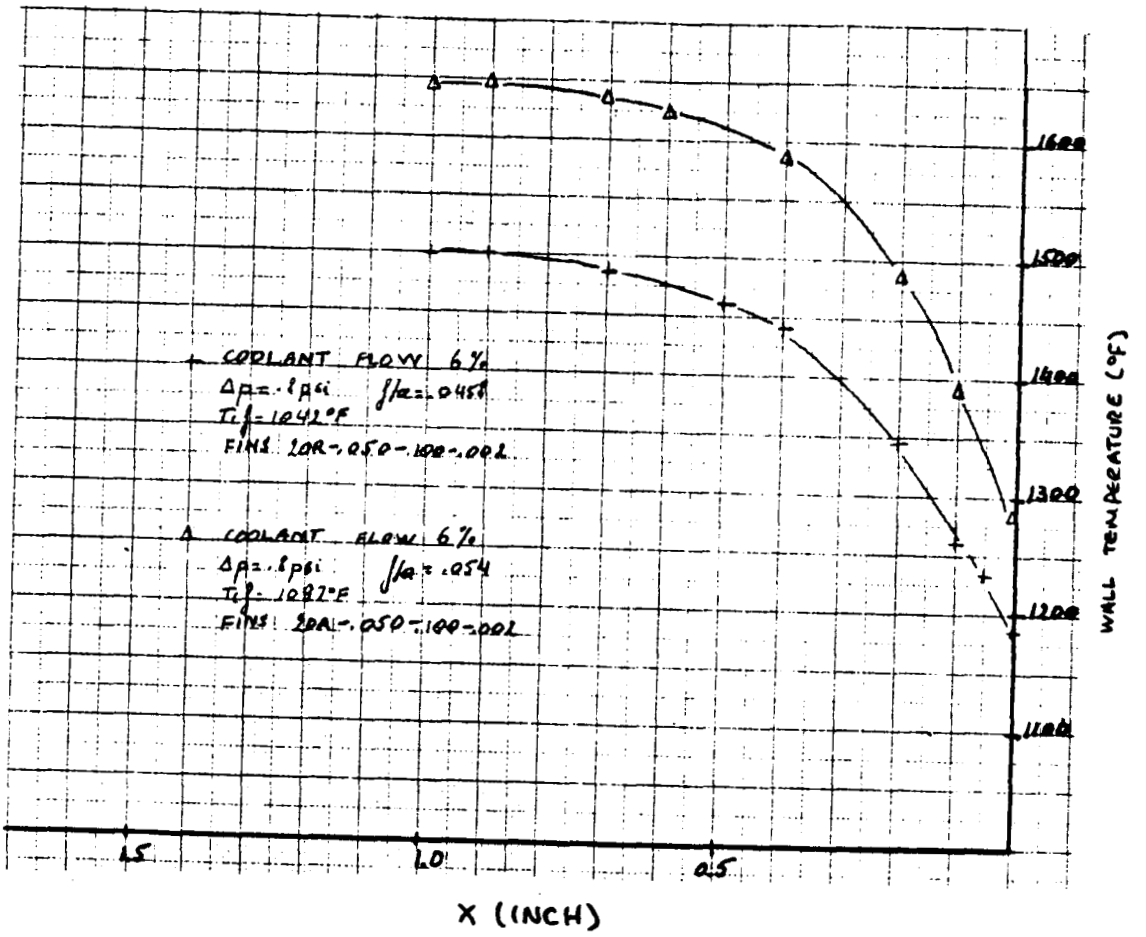

Figure 44. Outer Liner (First-Dilution Zone).

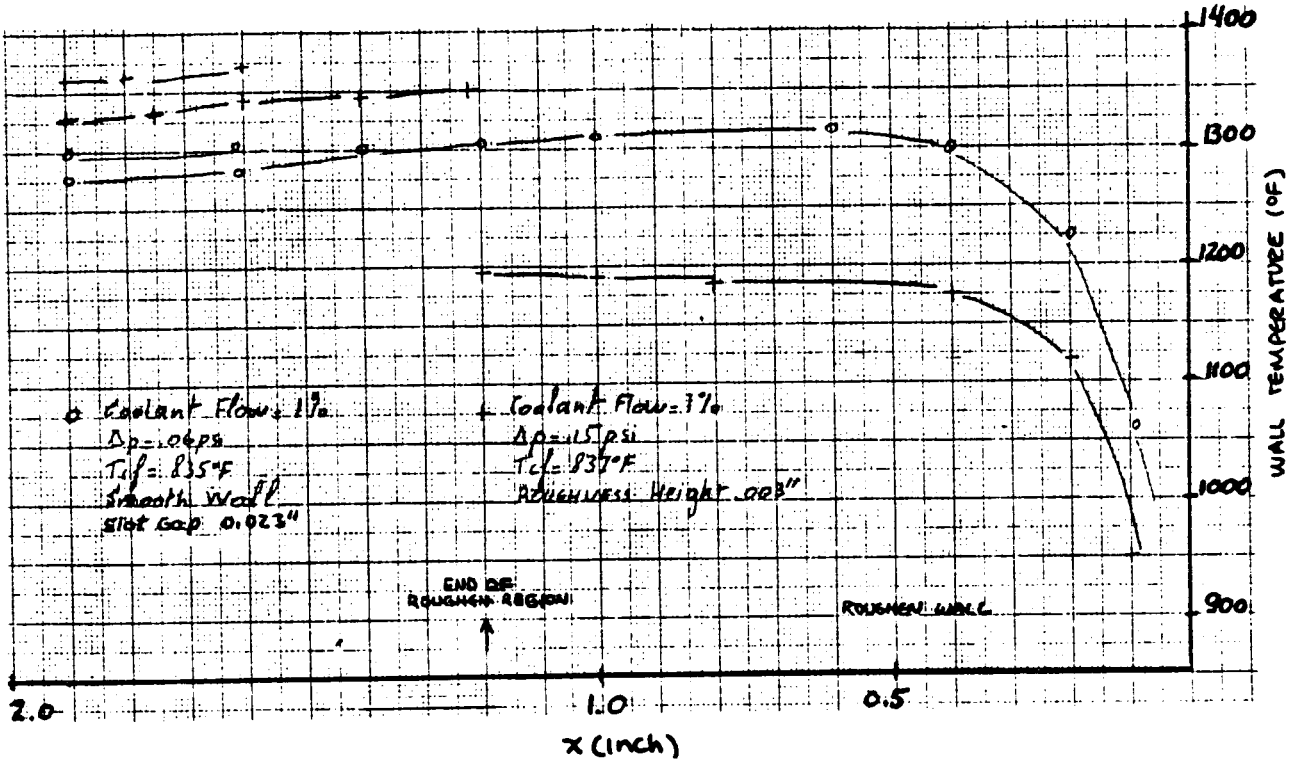

Figure 45. Outer Liner (Second-Dilution Zone).

The recommended cooling configuration gives a wall temperature distribution that is displayed in Figures 46 through 50.

Technique 3 - Extended Surface-Film Cooling

It is well known that the heat-transfer rate over a surface can be significantly increased (by as much as a factor of two) if a rough rather than a smooth wall is presented to the flow.

The determination of the roughness height required depends on such parameters as coolant passage geometry and flow Reynolds number.

The growing interest in turbulent flow across rough surfaces has been prompted by the need to accurately predict aircraft drag to evaluate aircraft performance. The prediction of the heat-transfer gain through increased turbulence and of the skin-friction penalty through increased drag greatly affects the design of a heat exchanger.

Different roughness conditions in a turbulent pipe flow have been observed and divided into three regions [Schlichting[1]]*.

HYDRAULIC SMOOTH $0 < \frac{k_s U_\tau}{v} \leqslant 5$ $Cf = Cf(Re)$

Cf = Coefficient of friction
U_τ = Friction velocity
k_s = Sand grain roughness height
v = Kinematic viscosity

The size of the roughness is so small that all protrusions are contoured within the laminar sublayer.

*References are listed at the end of Section 3.0.

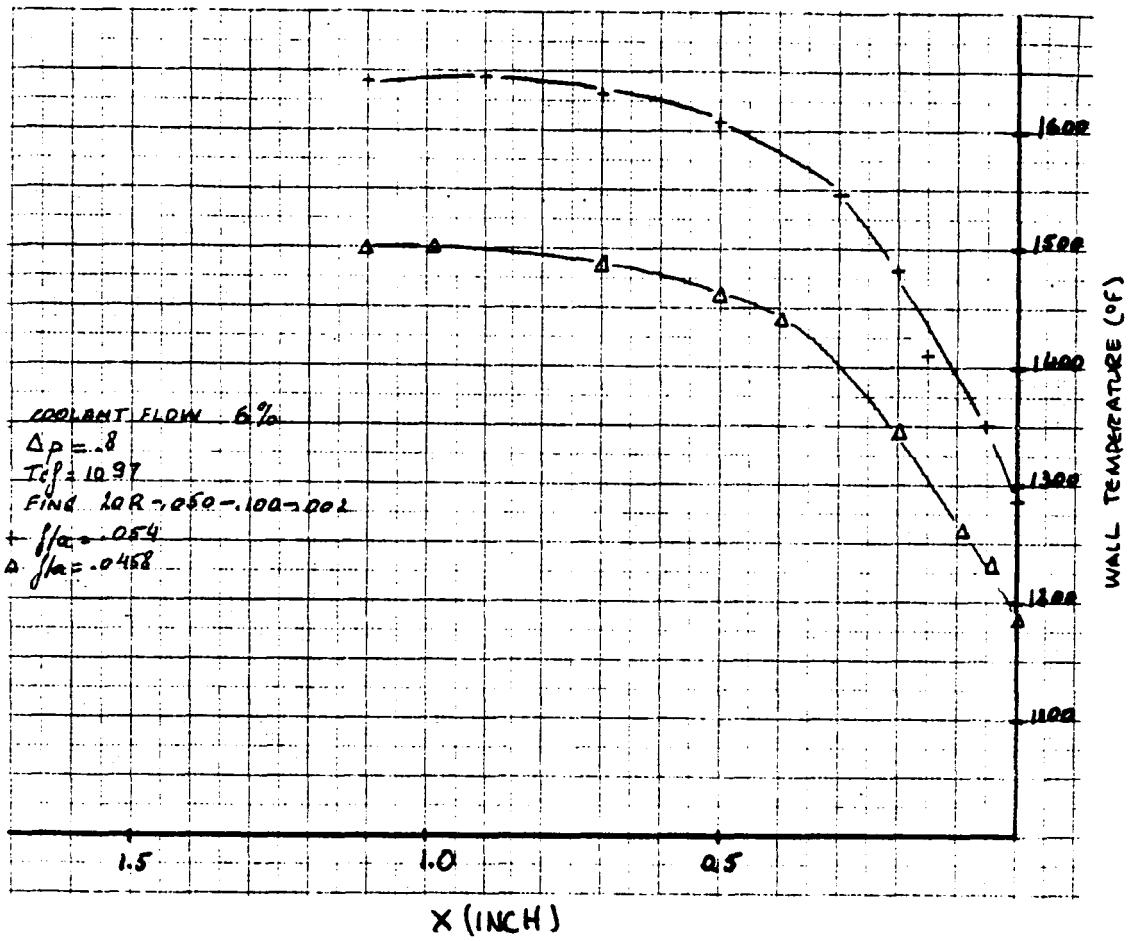

Figure 46. Outer Liner (First-Dilution Panel).

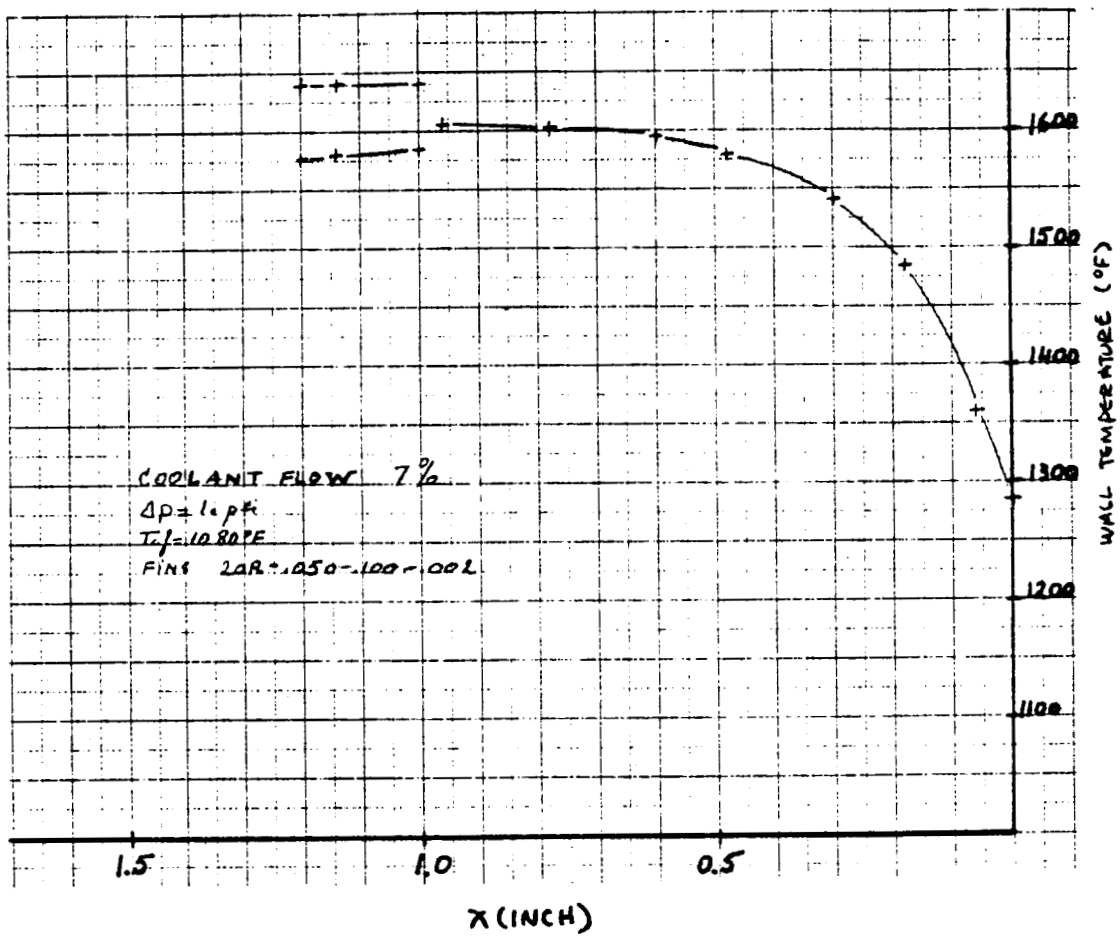

Figure 47. Outer Liner (Primary Zone).

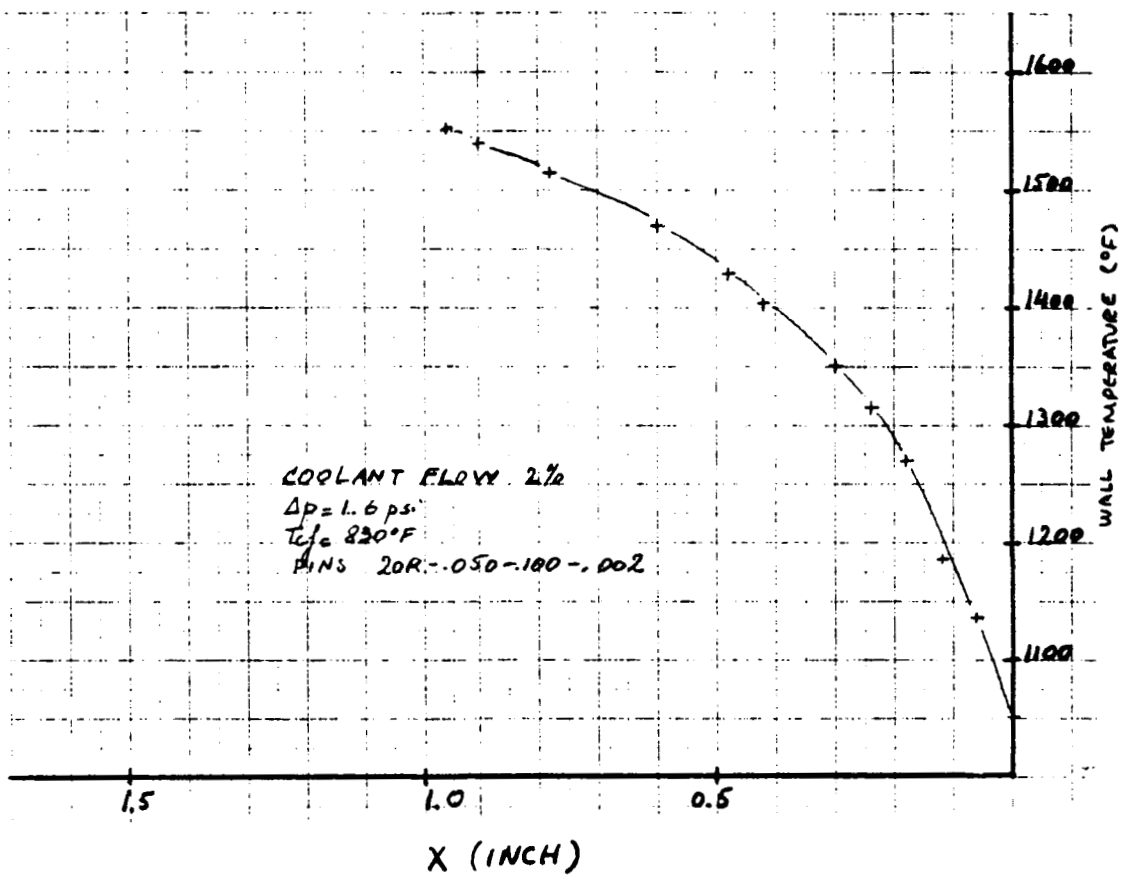

Figure 48. Inner Liner (Primary Zone).

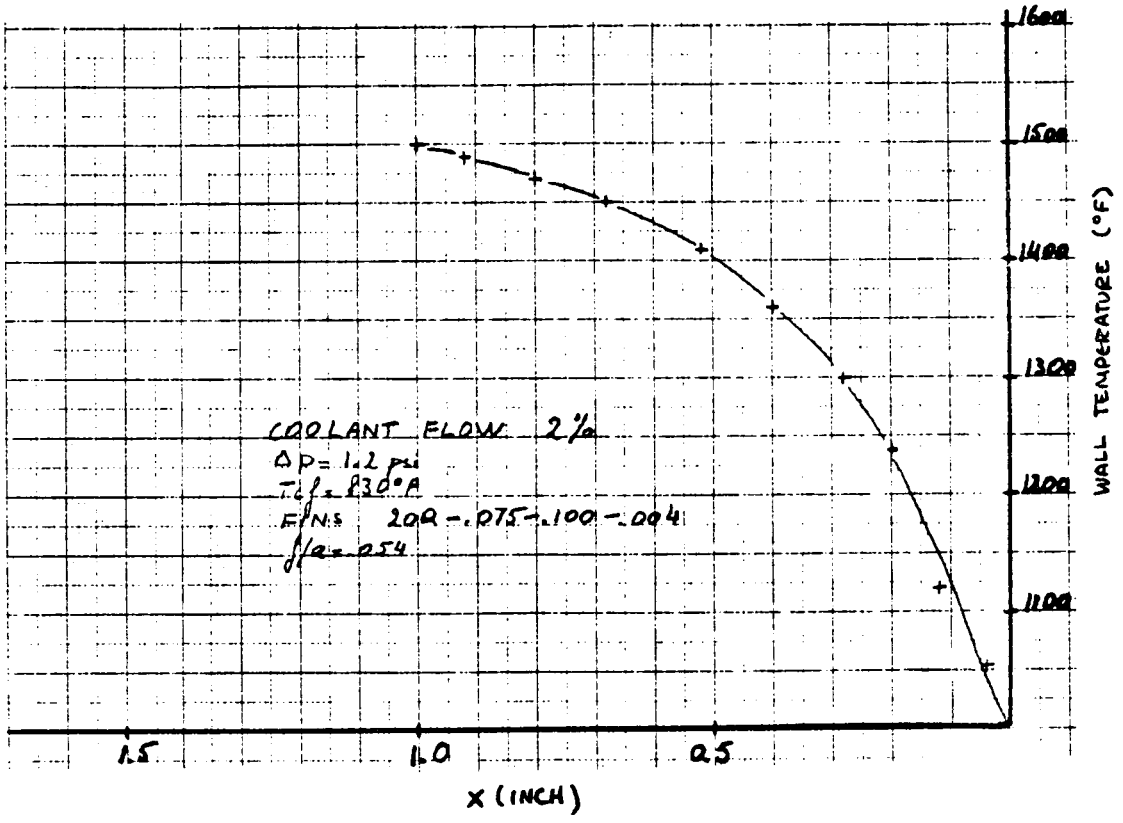

Figure 49. Inner Liner (First-Dilution Zone).

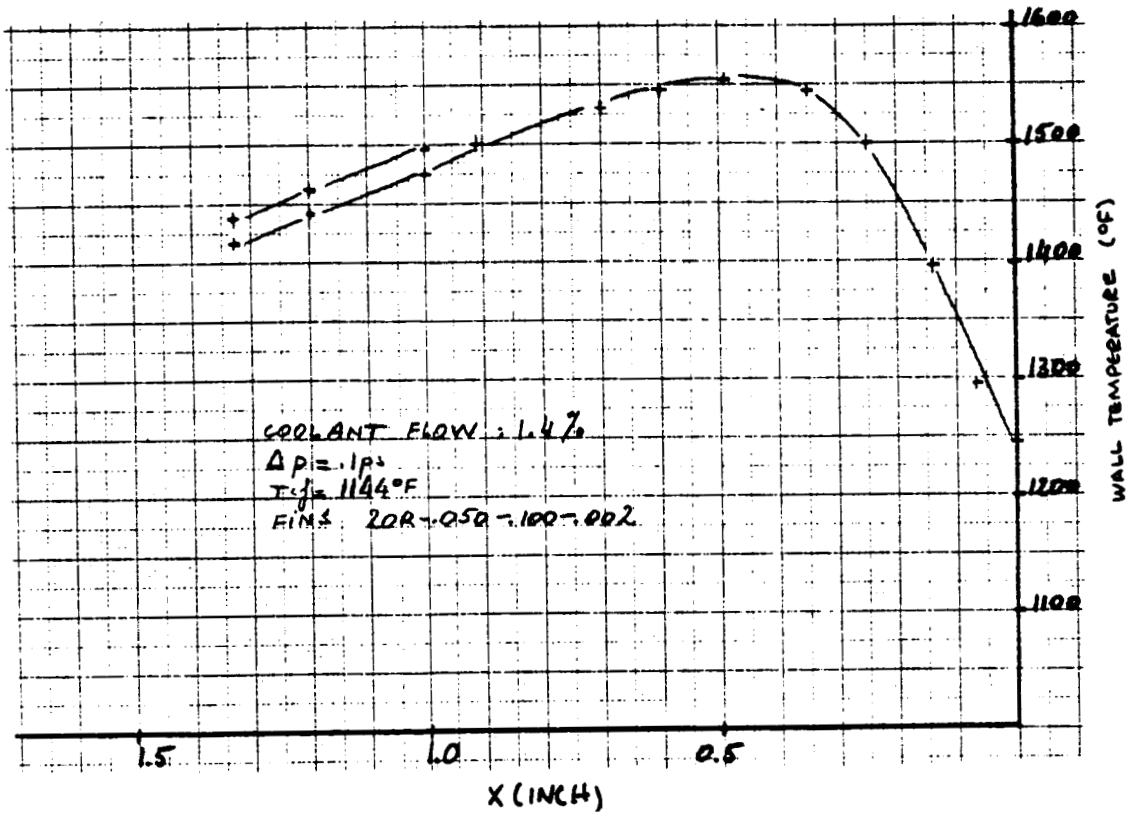

Figure 50. Inner Liner (Second-Dilution Zone).

$$\text{TRANSITION REGION } 5 \leqslant \frac{k_s U_\tau}{\nu} \leqslant 70 \qquad Cf = Cf\left(\frac{k_s}{D_h}, Re\right)$$

In the transition region protrusions extend partly outside the laminar sublayer.

$$\text{COMPLETELY ROUGH } \frac{k_s U_\tau}{\nu} \geqslant 70 \qquad Cf = Cf\left(\frac{k_s}{D_h}\right)$$

In the case of completely rough surface, a Stanton number based on the heat-transfer through the sublayer, and defined as $B = \frac{Q}{\rho c U_\tau (T_h - T_W)}$ has been related to a Stanton heat-transfer number based on the average flow properties:

$$St = \frac{Q}{\rho c U_m (T_m - T_W)}$$

where:

Q = heat-transfer
ρ = fluid density
c = specific heat
T_h = temperature at the edge of the sublayer
T_W = wall temperature
T_m = average temperature across a section
U_m = average velocity across a section
U_τ = friction velocity

The relation is:

$$\frac{1}{St} = \frac{U_m}{U_\tau}\left[\frac{U_m}{U_\tau} + \frac{1}{B} + 12.6\,\frac{U_\tau}{U_m}\right]$$

Owen and Thompson[2] have empirically determined the local Stanton number B to be approximately:

$$B = \frac{1}{\alpha}\left[\frac{u_t k}{v}\right]^{-0.45}[Pr]^{-0.8}$$

where: α = constant = 0.52
Pr = fluid Prandlt number
U_τ = friction velocity

Combining the two relationships and taking into account the definition of the friction velocity $U_\tau = U_m \sqrt{\frac{Cf}{2}}$ gives:

$$St = \frac{Cf}{2}\,\frac{1}{\left[1+0.52\ Re_k^{0.45}\ Pr^{0.8}\left[\frac{\mu_m}{\mu_w}\times\frac{\rho_w}{\rho_m}\right]^{0.45}\left[\frac{Cf}{2}\right]^{0.725} + 12.6\ \frac{Cf}{2}\right]}$$

where: $Re_k = \frac{U_m k}{\gamma_m}$

The knowledge of the friction coefficient cf is a prerequisite to compute the heat-transfer.

For a flow in a channel most of the incompressible skin friction laws are well approximated by the Prandlt-Schlichting[1] law as:

$$\lambda = \frac{1}{\left[2\ \mathrm{Log}\left(\frac{R_h}{k_s}\right) + 1.74\right]^2}$$

where: R_h = hydraulic radius
k_s = sand grain height
λ = Schlichting friction factor[1]

The Prandlt Schlichting law was derived from Nikuradse's experimental data obtained with sand grains. A great deal of effort was expended, correlating in a convenient manner any given roughness with its sand grain equivalence.

A correlation by Dirling[3] has been used here under the form:

$$\frac{k_s}{k} = 0.0164\ H^{3.78} \text{ of } H \leqslant 4.93$$

$$\frac{k_s}{k} = \frac{139}{H^{1.9}} \quad \text{if } H \leqslant 4.93$$

k_s = equivalent sand grain roughness height

k = roughness height

H is an empirical parameter relating the roughness size to its spacing:

$$H = \frac{lr}{k} \frac{As}{Ap}^{4/3}$$

where: l_r = spacing between roughness elements
k = roughness height
As = roughness surface area presented to the flow
Ap = projection of As on a plane perpendicular to the flow

The size of the roughness height was determined to provide high heat-transfer coefficient and low-pressure drop.

Several configurations of roughness and spacing were examined. Because the Dirling correlation has been extensively applied to hemispheric and conical roughness, a hemispherlike shape was used.

Figures 51 and 52 show the Stanton number variation with roughness height. The pressure drop penalty was clearly displayed.

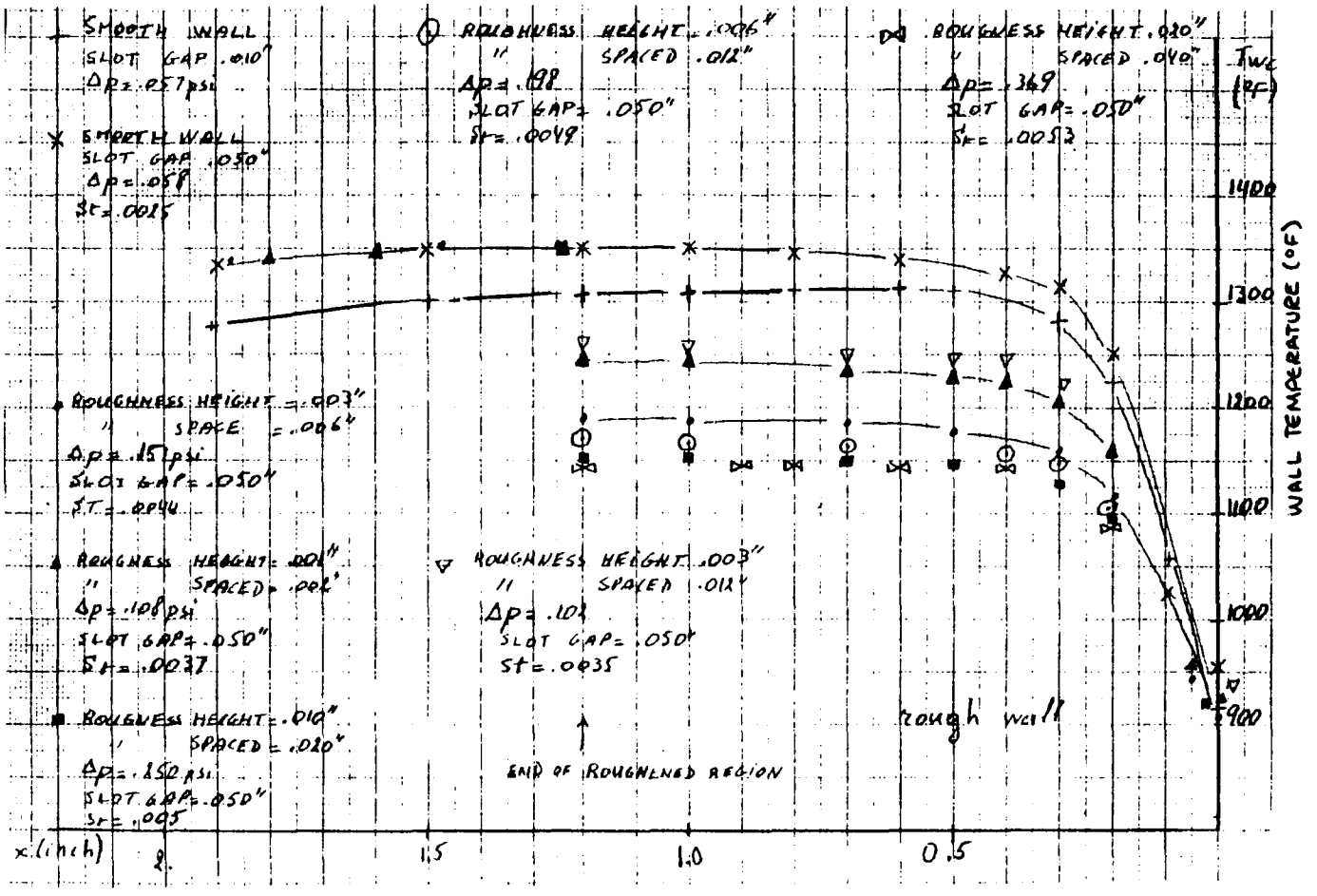

Figure 51. Second-Dilution Zone Outer-Liner Roughness Study.

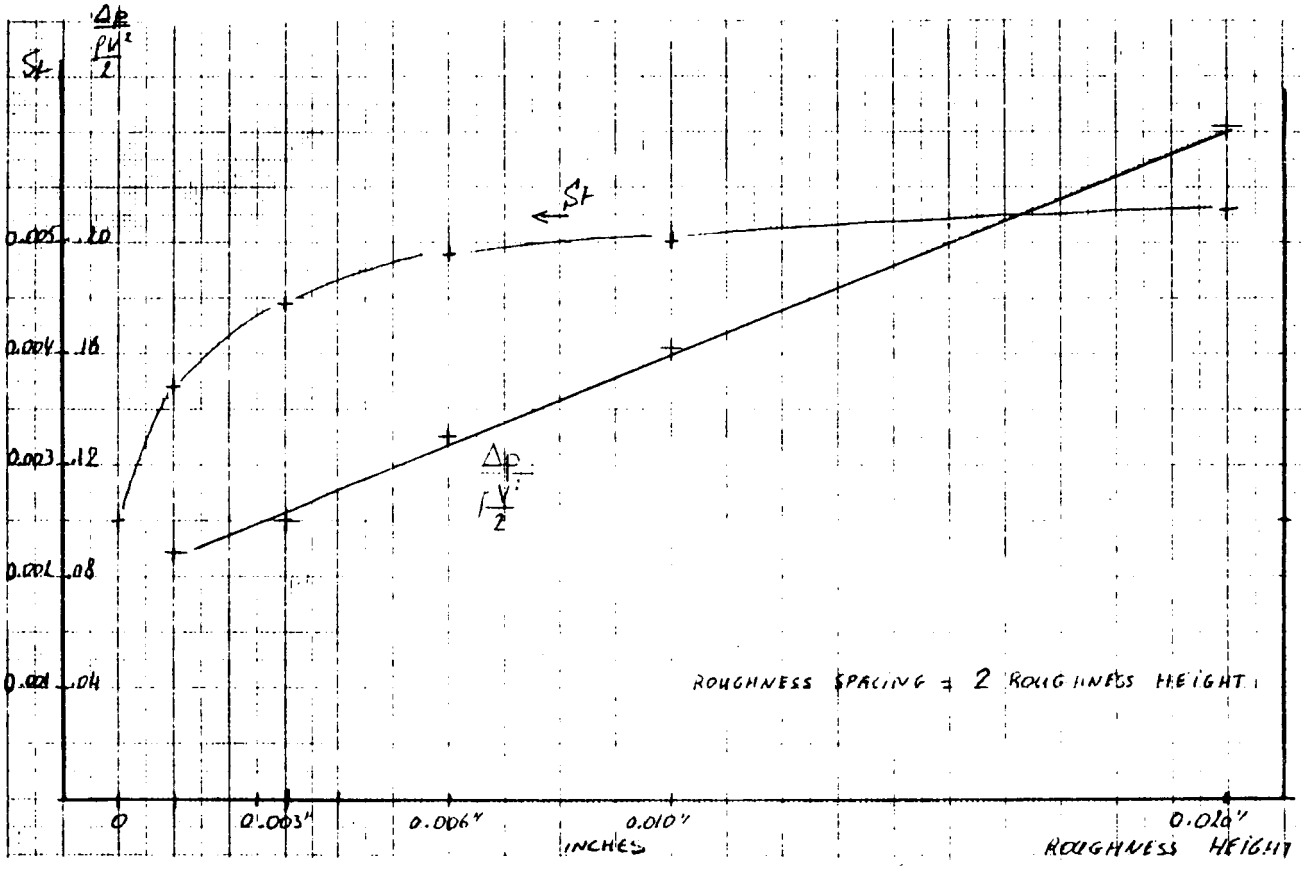

Figure 52. Heat Transfer and Pressure Drops Over a Roughened Wall.

2.2.2 Transition Liner

The flow distribution in the transition liners was restricted in order to minimize the amount of coolant and used a counter-flow scheme.

The considerable difficulty to fabricate transition liners with offset-fin plates prohibited their use in favor of the extended surface cooling technique. Because of manufacturing constraints, several equivalent roughness heights (relative to the sand-grain equivalence relationship) were made available for trial fabrication.

The first configuration called for an outer-transition liner that involved five independently-fed liner sections as shown previously in Figure 39. For the second dilution zone of the outer liner, an equivalent sand grain roughness height of 0.020 inch was selected to be the optimal sand grain roughness height. The wall temperature distribution achieved was given in Figure 45.

A comprehensive investigation was undertaken in the simplification of the transition-liner geometry. Although the above cooling configuration ensured an acceptable wall-temperature distribution along the outer-transition liner, existing potential difficulties in manufacturing and assembly accuracy called for a simplified configuration.

Combinations of two or more adjacent sections of the transition liners were examined. In order to retain the counterflow cooling scheme and maintain a constant flow velocity along the combined panels (see Figure 53), the flow-passage height along the downstream panel approximately doubled with the increased flow rate. As the flow changed from 4.2 percent to 2.4 percent from Panel II to Panel I, the panel heights changed from .06 to .03 inches, respectively.

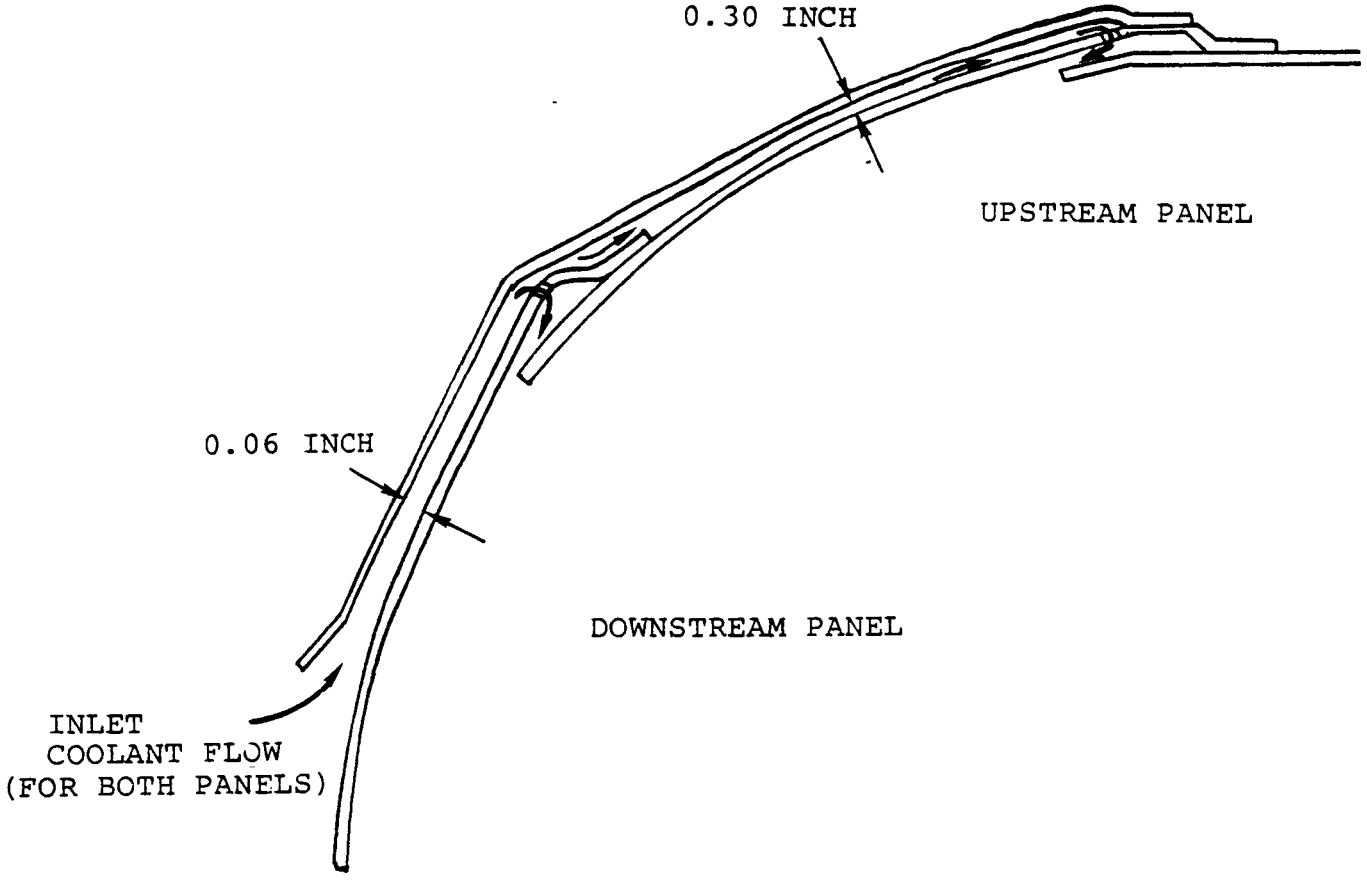

Figure 53. Panel Combination.

Although the wall temperatures were reduced significantly (as shown in Figures 54 and 55), the pressure drop (0.8 psi) resulting from the combination prohibited a longer combination. Panel III, therefore, was combined with Panel IV to make a single coolant passage. Temperature distributions are shown in Figures 56 through 58. Panel V was fed independently with the same coolant mass flow (1 percent).

A third configuration was derived from the thermal and stress analysis of the inner- and outer-transition liners and is discussed in the following paragraphs.

2.2.2.1 Outer-Transition Liner Thermal and Stress Analysis

A thermal and stress analysis was undertaken in order to determine the thermal deflections of the outer-transition liner's flow channels and slot gaps. Maintaining the specified channel and slot heights were critical to the correct cooling of the outer-transition liner.

The thermal deflection analysis was performed by applying the transition-liner's temperature distribution to the finite-element model, as shown in Figure 59. Only the first four panels of the outer-transition liner were modeled in the initial analysis. No temperature variation in the sheet-thickness direction was assumed in this analysis. Outer-sheet temperatures were calculated based on the cooling flow's heat-transfer coefficients and temperatures. Radiation was not included between the inner and outer sheets of the transition liner. The temperature distribution used in the thermal analysis is shown in Figure 60, and the resulting thermal deflections are shown in Figure 61.

Relative motions at the four dimple locations are also shown in Figure 61. The top two dimples showed closures for the maximum-

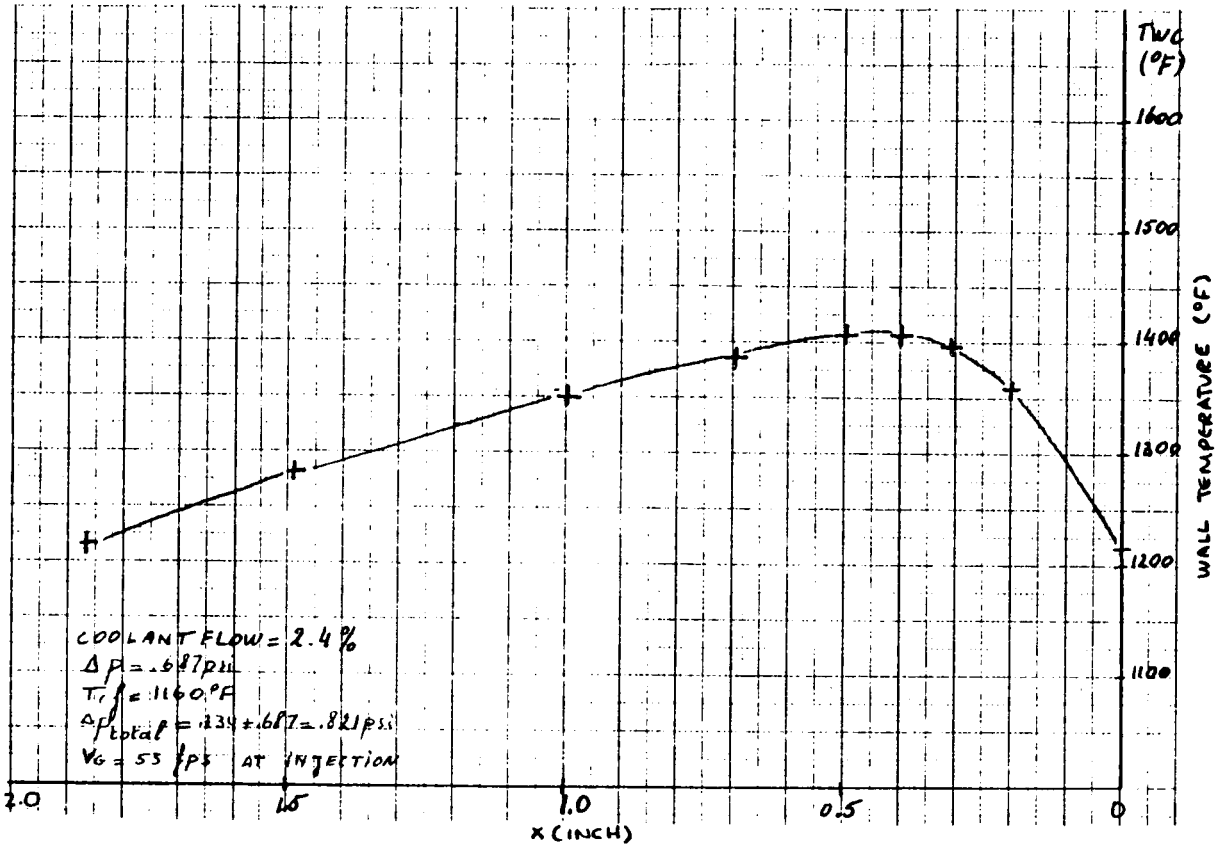

Figure 54. Transition Liner (Panel I).

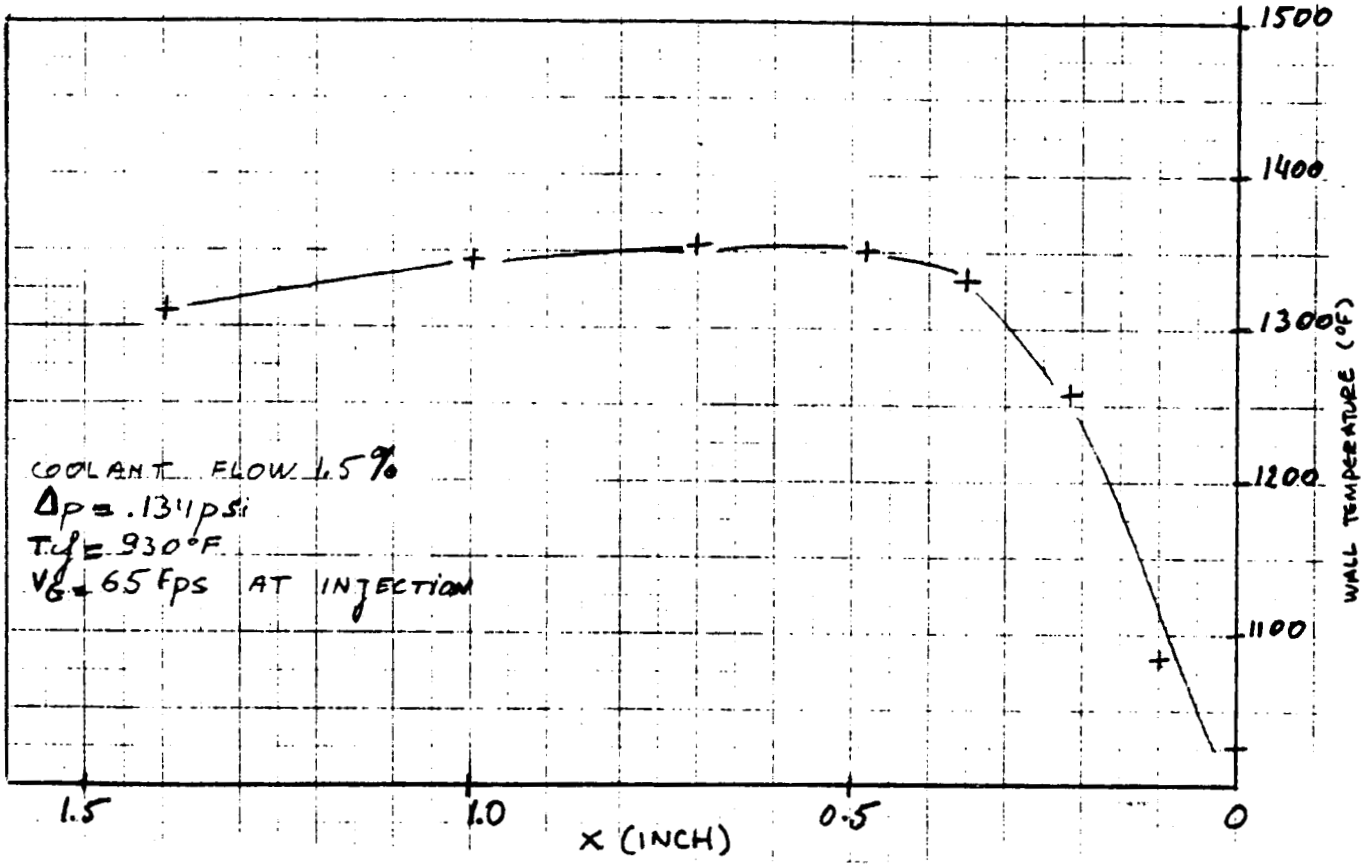

Figure 55. Transition Liner (Panel II).

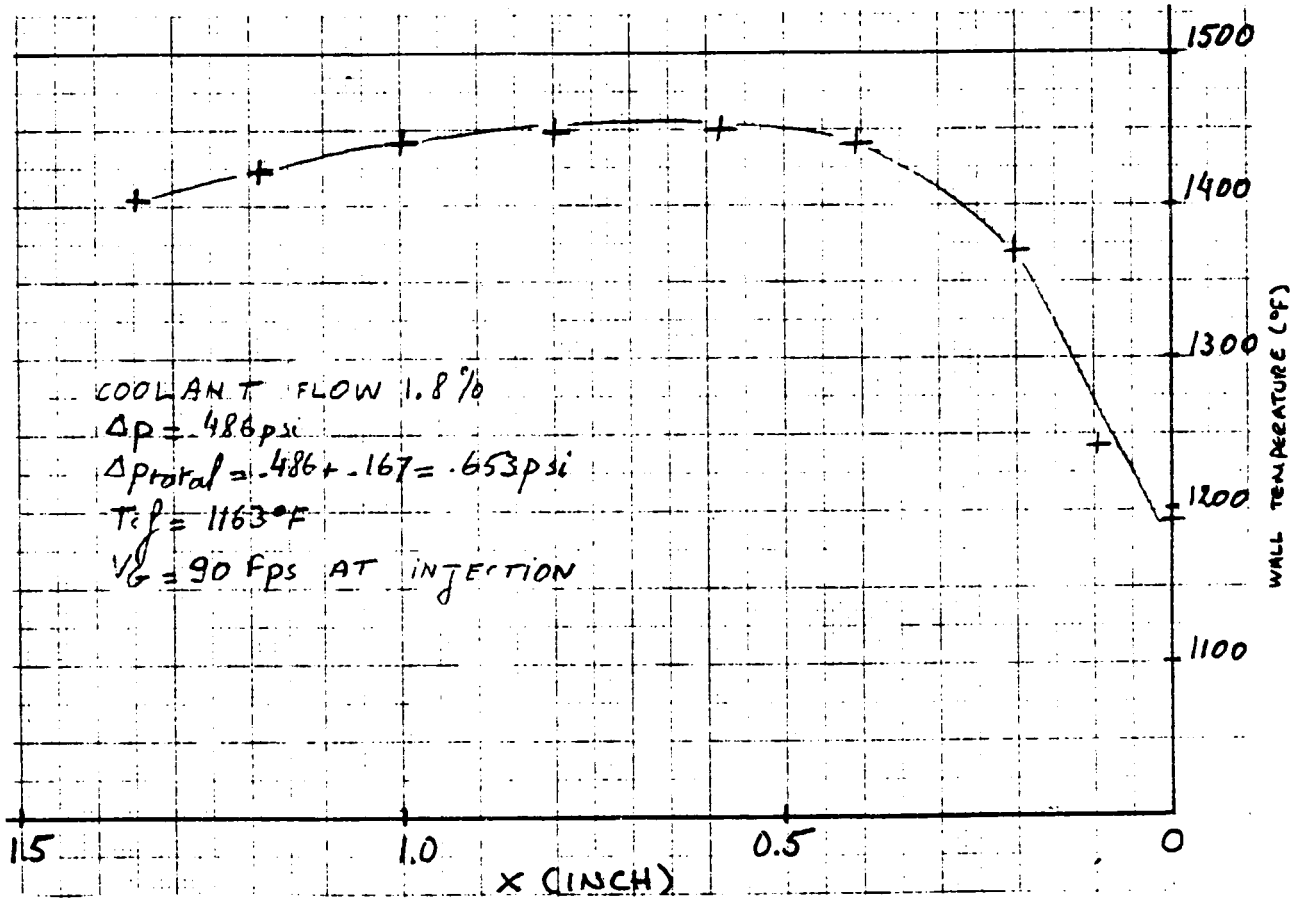

Figure 56. Transition Liner (Panel III).

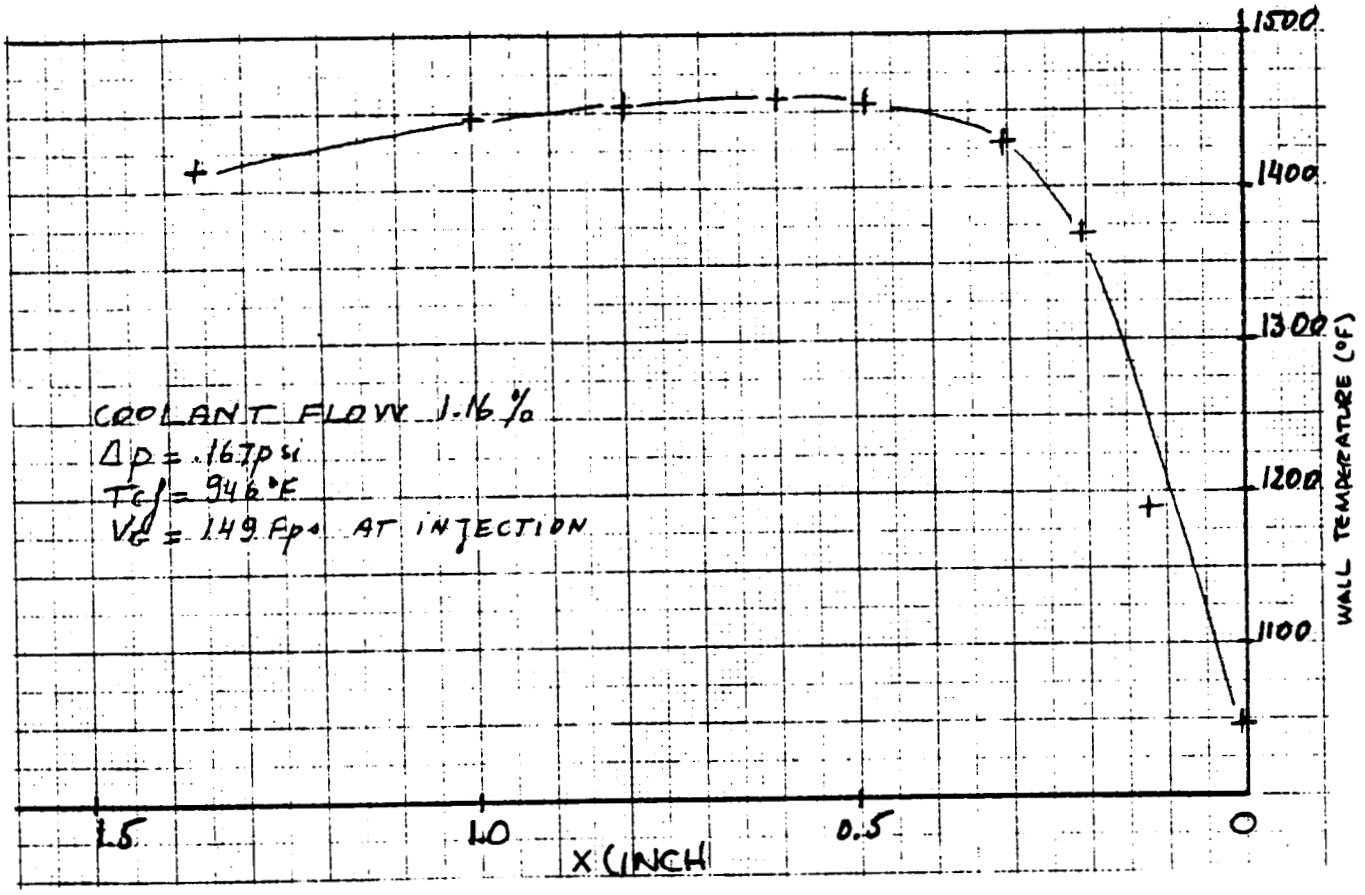

Figure 57. Transition Liner (Panel IV).

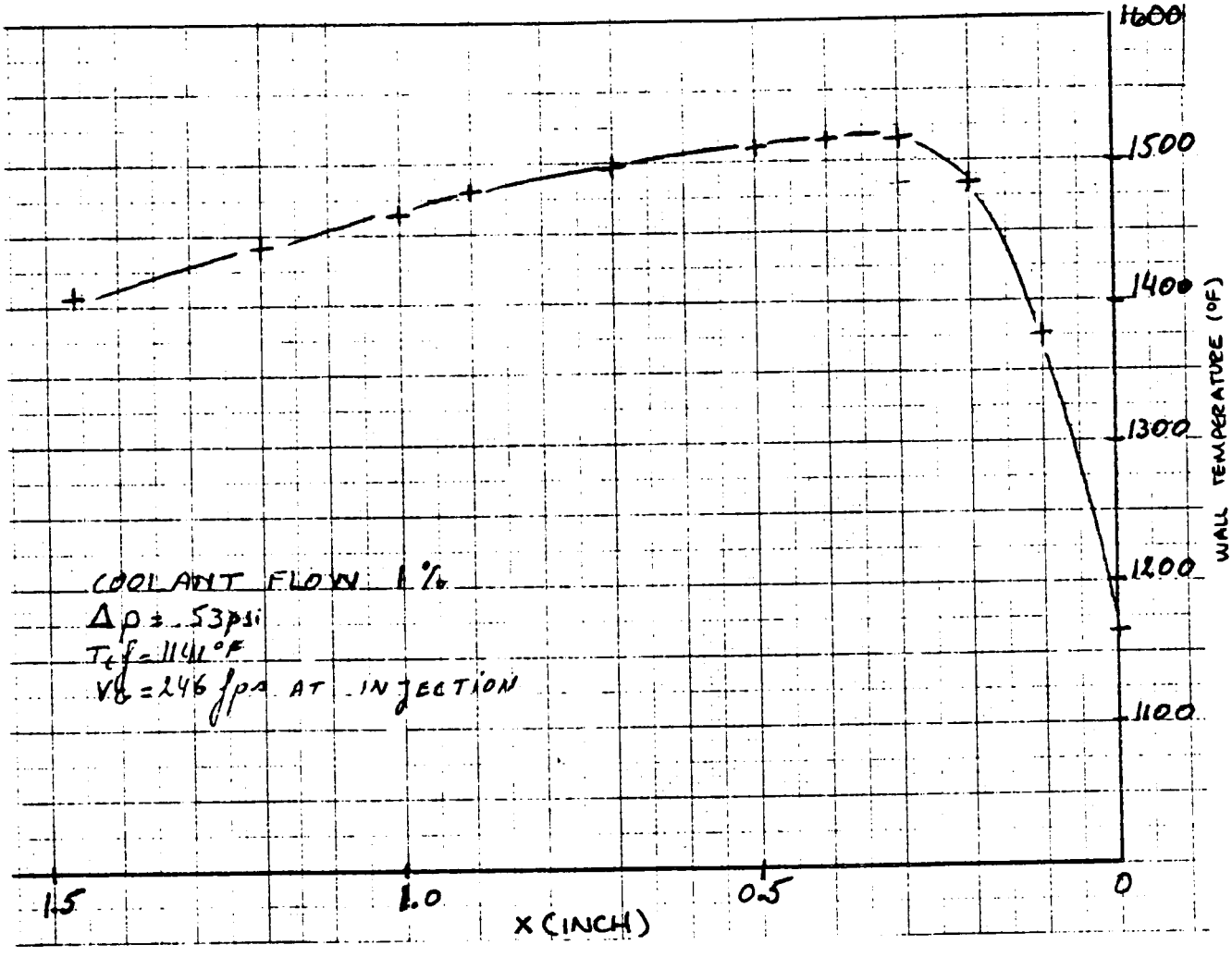

Figure 58. Transition Liner (Panel V).

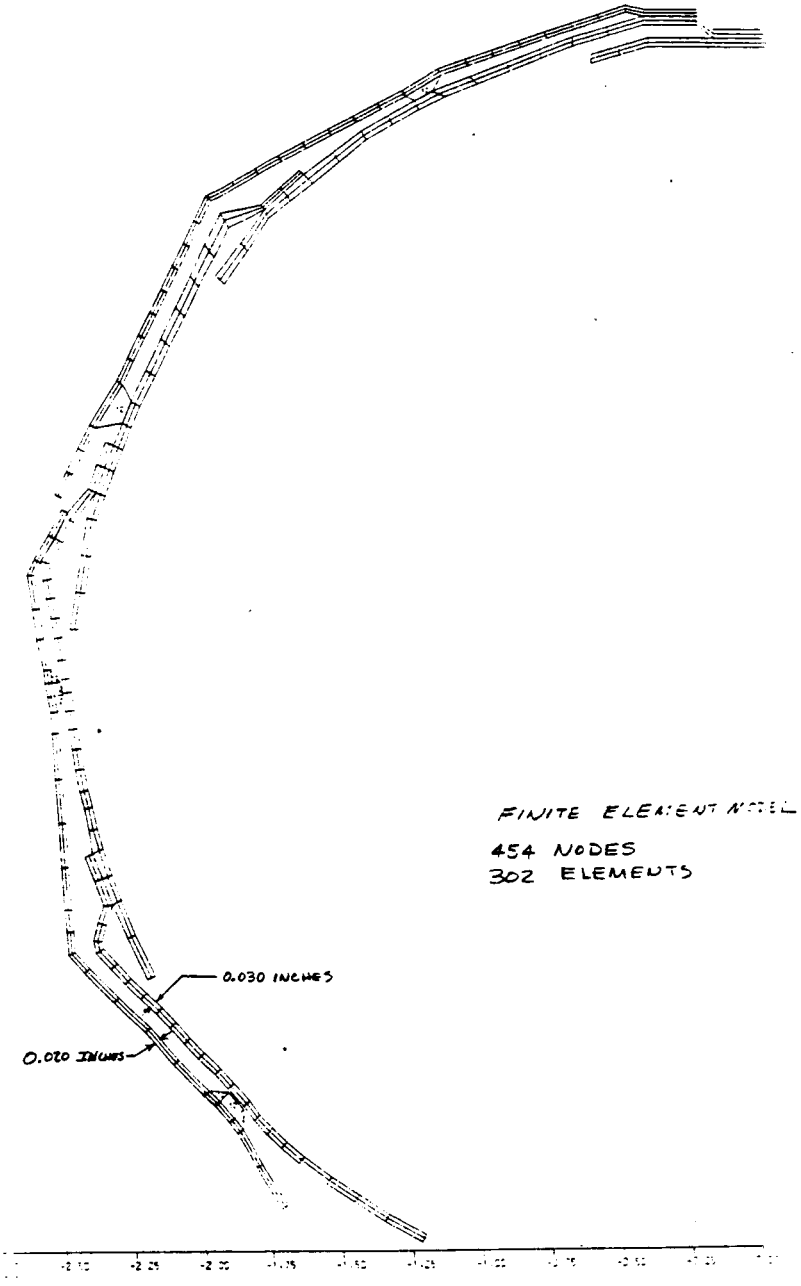

Figure 59. Initial Finite-Element Model.

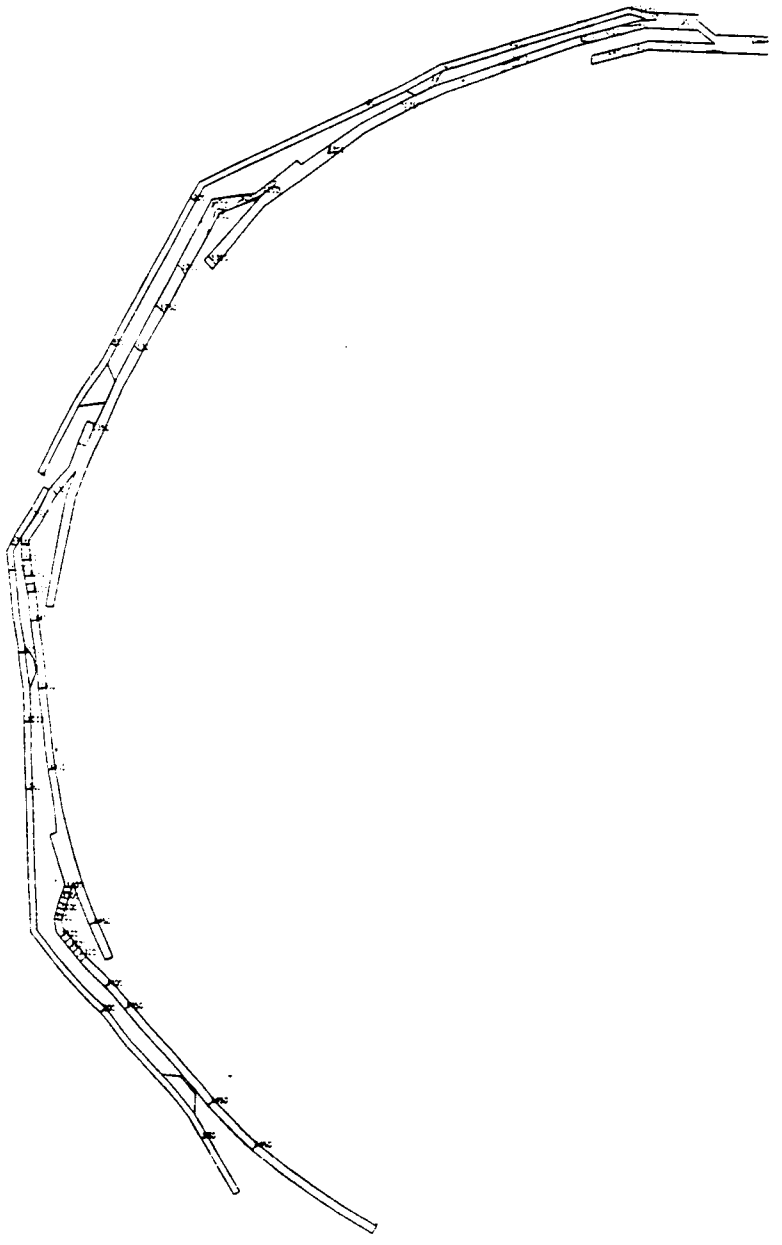

Figure 60. Initial Temperature Distribution.

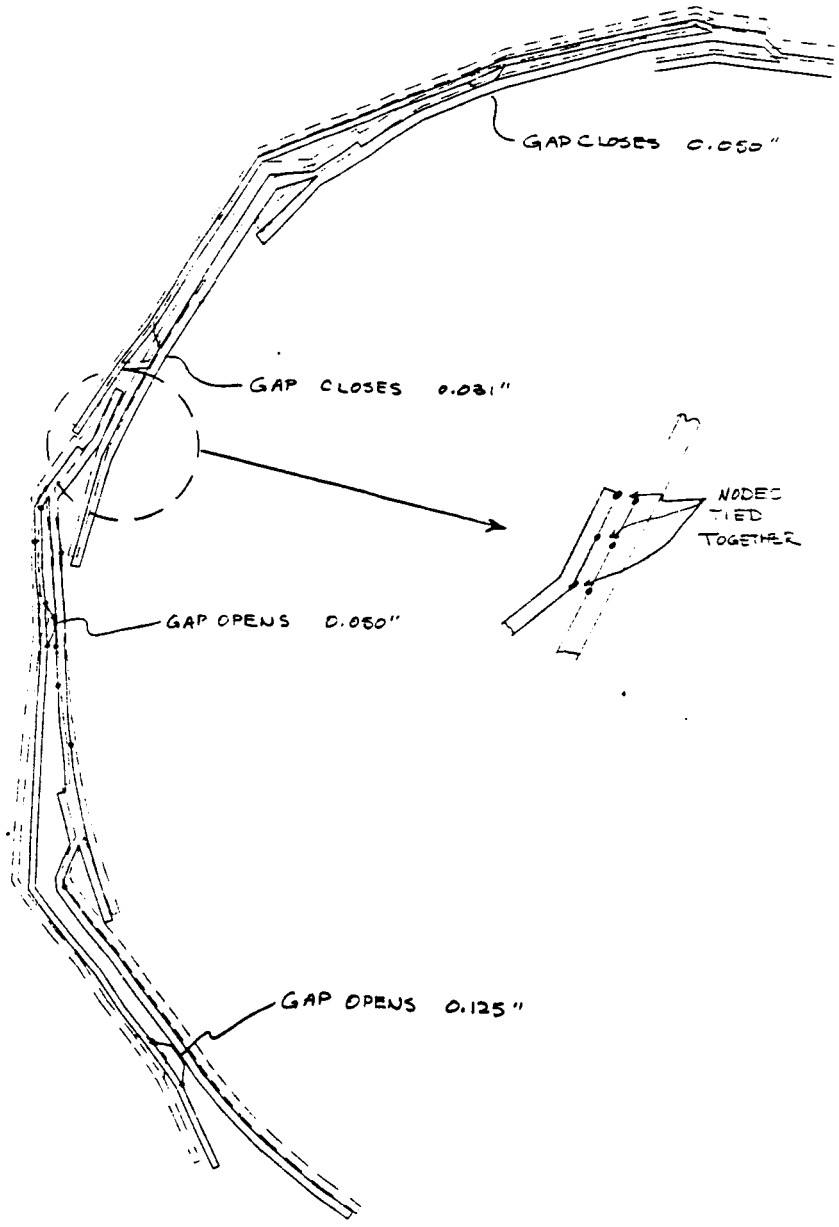

Figure 61. Thermal Deflections and Dimple Relative Motions.

temperature condition while relative motions were opening at the lower two dimple locations. Panels III and IV combined had specified channel heights of 0.030 inches and 0.060 inches, respectively, for the maximum design operating condition. Computed gaps due to thermal deflections only were approximately twice the specified operating gaps. Large thermal stresses also were computed at the double panel intersection location.

In order to reduce the stresses and deflections, the initial design was modified as shown in Figure 62. Panel V was added to the first model, and the other double panels were recombined in order to reduce the thermal stresses and deflections. (Panel I was made into a single panel. Panels II and III were combined into a double panel as were Panels IV and V.) The inner-panel sheet thickness was also increased to 0.050 inch. New temperature distributions were computed for the modified design (see Figure 63) and the resulting thermal deflections are shown in Figure 64. Relative motions at the dimple locations are also shown in this figure. The temperature distribution was recalculated for the new panel configuration, and the new distribution is shown in Figure 65.

Initial cold gaps were specified at the dimple locations that indicate closure at the operating condition. The lower two dimple locations were designed with an initial lower channel height that was allowed to open to the correct height at the operating condition.

2.2.2.2 Inner-Transition Liner Thermal and Stress Analysis

The analyses on the inner-transition liner indicated that it was an acceptable design. Figure 66 shows the result of the thermal analysis. A peak temperature of 1525°F is predicted near the interface of the combustor with the liner. The material for the liner, Hastelloy X, will adequately handle this temperature level.

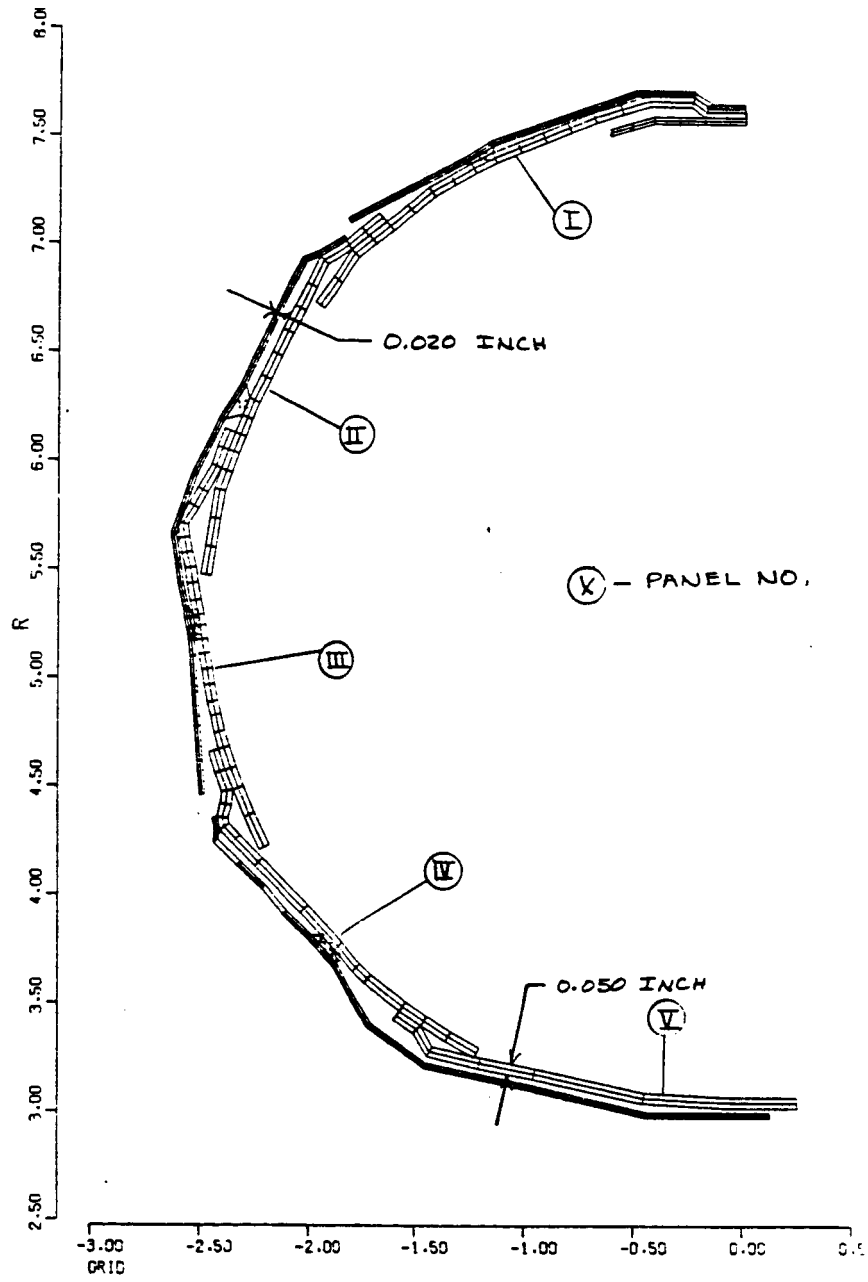

Figure 62. Modified Outer Transition Liner Design.

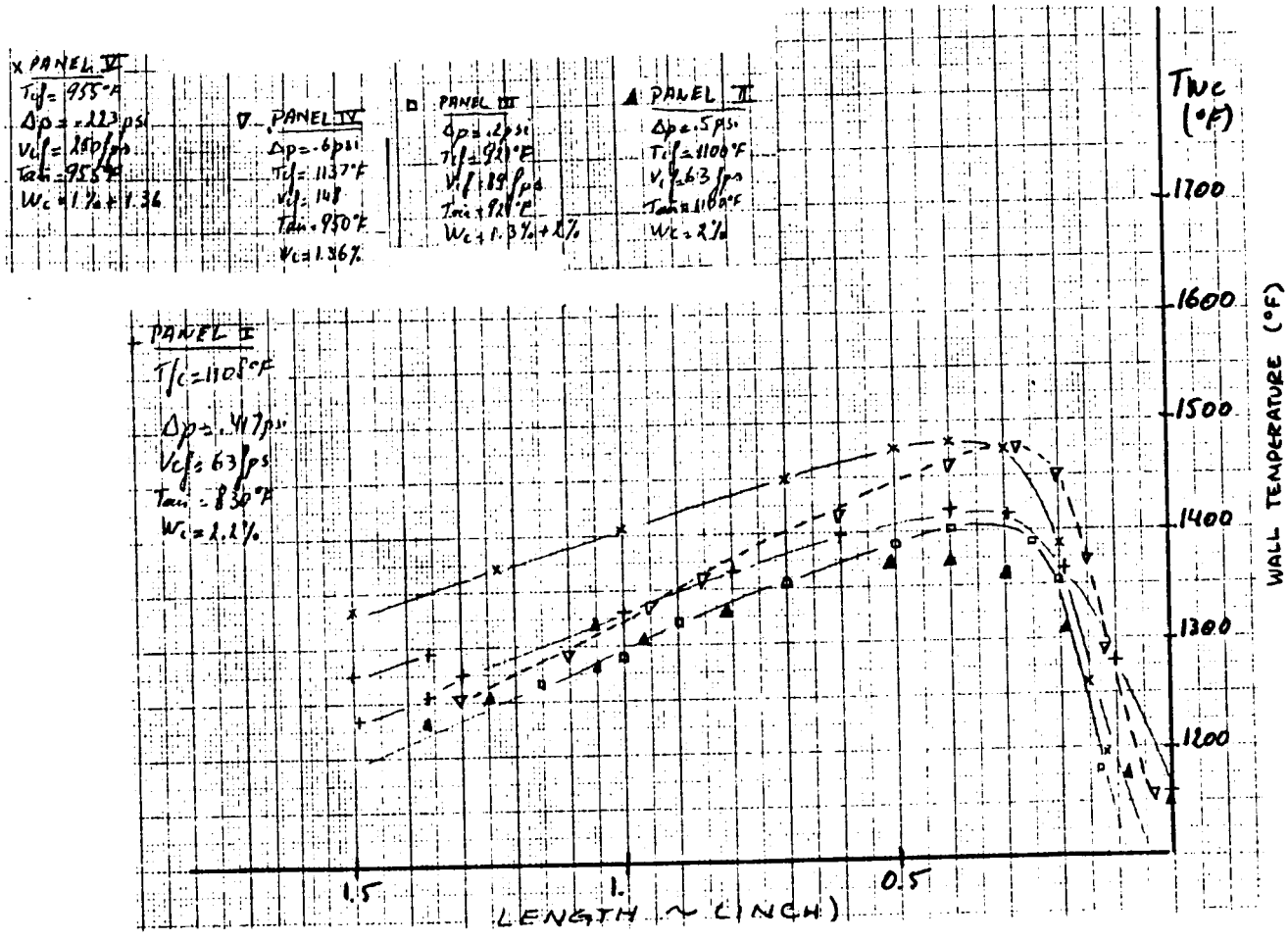

Figure 63. Panel Temperature Distributions.

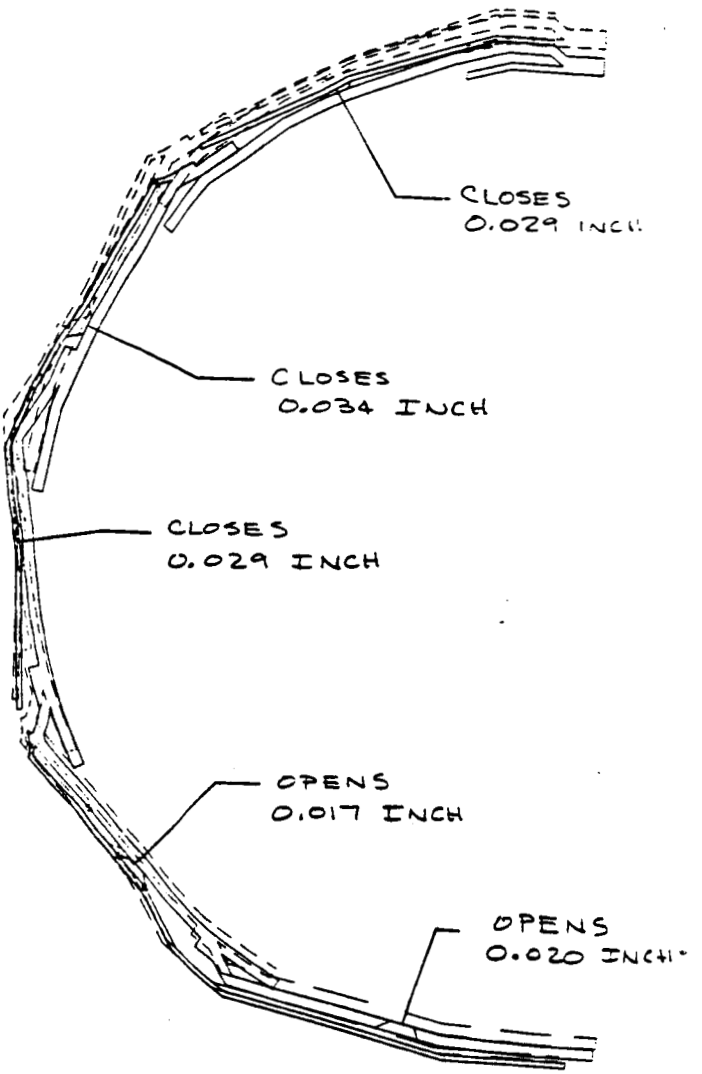

Figure 64. Modified Transition Liner Deflections and Dimple Relative Motions.

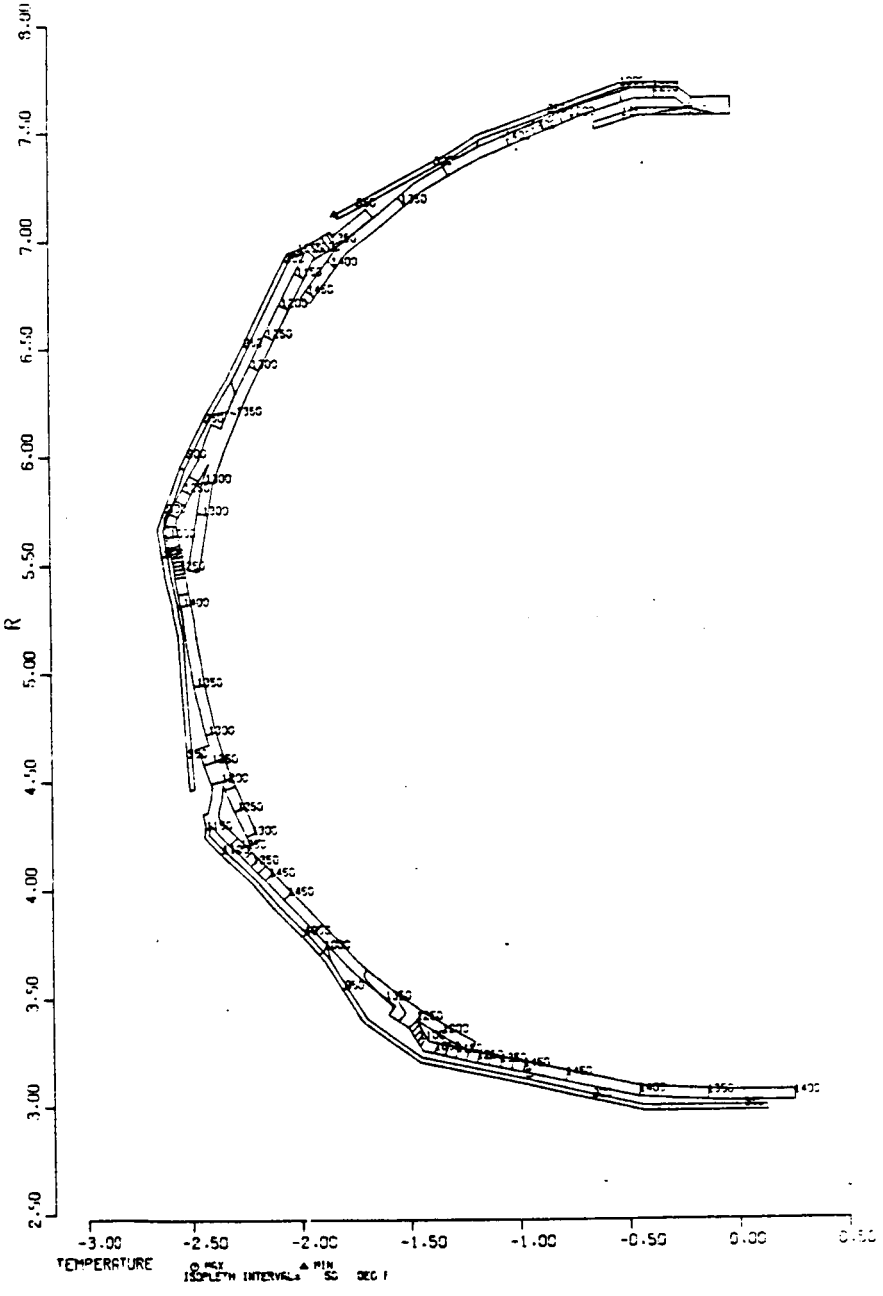

Figure 65. Modified Model Temperature Distribution.

1525

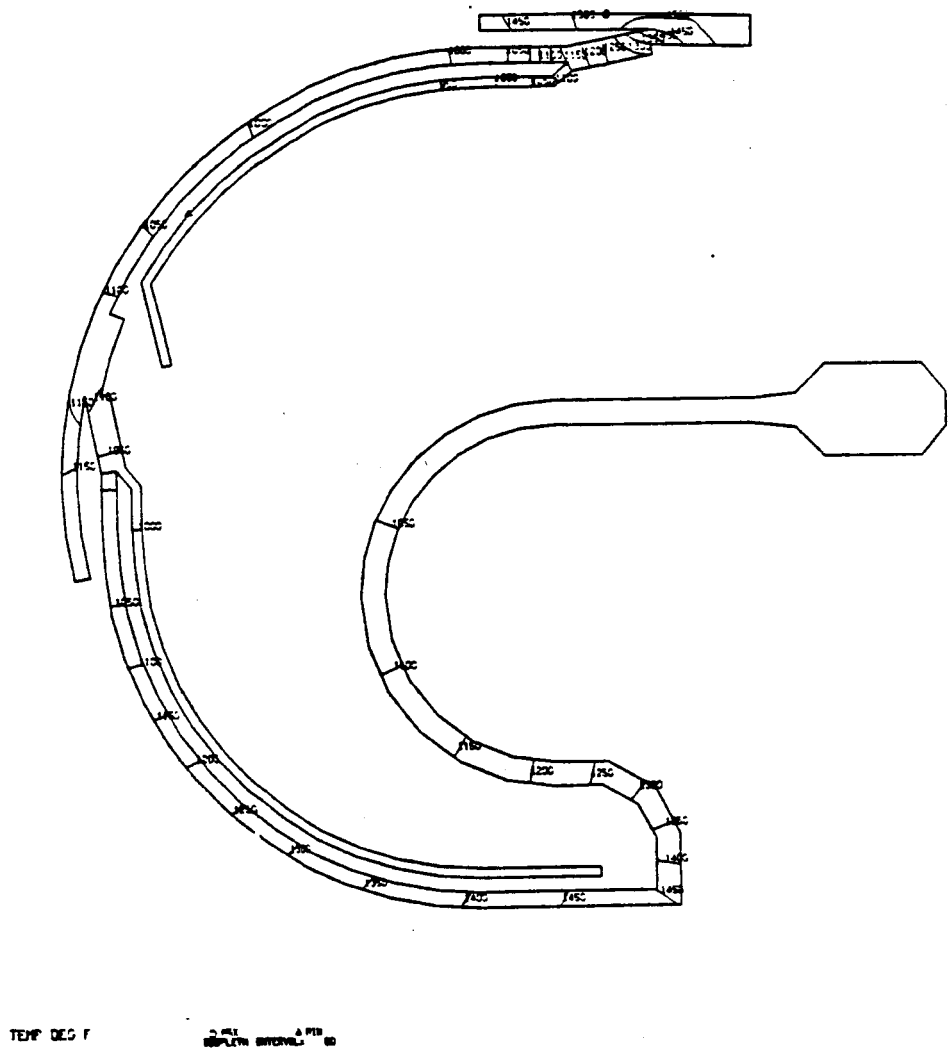

ALL TEMPERATURES IN °F

Figure 66. CFFC Inner Transition Liner Maximum Operating Temperatures.

The thermal analysis was based on 100-percent combustor efficiency at steady-state maximum operating condition. Film cooling of 2.0 percent was applied at the first inlet, and 1.54 percent was applied at the next downstream inlet. Convection heat transfer was applied at all of the model surfaces. Radiation was assumed only to be significant between the double walls of the liner. Zero-heat conduction was assumed at the junctions of the liner with the combustor and other mating parts.

Figure 67 shows the thermal stresses resulting from the temperatures of the steady-state maximum operating condition thermal analysis.

A maximum stress of 88.9 ksi was found at the dimple standoffs between the two liner walls. No stress relaxation was considered in this analysis. The results indicated that small localized yielding (creep) was likely to occur in this region, but should not affect the performance of this combustor.

Figure 68 shows the deflected shape of the inner-transition liner during steady-state maximum operating condition. The model was assumed fixed axially at the interface with the inner-combustor wall. The two cooling film inlets to the main flow both open up from the build condition. The first inlet opens up 0.0077 inches (radially), and the downstream inlet opens up 0.0015 inches (radially).

2.2.3 Detailed Analysis of Combustor Layout

A final iteration of the one-dimensional annulus flow model was used to match the liner geometry and the coolant-flow distribution. The detailed geometrical characteristics of the coolant-metering holes and their respective pressure drop along every single-liner section were inferred and summarized in Tables 1 and 2.

55.4

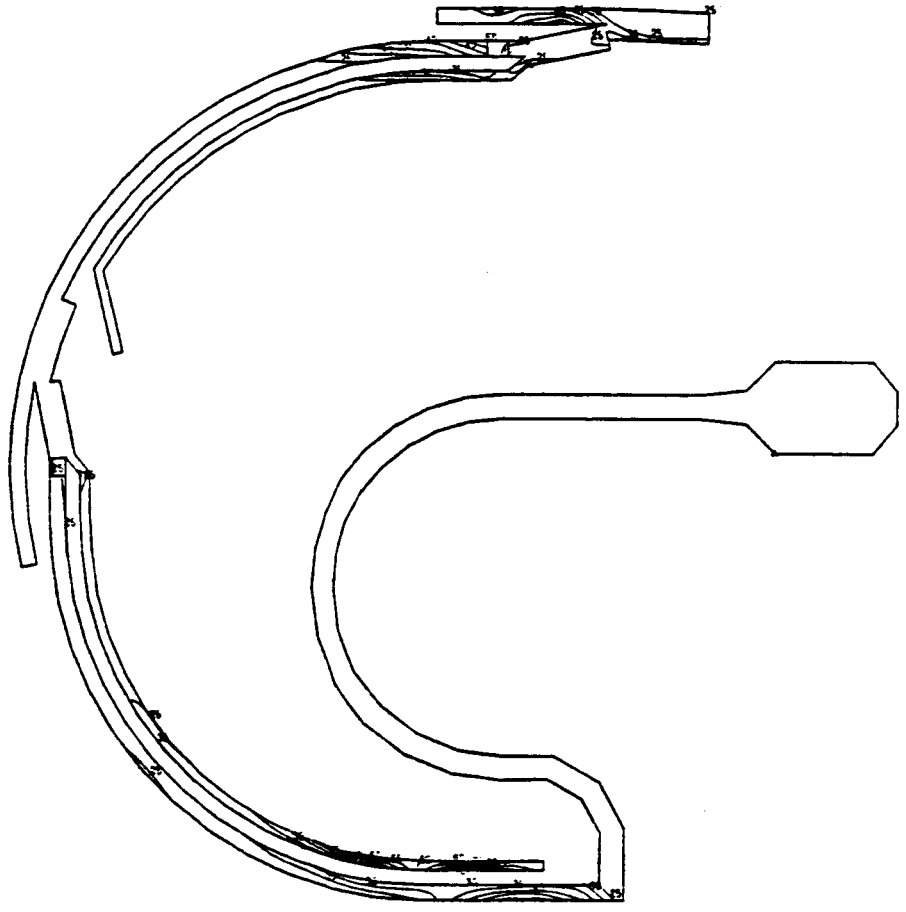

88.9

ALL STRESSES ARE EFFECTIVE AND IN KSI

Figure 67. CFFC Inner Transition Liner Maximum Operating Stresses.

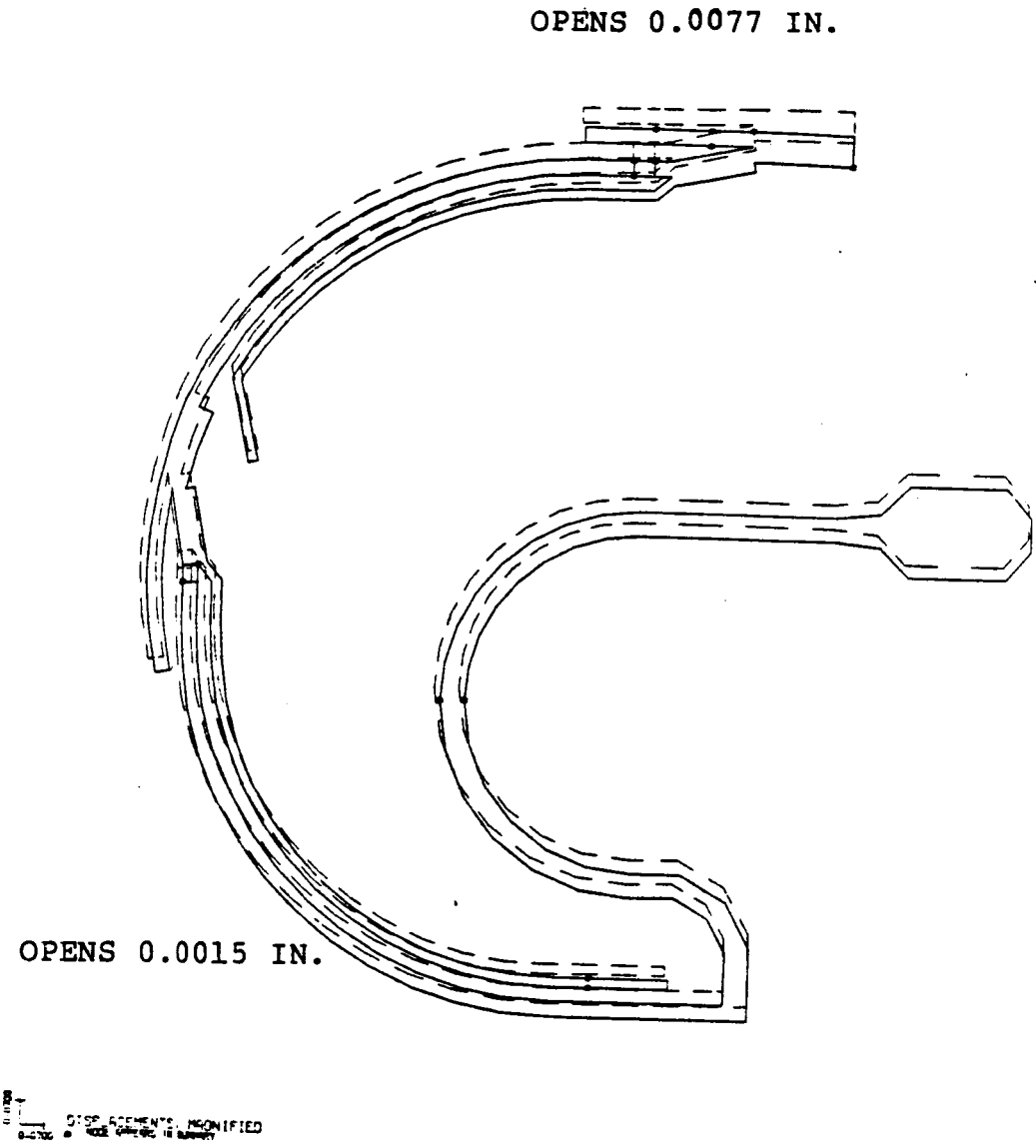

Figure 68. CFFC Inner Transition Liner Maximum Operating Deflections.

TABLE 1. TRANSITION LINERS.

LOCATION*	1	2	3	4	5	6	7	8	9	10	11	12	13	14	15
OUTER TRANSITION LINER															
Panel I	2.2	233.73	830	0.7076	2.15	192	0.6	0.0453	0.029	0.8	-0.0038	0.033	24	0.030	3.71
Panel II	2.0	233.80	921	0.653+ 0.442	1.99	181	0.6	0.454	0.025	0.63	-0.0167	0.042	18	0.030	2.92
Panel III	1.3+2	233.80	830	0.442	2.29	151	0.6	0.0370	0.018	0.57	-0.0037	0.022	12	0.060	3.81
Panel IV	1.36	233.64	955	0.608+ 0.822	1.85	116	0.6	0.0479	0.018	0.39	+0.0008	0.018	8	0.0131	2.12
Panel V	1+1.36	233.64	830	0.608	2.15	88	0.6	0.033	0.0106	0.39	+0.0024	0.010	6	0.0103	1.52
INNER TRANSITION LINER															
Panel I	2.0	231.95	885	0.596	1.45	150	0.6	0.0366	0.033	0.752	+0.008	0.025	10	0.017	2.97
Panel II	1.54	231.95	885	0.8	1.36	150	0.6	0.0464	0.0123	0.29	+0.0015	0.0123	9	0.030	1.38

*The transition-liner panels are as defined on Figure 39.

1. Cooling air mass flow (%)
2. Static pressure at entrance of panel (psi)
3. Cooling air temperature at the entrance of the panel (°F)
4. Pressure drop along panel (psi)
5. Pressure drop available at panel exit (%)
6. Number of cooling metering holes
7. Discharge coefficient C_D
8. Metering hole diameter, D inch
9. Cooling skirt height, s, inch
10. Parameter ψ for the cooling skirt
11. Cooling skirt height expansion, Δs, inch
12. Cooling skirt height at assembly
13. Number of dimpels
14. Dimpels height
15. Cooling slot area/metering holes total effective area ratio

GARRETT TURBINE ENGINE COMPANY
A DIVISION OF THE GARRETT CORPORATION
PHOENIX, ARIZONA

TABLE 2. CYLINDRICAL LINERS.

PANEL*	1	2	3	4	5	6	7	8	9	10	11	12	15	16	17
OUTER LINER															
Primary	7.0	233.71	830	1.195	1.94	192	0.6	0.086	0.070	0.68	0.010	0.080	3.0	58	1563
Primary Jets	10.03	233.82	830		2.48	36	0.529	0.204	-	-	-	-	-	10^4	-
First Dilution	6.0	233.7	830	0.9913	2.02	192	0.6	0.078	0.059	0.63	0.010	0.069	3.19	51	1547
Dilution Jets	12.47	233.88	830	-	2.51	36	0.56	0.229	-	-	-	-	-	-	-
Second Dilution	1.0	233.30	830	-	2.27	192	0.5137	0.0293	0.0113	0.527	0.047	0.058	5.0	24 4.1410^3	1363
INNER LINER															
Primary	2.0	231.85	830	-	1.66	196	0.584	0.0433	0.055	1.13	0.014	0.069	52	1417 6.310^3	
Primary Jets	7.57	231.85	830	1.56	1.0	36	0.6	0.232	-	-	-	-	-	-	-
First Dilution	2.0	231.86		-	1.66	140	0.6	0.051	0.036	1.05	0.006	0.030	6.3	53 6.710^3	1264
Dilution Jets	10.53	231.89		1.23	1.15	36	0.6	0.264	-	-	-	-	-	-	-
Second Dilution	1.4	231.91		0.1345	1.63	140	0.6	0.045	0.025	0.697	0.019	0.015	3.95	41 5.1210^3	1402

*See Table 1 for identification of 1 through 15

16 Cooling slot impingement
Nu and Re

17 Lip temperature (°F)

For each orifice opening along the combustor liner, the tables indicate the:

- Air flow is percentage of the total air flow, ω
- Pressure available at the section location, P (psi)
- Pressure drop through the fins or convective passage, ΔP
- Pressure drop available at the air injection, $\Delta P/P$ %
- Number of holes
- Geometric-hole diameter, D (inch)
- Cooling skirt height, S (inch)
- Cooling slot parameter, ψ
- Cooling film temperature at injection, T_f (°F)
- Cooling skirt temperature, T_{lip} (°F)
- Cooling skirt lip thermal grow (inch), Δs
- Reynold number and Nusselt number for the cooling impinging on the cooling skirt
- Ratio of metering hole diameter to cooling skirt gap, D/s
- Ratio of hole spacing to hole geometric diameter
- Ratio of cooling skirt flow area to the total holes area.

These parameters were derived to optimize the film cooling effectiveness. It was found that the initial film cooling flow characteristics had significant influence on the film effectiveness delays, and thereby on the liner-wall temperature. Based on Reference 4, a well-designed cooling slot criteria was followed. The extreme sensitivity of film effectiveness to the slot geometric details was quantified through the following criteria:

for slot with $D/s \leqslant 1.0$,
the "ideal" slot will be such that $\psi \leqslant 0.9$

slot with $D/s \leqslant 1.5$ $\psi \leqslant 1.3$

where D = geometric diameter of the coolant metering hole
s = slot height at the outlet.

The nondimensional parameter ψ is a function of the cooling configurations, such as double or single rows of metering orifices, axial-radial-hole injection angle. For the simple slot with a single row of metering orifices and no plenum considered in this design, ψ is related to the cooling skirt geometry by:

$$\psi = \frac{ps}{dL}$$

where d = metering-hole diameter
p = pitch length between metering holes
s = slot-outlet height
L = slot length from the metering hole axis to the end of the lip

ψ is given in Tables 1 and 2 for each film cooling location.

The pressure drop along the liner section includes the following:

- Fin or convective passage entrance pressure drop
- Pressure drop along the fins or convective cooling passages.
- Pressure drop due to dimple blockage along the transition liner.

The pressure drops across the swirlers and primary and dilution holes were given directly by the annulus-flow models for the exact-liner geometry (include fin outer panel).

The cooling slot gaps were estimated in two steps. For the first one, the slot height was estimated to match the film cooling velocity with the near-wall hot-gas velocity, as given by the three-dimensional analysis. The thermal growth, opening or closing, of each slot was computed from the temperature difference between the lip temperature and the liner local temperature. The enhanced cooling process from the metering hole impinging air was taken into account. The average Nusselt number along the lip and the impingement Reynolds number based on the metering hole diameter are also shown.

2.3 Technical Summary

The wall-temperature reduction obtained with the counterflow film-cooled combustor is shown in Figures 69 and 70. The wall-temperature distribution of the cylindrical liners are compared for both the original conventional convective-film cooling configuration and the present offset-fin/extended surface configuration. The first dilution zone-wall temperature profile has been estimated for two values of fuel/air ratio corresponding to the actual fuel/air ratio (0.046) in that region and a commonly assumed value (0.054) based on past experience.

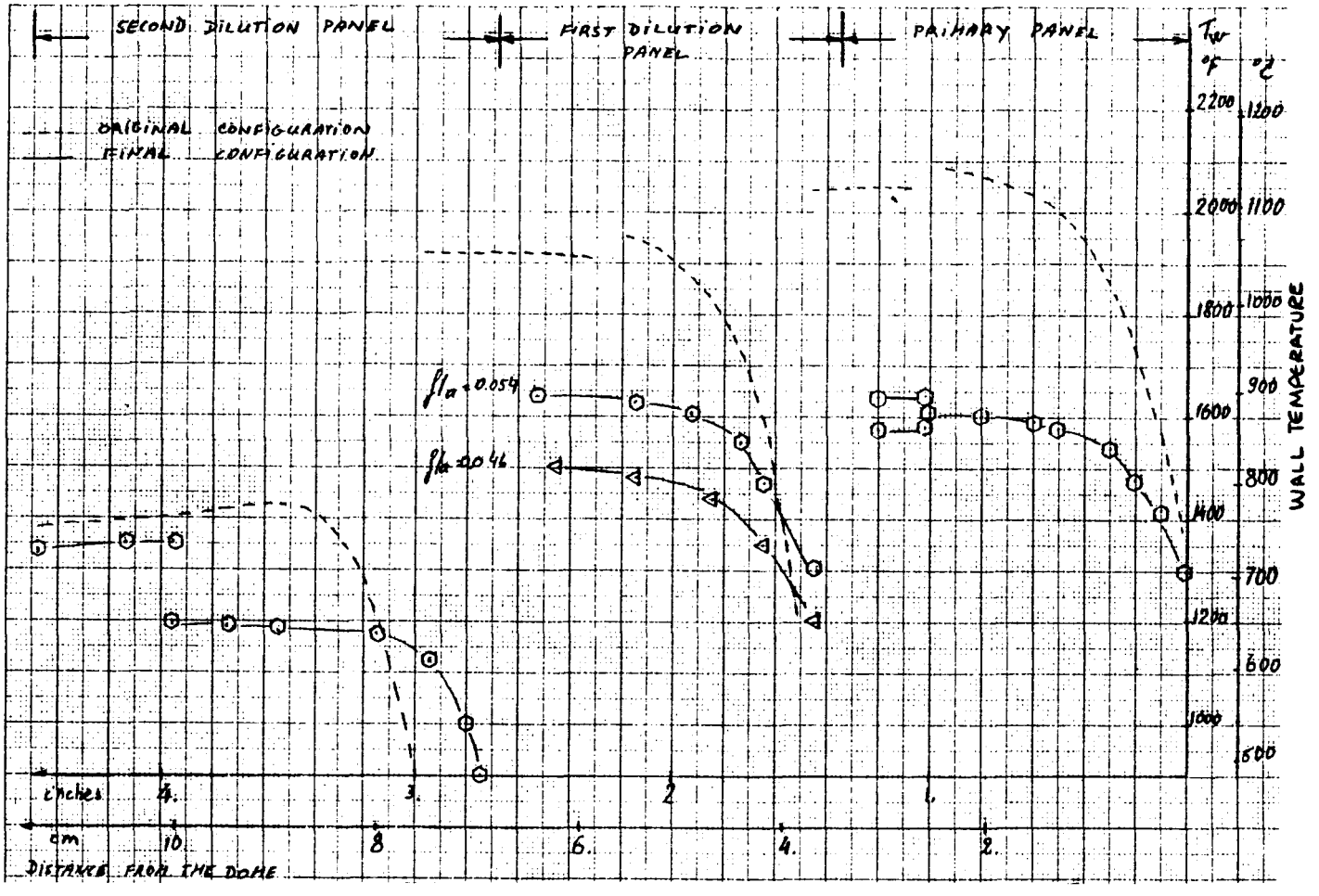

Figure 69. Temperature Distribution Outer Liner - Final Configuration.

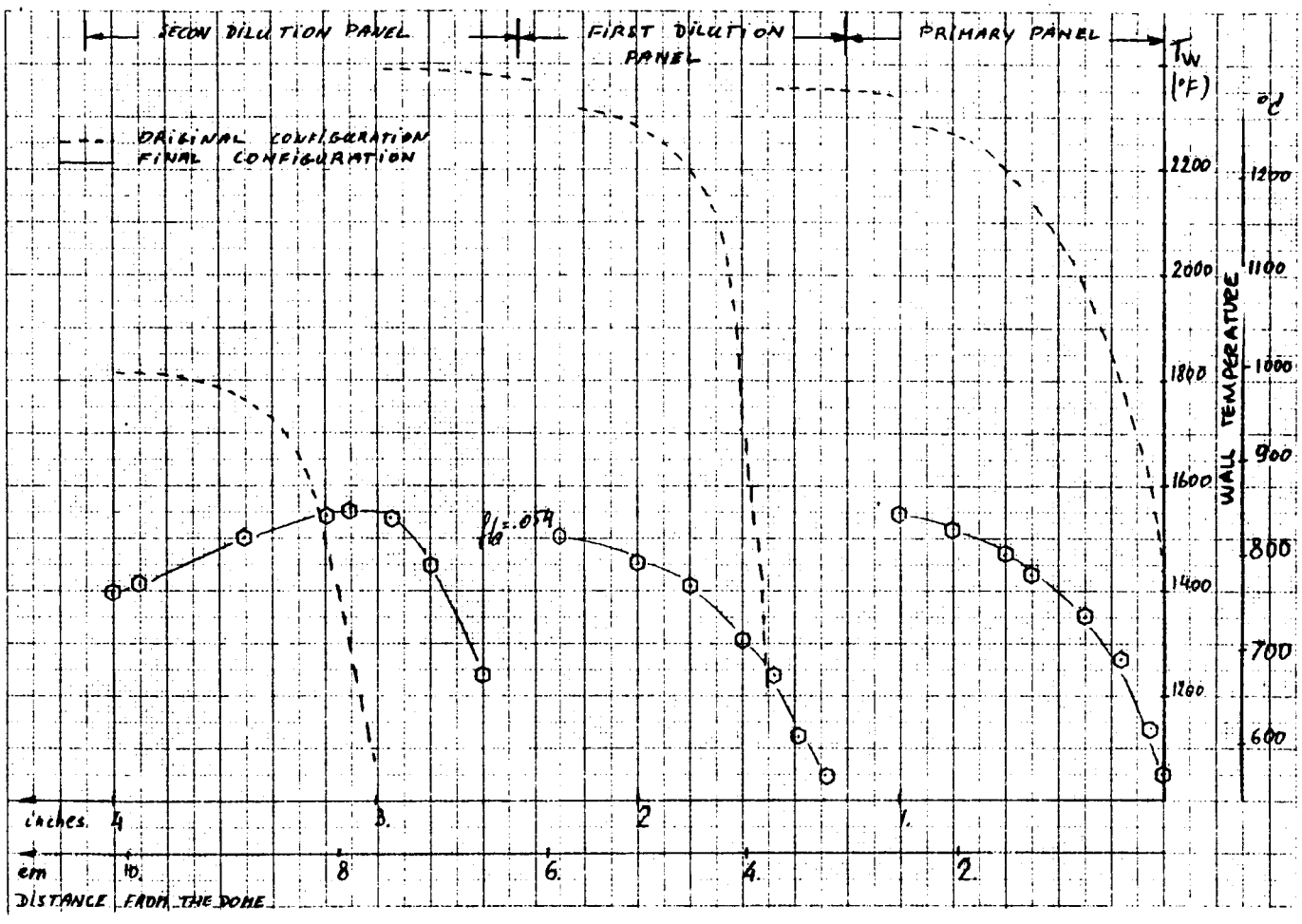

Figure 70. Inner Liner.

To evaluate the cooling performance between the original and final configuration, the parameters in Table 3 have been assembled for each liner section. They represent:

W_c = Amount of film cooling air (percent of the total airflow)

f/a = Fuel air ratio existing in the hot gas

T_G = Hot-gas temperature

T_f = Flame temperature (use in computing radiation flow to the wall)

$\frac{N_u}{N_{uo}}, \frac{St}{Sto}$ = Ratio of the Nusselt number and the Stanton number, respectively, for each region of the final configuration with respect to the conventional convective/cooling scheme. In the transition liner, the configuration of reference consists of the same forced convective passages but bearing no roughening elements.

The last two parameters illustrate the increased heat-transfer rate obtained around the combustor, when improved convection cooling techniques are used.

The reduction in the amount of air spent in cooling the liners represents a significant gain when compared to a conventionally cooled combustor. The "specific coolant flow" (i.e, the average coolant flow rate per liner surface area) has been plotted versus the combustor inlet pressure for a wide range of Garrett reverse-flow combustors as shown in Figure 71. The CFFC combustor would, a priori, require 0.0166 lbm/sec/in^2 (11.6910^{-4} kg/sec/cm^2) of cooling air to operate at the inlet pressure of 249.7 psia (16.98 atm). With the present

TABLE 3. COMBUSTOR COOLING PERFORMANCE.

LOCATION*	W_c %	f/a	T_G °F	T_f °F	Nu/Nuo	St/Sto
CYLINDRIC LINER						
Outer Liner						
1. Primary zone	7.0	0.0678	3439	3765	2.3	3.38
2. First dilution zone	6.0	0.054 0.046	3136 2859	3713 3136	2.50	3.51
3. Second dilution zone	1.0	0.031	2239	2592	1.7	1.74
Inner Liner						
1. Primary zone	2.0	0.0678	3439	3765	5.9	2.7
2. First dilution zone	2.0	0.054	3136	3713	7.8	2.78
3. Second dilution zone	1.4	0.0313	2239	2592	3.59	3.59
TRANSITION LINER						
Outer Liner						
1. Panel I	2.2	0.0284	2188	2592	2.66	1.47
2. Panel II	2.0	0.0277	2159	2492	2.15	1.30
3. Panel III	1.3+2	0.0273	2143	2471	2.35	1.5
4. Panel IV	1.36	0.0263	2100	2417	1.76	2.11
5. Panel V	1.36+1	0.0260	2084	2400	2.60	1.35

*The transition-liner panels are as defined on Figure 39.

Combustor Mass Flow = 8 lbm/sec = 3.63 kg/sec

Inlet Pressure P3 = 235 psi = 14.98 atm

Inlet Temperature T_3 = 830°F = 443°C

Pressure Drop $(\Delta p)_{liner}$ = 2.94%

Cylindrical Liner Surface = 2.585 ft^2 = 0.240 m^2

Cooling air mass flow required per unit of liner surface:

with conventional film cooling 0.0166 $lbm/sec/in^2$ = 11.6910^{-4} $kg/sec/cm^2$

with offset fins and extended surface 0.0081 $lbm/sec/in^2$ = 5.6710^{-4} $kg/sec/cm^2$

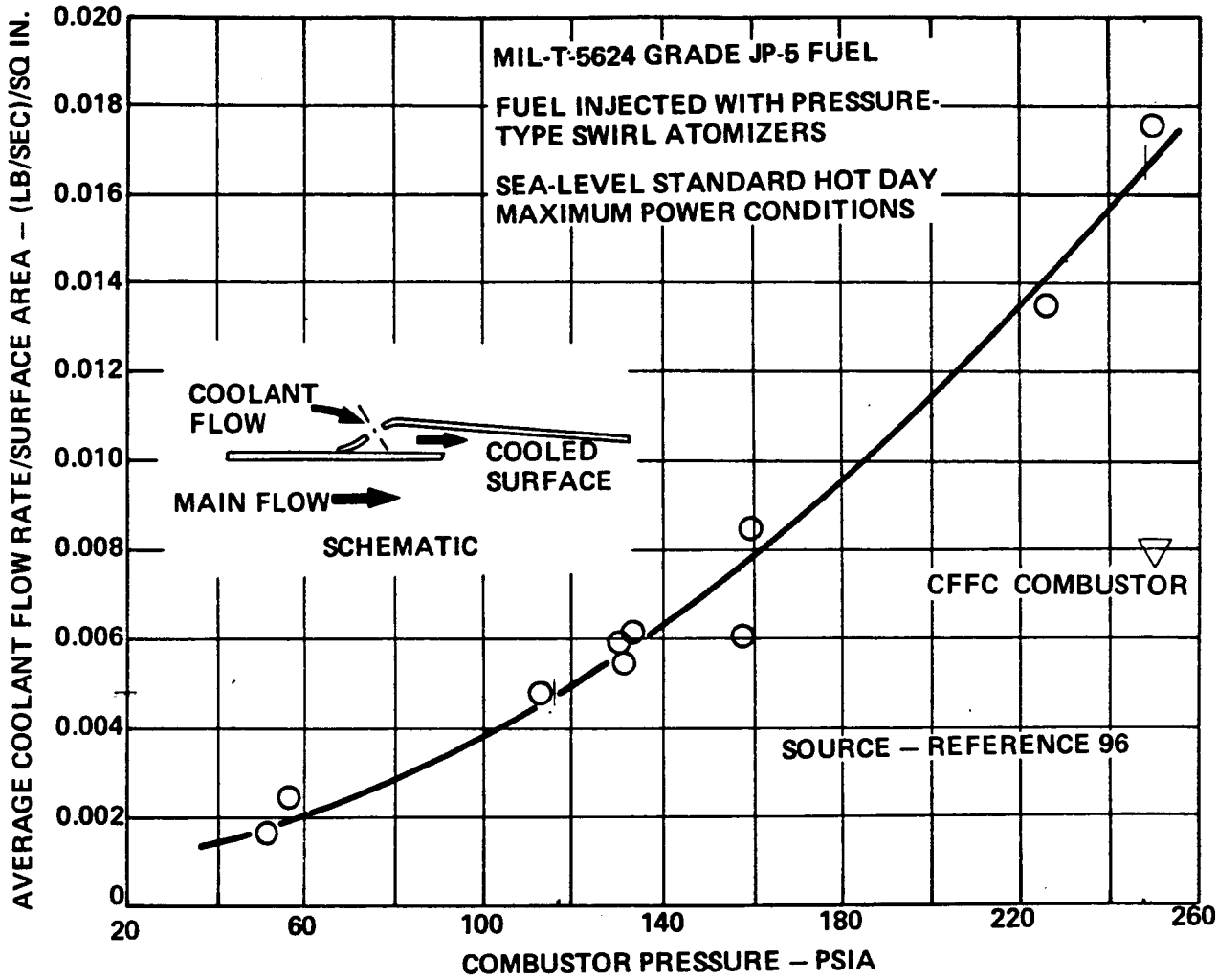

Figure 71. Experience Curve for Garrett Reverse-Flow Combustors, Comparing Average Coolant Flow Rates for Various Combustor Inlet Pressure Levels.

design, the specific coolant flow for the outer and inner liners (limited to the cylindrical liners to which Figure 71 applies only) are 0.0053 lbm/sec/in^2 ($3.72 10^{-4}$ kg/sec/cm^2) and 0.01176 lbm/sec in^2 ($8.26 10^{-4}$ kg/sec/cm^2), respectively. This leads to an overall specific coolant flow reduction of 52 percent, 0.008 lbm/sec/in^2 ($5.62 10^{-4}$ kg/sec/cm^2) instead of 0.0166 lbm/sec/in^2 ($11.69 10^{-4}$ kg/sec/cm^2) for a more conventional design.

The airflow distribution computer output along the cylindrical and transition liners is presented in Appendices I and II, respectively. For a given combustor geometry and specified airflow and pressure drop, the output consists of local velocities, pressures, orifices size, discharge coefficients, and jet velocities.

3.0 CONCLUSION

A comprehensive design study has been carried out to significantly reduce liner-wall temperature in a reverse-flow annular combustor.

A combination of high-performance offset-fin plates and extended surfaces have allowed increases in the local convective Stanton number up to a factor of 3.5. The offset-fin plates were distributed along the inner and outer cylindrical liners, while the transition liners complex geometry called for roughened wall to increase the heat transfer rate.

The specific coolant flow (i.e., the coolant mass flow per surface area) has been reduced by 52 percent with respect to a conventional convection-film cooling combustor.

Figure 72 shows the lay-out of the final configuration.

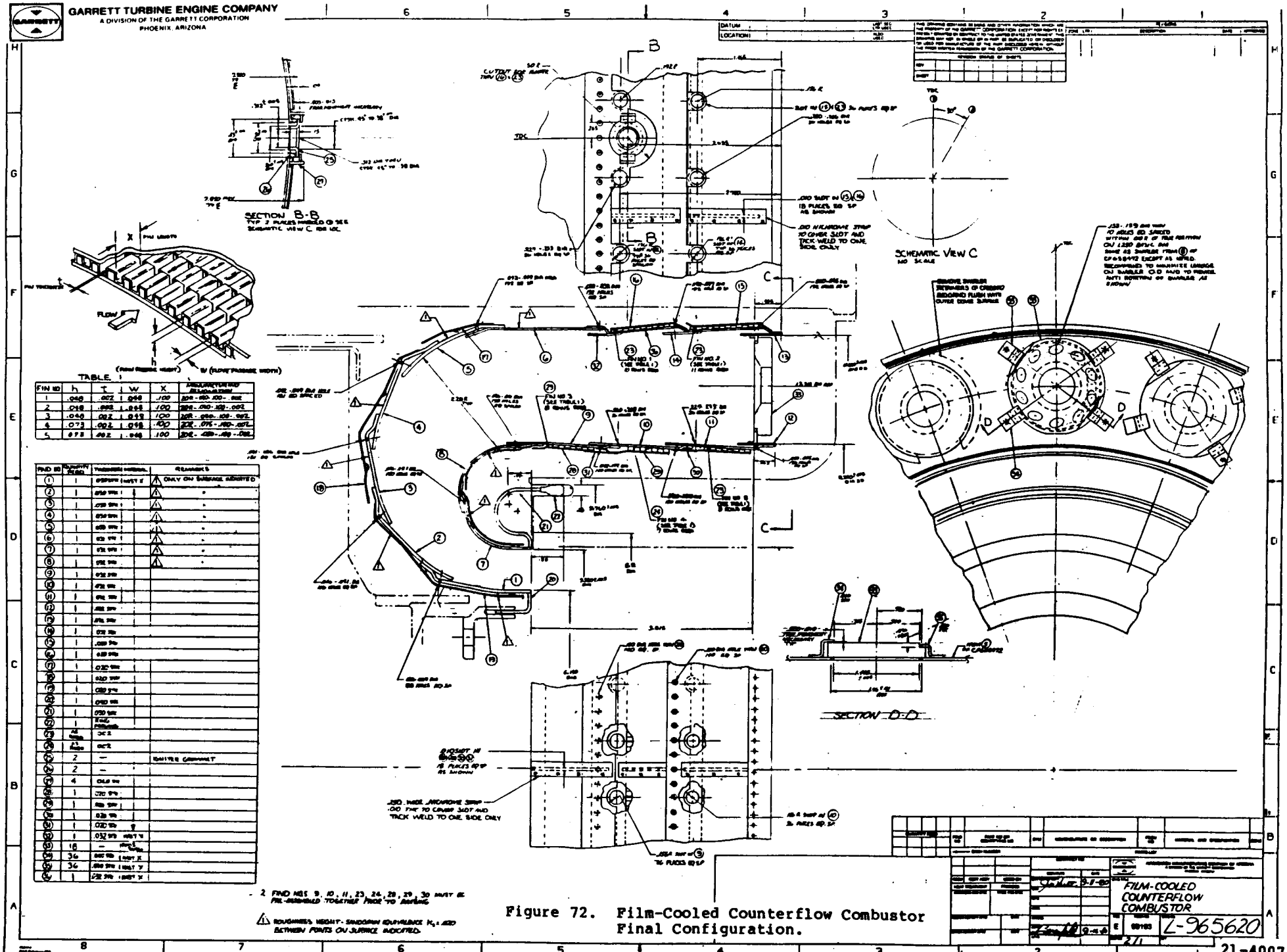

Figure 72. Film-Cooled Counterflow Combustor Final Configuration.

REFERENCES

1. H. Schlichting, "Boundary Layer Theory," McGraw Hill Book Co., 6th Edition, 1968.

2. Owen, P. R., and W. R. Thompson, "Heat-Transfer Across Rough Surfaces," Journal of Fluid Mechanics, Vol. 15, Part 3, March 1963, p 321-334.

3. Dirling, R. B., "A Method for Computing Roughwall Heat-Transfer Rates on Reentry Nosetips," AIAA Paper No. 73-763 presented at the AIAA 8th Thermophysics Conference, Palm Springs, California, July 16-18, 1973.

4. G. J. Sturgess, "Account of Film Turbulence for Predicting Film Cooling Effectiveness in Gas Turbine Combustors," ASME paper 79-GT-200.

APPENDIX 1

APPENDIX I

AIRFLOW DISTRIBUTION, CYLINDRICAL LINERS

(8 Pages)

GARRETT TURBINE ENGINE COMPANY
A DIVISION OF THE GARRETT CORPORATION
PHOENIX, ARIZONA

COMBUSTOR NASA AND95 SEPT.60

INPUT DATA -

PICTURE WILL NOT BE PLOTTED (IPIC = 0)
OUTPUT PRINTING OCCURS AFTER FINAL SOLUTION ONLY (IDBUG = 0)

OVERALL PRESSURE DROP - .0298
ANNULUS EFFECTIVE AREA FACTOR - .8300
AIR RATIO OF SPECIFIC HEATS - 1.400
AIR GAS CONSTANT - 52.300
ANNULUS WALL ROUGHNESS FACTOR - -0.0000
TANGENT OF SEPARATION SPREAD ANGLE - .1000
DRAG COEFFICIENT FOR INSERTED BLOCKAGE - 1.2000
NUMBER OF POSITION ELEMENTS - 58

DIMEN. AT DOWNSTREAM END OF ELEMENT

ELEM NO.	ELEM TYPE	XO OUTER LENGTH	RO OUTER RADIUS	XI INNER LENGTH	RI INNER RADIUS	CL ELEMENT LENGTH	WALL TEMP, R	INSERT AREA FACTOR	INSERT DIAMETER IN.	HOLE DIAM IN.	NUMBER OF HOLES	HOLE TYPE	DISCH COEFF	ORIFICE FLOW / FLOW IN
1	L	0.000	8.000	0.000	7.500	-0.000	1290.0	1.000	1.000					
2	L	1.000	8.000	1.000	7.500	-0.000	1290.0	1.000	1.000					
3	L	2.314	8.000	2.314	7.500	-0.000	1290.0	1.000	1.000					
5	L	3.000	8.000	3.000	7.300	-0.000	1290.0	1.000	1.000					
4	FB									-0.0000	0	0	*.0000	.0786
79	L	3.500	8.000	3.500	7.550	-0.000	1290.0	1.000	1.000					
6	L	4.250	8.000	4.250	7.650	-0.000	1860.0	1.000	1.000					
8	L	4.400	8.000	4.400	7.650	-0.000	1860.0	1.000	1.000					
7	L	4.425	8.000	4.425	7.600	-0.000	1860.0	1.000	1.000					
9	L	5.750	8.000	5.750	7.600	-0.000	1860.0	1.000	1.000					
10	L	5.840	8.000	5.840	7.630	-0.000	1860.0	1.000	1.000					
11	L	6.035	8.000	6.035	7.630	-0.000	1860.0	1.000	1.000					
13	FF									-0.0000	192	1	*.0000	.0100
12	L	6.230	8.000	6.230	7.550	-0.000	1290.0	1.000	1.000					
14	L	6.240	8.000	6.240	7.550	-0.000	1290.0	1.000	1.000					
15	FF									-0.0000	192	1	*.0000	.0600
16	FF									-0.0000	36	1	*.0000	.1247
17	L	6.242	8.000	6.242	7.600	-0.000	1290.0	1.000	1.000					
18	L	7.275	8.000	7.275	7.725	-0.000	1290.0	1.000	1.000					
19	L	7.500	8.000	7.500	7.575	-0.000	1290.0	1.000	1.000					
20	FF									-0.0000	192	1	*.0000	.0700
21	FF									-0.0000	36	1	*.0000	.1003
22	L	7.510	8.000	7.510	7.700	-0.000	1290.0	1.000	1.000					
23	L	7.620	8.000	7.620	7.650	-0.000	1290.0	1.000	1.000					
24	L	8.800	8.000	8.800	7.725	-0.000	1290.0	1.000	1.000					
25	L	9.025	8.000	9.025	7.507	-0.000	1290.0	1.000	1.000					
26	L	9.200	8.000	9.200	7.507	-0.000	1290.0	1.000	1.000					
27	L	10.040	8.000	9.200	7.507	-0.000	1290.0	1.000	1.000					
28	L	10.040	7.447	9.050	7.447	-0.000	1290.0	1.000	1.000					
29	L	10.040	6.659	9.050	6.659	-0.000	1290.0	1.000	1.000					
30	FF									-0.0000	1	1	*.0000	.0317
31	FF									-0.0000	180	5	.6000	.2543
32	L	10.040	5.650	9.050	5.650	-0.000	1290.0	1.000	1.000					
33	L	9.850	5.200	9.050	5.650	-0.000	1290.0	1.000	1.000					
78	L	9.200	4.954	9.050	5.600	-0.000	1290.0	1.000	1.000					
34	L	8.850	4.954	8.850	5.550	-0.000	1290.0	1.000	1.000					
35	L	8.800	4.954	8.800	5.500	-0.000	1290.0	1.000	1.000					

ELEM NO.	ELEM TYPE	XO OUTER LENGTH	RO OUTER RADIUS	XI INNER LENGTH	RI INNER RADIUS	CL ELEMENT LENGTH	WALL TEMP, R	INSERT AREA FACTOR	INSERT DIAMETER IN.	HOLE DIAM IN.	NUMBER OF HOLES	HOLE TYPE	DISCH COEFF	ORIFICE FLOW / FLOW IN
36	FF									-0.0000	196	1	*.0000	.0200
37	L	8.760	4.954	8.760	5.495	-0.000	1290.0	1.000	1.000					
38	L	8.680	4.954	8.680	5.495	-0.000	1290.0	1.000	1.000					
~~39~~	~~F~~									~~-0.0000~~	~~36~~	~~1~~	~~*.0000~~	~~.0757~~
40	L	8.670	4.954	8.670	5.420	-0.000	1290.0	1.000	1.000					
41	L	7.400	4.954	7.400	5.450	-0.000	1290.0	1.000	1.000					
42	FF									-0.0000	140	1	*.0000	.0200
43	L	7.290	4.954	7.290	5.500	-0.000	1290.0	1.000	1.000					
44	FF									-0.0000	36	1	*.0000	~~.1053~~
45	L	7.270	4.954	7.270	5.405	-0.000	1290.0	1.000	1.000					
46	L	6.560	4.954	6.560	5.450	-0.000	1290.0	1.000	1.000					
47	L	6.410	4.954	6.410	5.400	-0.000	1290.0	1.000	1.000					
48	L	4.930	4.954	4.930	5.500	-0.000	1290.0	1.000	1.000					
49	L	4.920	4.954	4.920	5.550	-0.000	1290.0	1.000	1.000					
50	FF									-0.0000	140	1	*.0000	.0140
51	L	4.710	4.954	4.710	5.500	-0.000	1290.0	1.000	1.000					
52	L	3.750	4.750	4.425	4.750	-0.000	1290.0	1.000	1.000					
53	L	3.720	4.740	4.425	4.740	-0.000	1290.0	1.000	1.000					
54	FF									-0.0000	150	1	*.0000	.0200
55	L	4.650	4.000	4.550	3.750	-0.000	1290.0	1.000	1.000					
56	FF									-0.0000	150	1	*.0000	.0154

START ITERATION NO. 1

COMBUSTOR NASA ANDSS SEPT.90

OUTPUT RESULTS - PAGE 1

ELEM NO	ELEM TYPE	SWIRL ANGLE	FLOW RATE LB/S	MACH NO	FLOW VEL FPS	AXIAL VEL FPS	TANG VEL FPS	TOTAL TEMP, R	STATIC TEMP, R	TOTAL PRESS, PSIA	STATIC PRESS, PSIA	DENSITY LB/FT3	DYNAM HEAD, PSIA	DYN HD /PTOT --
1	L	30.90	8.000	.0755	131.61	113.98	65.81	1290.0	1288.5	235.00	234.06	.5002	.935	.0040
2	L	28.52	8.000	.0745	129.77	114.00	61.99	1290.0	1288.6	234.93	234.02	.5000	.909	.0039
3	L	26.72	8.000	.0733	127.68	114.03	57.43	1290.0	1288.6	234.85	233.97	.4999	.879	.0037
5	L	29.16	8.000	.0657	114.49	99.97	55.82	1290.0	1288.9	234.81	234.10	.5001	.707	.0030
4	FB	31.21	7.371	.0618	107.68	92.09	55.82	1290.0	1289.0	234.81	234.18	.5002	.626	.0027
79	L	24.70	7.371	.0735	128.15	116.41	53.57	1290.0	1288.6	234.76	233.88	.4997	.886	.0038
6	L	18.62	7.371	.0903	157.55	149.29	50.34	1292.6	1290.5	234.66	233.32	.4978	1.334	.0057
8	L	18.27	7.371	.0902	157.32	149.38	49.33	1293.3	1291.2	234.64	233.31	.4975	1.329	.0057
7	L	18.28	7.371	.0895	156.19	148.30	49.01	1293.4	1291.4	234.62	233.31	.4974	1.310	.0056
9	L	18.71	7.371	.0795	139.02	131.67	44.62	1299.0	1297.3	234.49	233.45	.4955	1.033	.0044
10	L	17.16	7.371	.0851	148.81	142.18	43.92	1299.3	1297.5	234.48	233.30	.4951	1.183	.0050
11	L	16.79	7.371	.0850	148.62	142.28	42.94	1300.1	1298.3	234.46	233.28	.4947	1.179	.0050
13	FF	16.96	7.291	.0841	147.13	140.72	42.94	1300.1	1298.3	234.45	233.30	.4948	1.156	.0049
12	L	17.50	7.291	.0802	140.39	133.89	42.24	1300.1	1298.4	234.43	233.38	.4949	1.053	.0045
14	L	17.43	7.291	.0800	139.96	133.53	41.96	1300.1	1298.4	234.43	233.38	.4949	1.046	.0045
15	FF	21.13	6.811	.0665	116.34	108.51	41.96	1300.1	1299.0	234.43	233.70	.4954	.724	.0031
16	FF	24.37	5.814	.0581	101.64	92.57	41.96	1300.1	1299.2	234.43	233.88	.4956	.553	.0024
17	L	21.75	5.814	.0639	111.82	103.85	41.45	1300.1	1299.0	234.42	233.75	.4954	.668	.0029
18	L	13.93	5.814	.0885	154.77	150.22	37.28	1300.0	1298.0	234.28	233.00	.4942	1.278	.0055
19	L	14.61	5.814	.0822	143.92	139.26	36.32	1300.0	1298.3	234.19	233.09	.4943	1.105	.0047
20	FF	22.30	5.254	.0546	95.66	88.50	36.32	1300.0	1299.2	234.19	233.71	.4953	.489	.0021
21	FF	25.84	4.451	.0476	83.29	74.95	36.32	1300.0	1299.4	234.19	233.82	.4954	.371	.0016
22	L	18.58	4.451	.0636	111.25	105.45	35.47	1300.0	1299.0	234.16	233.50	.4949	.661	.0028
23	L	18.85	4.451	.0614	107.52	101.74	34.76	1300.0	1299.0	234.14	233.53	.4950	.617	.0026
24	L	14.69	4.451	.0679	118.82	114.94	30.15	1299.9	1298.7	234.03	233.28	.4946	.754	.0032
25	L	15.37	4.451	.0631	110.46	106.51	29.29	1299.9	1298.8	234.02	233.37	.4947	.651	.0028
26	L	16.01	4.451	.0597	104.49	100.43	28.83	1299.8	1298.9	234.01	233.43	.4948	.583	.0025
27	L	17.54	4.451	.0529	92.96	88.63	28.03	1299.8	1299.1	233.12	232.67	.4931	.460	.0020
28	L	18.81	4.451	.0508	89.64	84.85	28.91	1299.8	1299.1	232.30	231.88	.4914	.426	.0018
29	L	22.00	4.451	.0479	84.57	78.40	31.70	1299.7	1299.1	232.25	231.88	.4914	.379	.0016
30	FF	41.54	4.198	.0271	47.78	35.75	31.70	1299.7	1299.5	232.25	232.13	.4918	.121	.0005
31	FF	59.81	2.163	.0208	36.66	18.42	31.70	1299.7	1299.6	232.25	232.18	.4919	.071	.0003
32	L	58.06	2.163	.0233	41.08	21.71	34.87	1299.7	1299.5	232.23	232.15	.4918	.090	.0004
33	L	55.52	2.163	.0244	43.13	24.40	35.56	1299.7	1299.5	232.14	232.04	.4916	.099	.0004
78	L	45.55	2.163	.0281	49.64	34.75	35.45	1299.6	1299.4	231.96	231.84	.4912	.131	.0006
34	L	41.62	2.163	.0294	51.98	38.85	34.54	1299.6	1299.4	231.95	231.81	.4912	.143	.0006
35	L	38.74	2.163	.0309	54.65	42.61	34.21	1299.6	1299.4	231.95	231.79	.4912	.158	.0007
36	FF	40.90	2.003	.0296	52.22	39.46	34.21	1299.6	1299.4	231.95	231.81	.4912	.145	.0006
37	L	40.26	2.003	.0296	52.23	39.84	33.77	1299.6	1299.4	231.95	231.81	.4912	.145	.0006
38	L	39.77	2.003	.0294	51.85	39.84	33.18	1299.6	1299.4	231.95	231.81	.4912	.143	.0006
39	F	50.03	1.398	.0245	43.29	27.79	33.18	1299.6	1299.5	231.95	231.85	.4912	.099	.0004
40	L	45.26	1.398	.0262	46.19	32.50	32.82	1299.6	1299.4	231.94	231.83	.4912	.113	.0005
41	L	41.32	1.398	.0230	40.55	30.44	26.79	1299.5	1299.4	231.93	231.84	.4913	.087	.0004
42	FF	44.80	1.238	.0215	38.00	26.96	26.79	1299.5	1299.4	231.93	231.86	.4913	.077	.0003
43	L	44.92	1.238	.0208	36.73	26.00	25.94	1299.5	1299.4	231.93	231.86	.4913	.072	.0003
44	FF	73.27	.395	.0153	27.09	7.78	25.94	1299.5	1299.4	231.93	231.89	.4914	.039	.0002
45	L	69.13	.395	.0151	26.73	9.51	24.98	1299.5	1299.4	231.93	231.89	.4914	.038	.0002
46	L	65.15	.395	.0116	20.51	8.61	18.61	1299.3	1299.3	231.92	231.90	.4914	.022	.0001
47	L	61.02	.395	.0112	19.87	9.62	17.38	1299.3	1299.3	231.92	231.90	.4914	.021	.0001
48	L	51.20	.395	.0070	12.42	7.78	9.68	1299.0	1299.0	231.92	231.91	.4915	.008	.0000
49	L	50.90	.395	.0069	12.19	7.68	9.46	1299.0	1299.0	231.92	231.91	.4915	.008	.0000

COMBUSTOR NASA AND95 SEPT.80

OUTPUT RESULTS - PAGE 1

ELEM NO	ELEM TYPE	SWIRL ANGLE	FLOW RATE LB/S	MACH NO	FLOW VEL FPS	AXIAL VEL FPS	TANG VEL FPS	TOTAL TEMP, R	STATIC TEMP, R	TOTAL PRESS, PSIA	STATIC PRESS, PSIA	DENSITY LB/FT3	DYNAM HEAD, PSIA	DYN HD /PTOT --
50	FF	61.72	.283	.0061	10.74	5.08	9.46	1299.0	1299.0	231.92	231.91	.4915	.006	.0000
51	L	57.25	.283	.0058	10.31	5.57	8.68	1299.0	1299.0	231.92	231.91	.4916	.006	.0000
52	L	54.44	.283	.0048	8.53	4.96	6.95	1298.9	1298.9	231.95	231.95	.4917	.004	.0000
53	L	54.13	.283	.0048	8.45	4.95	6.85	1298.9	1298.9	231.95	231.95	.4917	.004	.0000
54	FF	73.14	.123	.0041	7.16	2.07	6.85	1298.9	1298.9	231.95	231.95	.4917	.003	.0000
55	L	31.51	.123	.0047	8.38	7.14	4.36	1298.7	1298.7	231.95	231.95	.4917	.004	.0000
56	FF	89.02	.001	.0025	4.38	.07	4.38	1298.7	1298.7	231.95	231.95	.4917	.001	.0000

COMBUSTOR NASA AND95 SEPT.80

OUTPUT RESULTS - PAGE 2

		/********** ANNULUS GEOMETRIC PARAMETERS ******** /							********** ORIFICE PARAMETERS ********** /							
ELEM NO.	ELEM TYPE	MEAN RADIUS IN.	CHANNEL WIDTH IN.	ANN AREA IN2	AN EFF AREA IN2	WAKE AREA FACTOR	SEPAR AREA FACTOR	ATTCH LENGTH IN.	HOLE DIAM IN.	DISCH COEFF -	JET ANGLE DEG	ORIF GEOM AREA	ORIF EFF AREA	ORIF CUMUL EF AREA	JET VELOCITY FPS	ORIF FLOW /WIN
1	L	7.750	.500	24.35	17.50	1.000	1.000	0.000								
2	L	7.750	.500	24.35	17.75	1.000	1.000	0.000								
3	L	7.750	.500	24.35	18.05	1.000	1.000	0.000								
5	L	7.650	.700	33.65	20.12	1.000	.825	0.000								
4	FB	7.650	.700	33.65	19.71	1.000	.825	0.000	-0.0000	*.0000	0.00	0.000	0.000	0.000	0.00	.0786
79	L	7.775	.450	21.98	16.58	1.000	1.000	0.000								
6	L	7.825	.350	17.21	13.53	1.000	1.000	0.000								
8	L	7.825	.350	17.21	13.56	1.000	1.000	0.000								
7	L	7.800	.400	19.60	13.66	1.000	.884	0.000								
9	L	7.800	.400	19.60	15.41	1.000	1.000	.439								
10	L	7.815	.370	18.17	14.41	1.000	1.000	0.000								
11	L	7.815	.370	18.17	14.44	1.000	1.000	0.000								
13	FF	7.815	.370	18.17	14.42	1.000	1.000	0.000	.0293	.5154	65.03	.129	.067	.067	350.11	.0100
12	L	7.775	.450	21.98	15.11	1.000	.868	0.000								
14	L	7.775	.450	21.98	15.16	1.000	.871	0.000								
15	FF	7.775	.450	21.98	17.02	1.000	1.000	0.000	.0707	.5306	67.20	.753	.400	.466	349.34	.0600
16	FF	7.775	.450	21.98	16.62	1.000	1.000	0.000	.2289	.5601	72.03	1.482	.830	1.296	349.41	.1247
17	L	7.800	.400	19.60	15.11	1.000	1.000	0.000								
18	L	7.862	.275	13.59	10.94	1.000	1.000	0.000								
19	L	7.787	.425	20.80	11.77	1.000	.705	0.000								
20	FF	7.787	.425	20.80	15.97	1.000	1.000	0.000	.0775	.5254	66.46	.905	.476	1.772	342.95	.0700
21	FF	7.787	.425	20.80	15.53	1.000	1.000	0.000	.2044	.5757	75.08	1.181	.680	2.452	343.08	.1003
22	L	7.850	.300	14.80	11.64	1.000	1.000	0.000								
23	L	7.825	.350	17.21	12.04	1.000	.891	0.000								
24	L	7.862	.275	13.59	10.91	1.000	1.000	0.000								
25	L	7.754	.493	23.49	11.73	1.000	.611	0.000								
26	L	7.754	.493	23.99	12.40	1.000	.648	0.000								
27	L	7.754	.974	47.44	13.98	1.000	.372	0.000								
28	L	7.447	.990	46.32	14.55	1.000	.400	0.000								
29	L	6.659	.990	41.42	15.42	1.000	.484	0.000								

		/********** ANNULUS GEOMETRIC PARAMETERS ******** /							********** ORIFICE PARAMETERS **********							
ELEM NO.	ELEM TYPE	MEAN RADIUS IN.	CHANNEL WIDTH IN.	ANN AREA IN2	AN EFF AREA IN2	WAKE AREA FACTOR	SEPAR AREA FACTOR	ATTCH LENGTH IN.	HOLE DIAM IN.	DISCH COEFF -	JET ANGLE DEG	ORIF GEOM AREA	ORIF EFF AREA	ORIF CUMUL EF AREA	JET VELOCITY FPS	ORIF FLOW /WIN
30	FF	6.659	.990	41.42	25.72	1.000	1.000	0.000	.7659	.5667	73.22	.461	.261	2.713	234.59	.0317
31	FF	6.659	.990	41.42	17.27	1.000	1.000	0.000	.1571	.6000	90.00	3.488	2.093	4.806	284.64	.2543
32	L	5.650	.990	35.14	15.42	1.000	1.000	0.000								
33	L	5.425	.916	31.29	14.69	1.000	1.000	0.000								
78	L	5.277	.663	21.99	12.77	1.000	1.000	0.000								
34	L	5.252	.596	19.67	12.20	1.000	1.000	0.000								
35	L	5.227	.546	17.93	11.61	1.000	1.000	0.000								
36	FF	5.227	.546	17.93	11.25	1.000	1.000	0.000	.0433	.5916	78.95	.289	.171	4.977	274.48	.0200
37	L	5.225	.541	17.76	11.24	1.000	1.000	0.000								
38	L	5.225	.541	17.76	11.33	1.000	1.000	0.000								
39	F	5.225	.541	17.76	9.46	1.000	1.000	0.000	.1958	.5972	80.77	1.084	.647	5.624	274.39	.0757
40	L	5.187	.466	15.19	8.87	1.000	1.000	0.000								
41	L	5.202	.496	16.21	10.10	1.000	1.000	.211								
42	FF	5.202	.496	16.21	9.54	1.000	1.000	0.000	.0509	.6007	81.97	.285	.171	5.795	273.83	.0200
43	L	5.227	.546	17.93	9.68	1.000	.938	0.000								
44	FF	5.227	.546	17.93	4.28	1.000	1.000	0.000	.2294	.6062	84.92	1.433	.902	6.697	273.79	.1053
45	L	5.179	.451	14.68	4.33	1.000	1.000	0.000								
46	L	5.202	.496	16.21	5.65	1.000	1.000	.160								
47	L	5.177	.446	14.51	5.83	1.000	1.000	0.000								
48	L	5.227	.546	17.93	9.32	1.000	1.000	.485								
49	L	5.252	.596	19.67	9.50	1.000	.923	0.000								
50	FF	5.252	.596	19.67	7.73	1.000	1.000	0.000	.0423	.6102	87.81	.197	.120	6.817	273.40	.0140
51	L	5.227	.546	17.93	8.05	1.000	1.000	0.000								
52	L	4.750	.675	20.15	9.72	1.000	1.000	.698								
53	L	4.740	.705	21.00	9.61	1.000	.962	0.000								
54	FF	4.740	.705	21.00	5.04	1.000	1.000	0.000	.0487	.6107	88.73	.279	.171	6.987	274.55	.0200
55	L	3.875	.250	6.09	4.31	1.000	1.000	0.000								
56	FF	3.875	.250	6.09	.08	1.000	1.000	0.000	.0427	.6108	89.13	.215	.131	7.119	274.49	.0154

OVERALL FLOW COEFFICIENT = .4856
INLET CORRECTED FLOW, LB/S = .789
DISCHARGE PRESSURE, PSIA = 228.00
PRESSURE DROP / PT INLET = .0298
TOTAL GEOMETRIC AREA, IN2 = 12.236

COMBUSTOR NASA - TRANSITION LINER

ORIFICE ELEM 27 F	
WO	0.2799
NO	192
DO	0.0346
GA	0.181
EA	0.155
CD	0.855
JA	0.00
JV	335.

ORIFICE ELEM 28 F	
WO	0.2544
NO	181
DO	0.0341
GA	0.165
EA	0.141
CD	0.853
JA	0.00
JV	335.

ORIFICE ELEM 29 F	
WO	0.1654
NO	151
DO	0.0300
GA	0.107
EA	0.091
CD	0.854
JA	0.00
JV	335.

INLET ELEM 1	ANNULUS ELEM 2	ANNULUS ELEM 3	ANNULUS ELEM 4	ANNULUS ELEM 5	ANNULUS ELEM 6	ANNULUS ELEM 7	ANNULUS ELEM 8	ANNULUS ELEM 9	ANNULUS ELEM 10	ANNULUS ELEM 11	ANNULUS ELEM 12	ANNULUS ELEM 13	ANNULUS ELEM 14	ANNULUS ELEM 15	ANNULUS ELEM 16	ANNULUS ELEM 17	ANNULUS ELEM 18	ANNULUS ELEM 19	ANNULUS ELEM 20
W	0.629	0.629	0.629	0.629	0.453	0.453	0.453	0.453	0.453	0.453	0.453	0.453	0.453	0.453	0.453	0.189	0.189	0.189	0.189
TT	1290.	1290.	1290.	1290.	1290.	1290.	1290.	1290.	1290.	1290.	1290.	1290.	1290.	1290.	1290.	1290.	1290.	1290.	1290.
PT	233.83	233.83	233.83	233.83	233.83	233.83	233.83	233.83	233.83	233.83	233.83	233.83	233.83	233.83	233.83	233.83	233.83	233.83	233.83
PS	233.82	233.82	233.82	233.82	233.82	233.82	233.82	233.82	233.81	233.81	233.81	233.81	233.79	233.79	233.79	233.81	233.81	233.81	233.81
M	0.005	0.009	0.008	0.007	0.006	0.007	0.006	0.007	0.010	0.010	0.010	0.012	0.015	0.014	0.014	0.008	0.009	0.009	0.010
SA	30.00	29.84	33.96	40.35	52.09	48.41	51.76	53.04	35.77	36.39	38.49	30.85	25.46	30.48	31.48	66.83	65.73	68.00	73.45
V	16.	16.	15.	13.	11.	12.	11.	12.	17.	17.	17.	21.	26.	25.	24.	15.	15.	16.	17.
AV	14.	14.	12.	10.	7.	8.	7.	7.	14.	14.	13.	18.	23.	21.	21.	6.	6.	6.	5.
TV	8.	8.	8.	8.	9.	9.	9.	10.	10.	10.	10.	11.	11.	13.	13.	13.	14.	15.	16.
DE	0.490	0.490	0.490	0.490	0.490	0.490	0.490	0.490	0.490	0.490	0.490	0.490	0.490	0.490	0.490	0.490	0.490	0.490	0.490
Q	0.0001	0.0001	0.0000	0.0000	0.0000	0.0000	0.0000	0.0000	0.0001	0.0001	0.0001	0.0001	0.0001	0.0001	0.0001	0.0000	0.0001	0.0001	0.0001

8.00

7.68

FIXED INPUT VALUES -

ANNULUS WALL ROUGHNESS FACTOR	=	0.0000
ANNULUS EFFECTIVE AREA FACTOR	=	0.8300
TANGENT OF SEPARATION SPREAD ANGLE	=	0.1000
DRAG COEFFICIENT FOR INSERTED BLOCKAGE	=	1.2000
AIR RATIO OF SPECIFIC HEATS	=	1.4000
AIR GAS CONSTANT	=	53.3000

OVERALL OUTPUT VALUES -

INLET CORRECTED FLOW, LB/S	=	0.0623
OVERALL PRESSURE DROP	=	0.0249
TOTAL GEOMETRIC AREA, IN2	=	0.6475
OVERALL FLOW COEFFICIENT	=	0.8601
DISCHARGE PRESSURE, PSIA	=	228.0006

NOMENCLATURE

ORIFICE ELEMENT XX F = FIXED FLOW PERCENT
ORIFICE ELEMENT XX D = FIXED HOLE DIAMETER
ORIFICE ELEMENT XX B = BLEED FLOW EXTRACTED

W = AIR MASS FLOW RATE, LB/SEC
TT = TOTAL TEMPERATURE, R
PT = TOTAL PRESSURE, PSIA
PS = STATIC PRESSURE, PSIA
M = MACH NUMBER
SA = SWIRL ANGLE, DEGREES FROM AXIAL
V = TOTAL FLOW VELOCITY, FPS
AV = AXIAL FLOW VELOCITY, FPS
TV = TANGENTIAL FLOW VELOCITY, FPS
DE = DENSITY, LB/CU FT
Q = DYNAMIC HEAD / PT LOCAL
WO = ORIFICE FLOW / INLET FLOW
NO = NUMBER OF ORIFICES
DO = ORIFICE DIAMETER, IN.
GA = STATION GEOMETRIC AREA, SQ. IN.
EA = STATION EFFECTIVE AREA, SQ. IN.
CD = ORIFICE DISCHARGE COEFFICIENT
JA = JET INJECTION ANGLE, DEGREES
JV = JET INJECTION VELOCITY, FPS

2.97

2.50

ANNULUS ELEM 26	ANNULUS ELEM 25	ANNULUS ELEM 24	ANNULUS ELEM 23	ANNULUS ELEM 22	ANNULUS ELEM 21
W	0.189	0.189	0.189	0.189	0.189
TT	1290.	1290.	1290.	1290.	1290.
PT	233.81	233.81	233.82	233.82	233.83
PS	233.75	233.74	233.66	233.80	233.81
M	0.019	0.021	0.031	0.012	0.011
SA	35.60	34.18	20.04	60.96	70.84
V	34.	36.	54.	21.	19.
AV	28.	30.	51.	10.	6.
TV	20.	20.	19.	18.	18.
DE	0.490	0.490	0.489	0.490	0.490
Q	0.0003	0.0003	0.0007	0.0001	0.0001

ORIFICE ELEM 31 F	
WO	0.1272
NO	88
DO	0.0345
GA	0.082
EA	0.070
CD	0.854
JA	0.00
JV	334.

ORIFICE ELEM 30 F	
WO	0.1730
NO	116
DO	0.0351
GA	0.112
EA	0.096
CD	0.851
JA	0.00
JV	334.

ORIFICE ELEM 4 B	ORIFICE ELEM 13 F	ORIFICE ELEM 15 F
WO 0.0786	WO 0.0100	WO 0.0600
NO 0	NO 192	NO 192
DO 0.0000	DO 0.0294	DO 0.0712
GA 0.000	GA 0.131	GA 0.764
EA 0.000	EA 0.067	EA 0.404
CD 0.000	CD 0.514	CD 0.529
JA 0.00	JA 64.80	JA 66.96
JV 0.	JV 347.	JV 346.

INLET ELEM 1	ANNULUS ELEM 2	ANNULUS ELEM 3	ANNULUS ELEM 5.	ANNULUS ELEM 79	ANNULUS ELEM 6	ANNULUS ELEM 8	ANNULUS ELEM 7	ANNULUS ELEM 9	ANNULUS ELEM 10	ANNULUS ELEM 11	ANNULUS ELEM 12	ANNULUS ELEM 14
W 8.000	W 8.000	W 8.000	W 8.000	W 7.371	W 7.371	W 7.371	W 7.371	W 7.371	W 7.371	W 7.371	W 7.291	W 7.291
TT 1290.	TT 1290.	TT 1290.	TT 1290.	TT 1290.	TT 1293.	TT 1293.	TT 1293.	TT 1299.	TT 1299.	TT 1300.	TT 1300.	TT 1300.
PT 235.00	PT 234.93	PT 234.85	PT 234.77	PT 234.68	PT 234.57	PT 234.55	PT 234.52	PT 234.39	PT 234.37	PT 234.35	PT 234.30	PT 234.30
PS 234.06	PS 234.02	PS 233.97	PS 234.06	PS 233.80	PS 233.23	PS 233.22	PS 233.21	PS 233.35	PS 233.19	PS 233.17	PS 233.25	PS 233.26
M 0.076	M 0.074	M 0.073	M 0.066	M 0.074	M 0.090	M 0.090	M 0.090	M 0.080	M 0.085	M 0.085	M 0.080	M 0.080
SA 30.00	SA 28.52	SA 26.72	SA 29.16	SA 24.69	SA 18.62	SA 18.26	SA 18.27	SA 18.70	SA 17.15	SA 16.78	SA 17.49	SA 17.43
V 132.	V 130.	V 128.	V 115.	V 128.	V 158.	V 157.	V 156.	V 139.	V 149.	V 149.	V 140.	V 140.
AV 114.	AV 114.	AV 114.	AV 100.	AV 116.	AV 149.	AV 149.	AV 148.	AV 132.	AV 142.	AV 142.	AV 134.	AV 134.
TV 66.	TV 62.	TV 57.	TV 56.	TV 54.	TV 50.	TV 49.	TV 49.	TV 45.	TV 44.	TV 43.	TV 42.	TV 42.
DE 0.500	DE 0.500	DE 0.500	DE 0.500	DE 0.500	DE 0.498	DE 0.497	DE 0.497	DE 0.495	DE 0.495	DE 0.495	DE 0.495	DE 0.495
Q 0.0040	Q 0.0039	Q 0.0037	Q 0.0030	Q 0.0038	Q 0.0057	Q 0.0057	Q 0.0056	Q 0.0044	Q 0.0050	Q 0.0050	Q 0.0045	Q 0.0045

8.00

7.50

FIXED INPUT VALUES -

ANNULUS WALL ROUGHNESS FACTOR	=	0.0000
ANNULUS EFFECTIVE AREA FACTOR	=	0.8300
TANGENT OF SEPARATION SPREAD ANGLE	=	0.1000
DRAG COEFFICIENT FOR INSERTED BLOCKAGE	=	1.2000
AIR RATIO OF SPECIFIC HEATS	=	1.4000
AIR GAS CONSTANT	=	52.3000

OVERALL OUTPUT VALUES -

INLET CORRECTED FLOW, LB/S	=	0.7892
OVERALL PRESSURE DROP	=	0.0298
TOTAL GEOMETRIC AREA, IN2	=	12.8128
OVERALL FLOW COEFFICIENT	=	0.4637
DISCHARGE PRESSURE, PSIA	=	227.9970

ORIFICE ELEM 16 F	ORIFICE ELEM 20 F	ORIFICE ELEM 21 F	ORIFICE ELEM 30 F	ORIFICE ELEM 31 F
WO 0.1247	WO 0.0700	WO 0.1003	WO 0.0317	WO 0.2543
NO 36	NO 192	NO 36	NO 1	NO 180
DO 0.2303	DO 0.0786	DO 0.2069	DO 0.8182	DO 0.1611
GA 1.500	GA 0.932	GA 1.210	GA 0.526	GA 3.669
EA 0.839	EA 0.486	EA 0.695	EA 0.275	EA 2.201
CD 0.559	CD 0.522	CD 0.574	CD 0.523	CD 0.600
JA 71.83	JA 65.92	JA 74.75	JA 66.07	JA 90.00
JV 346.	JV 336.	JV 336.	JV 271.	JV 271.

ANNULUS ELEM 17	ANNULUS ELEM 18	ANNULUS ELEM 19	ANNULUS ELEM 22	ANNULUS ELEM 23	ANNULUS ELEM 24	ANNULUS ELEM 25	ANNULUS ELEM 26	ANNULUS ELEM 27	ANNULUS ELEM 28	ANNULUS ELEM 29
W 5.814	W 5.814	W 5.814	W 4.451	W 4.451	W 4.451	W 4.451	W 4.451	W 4.451	W 4.451	W 4.451
TT 1300.	TT 1300.	TT 1300.	TT 1300.	TT 1300.	TT 1300.	TT 1300.	TT 1300.	TT 1300.	TT 1300.	TT 1300.
PT 234.30	PT 234.11	PT 233.94	PT 233.91	PT 233.89	PT 233.76	PT 233.62	PT 233.61	PT 232.65	PT 231.87	PT 231.85
PS 233.63	PS 232.83	PS 232.84	PS 233.25	PS 233.28	PS 233.01	PS 232.97	PS 233.03	PS 232.19	PS 231.45	PS 231.19
M 0.064	M 0.088	M 0.082	M 0.064	M 0.061	M 0.068	M 0.063	M 0.060	M 0.053	M 0.051	M 0.064
SA 21.73	SA 13.92	SA 14.59	SA 18.56	SA 18.84	SA 14.67	SA 15.34	SA 15.98	SA 17.51	SA 18.77	SA 16.30
V 112.	V 155.	V 144.	V 111.	V 108.	V 119.	V 111.	V 105.	V 93.	V 90.	V 113.
AV 104.	AV 150.	AV 139.	AV 106.	AV 102.	AV 115.	AV 107.	AV 101.	AV 89.	AV 85.	AV 109.
TV 41.	TV 37.	TV 36.	TV 35.	TV 35.	TV 30.	TV 29.	TV 29.	TV 28.	TV 29.	TV 32.
DE 0.495	DE 0.494	DE 0.494	DE 0.494	DE 0.494	DE 0.494	DE 0.494	DE 0.494	DE 0.492	DE 0.491	DE 0.490
Q 0.0029	Q 0.0055	Q 0.0047	Q 0.0028	Q 0.0026	Q 0.0032	Q 0.0028	Q 0.0025	Q 0.0020	Q 0.0018	Q 0.0029

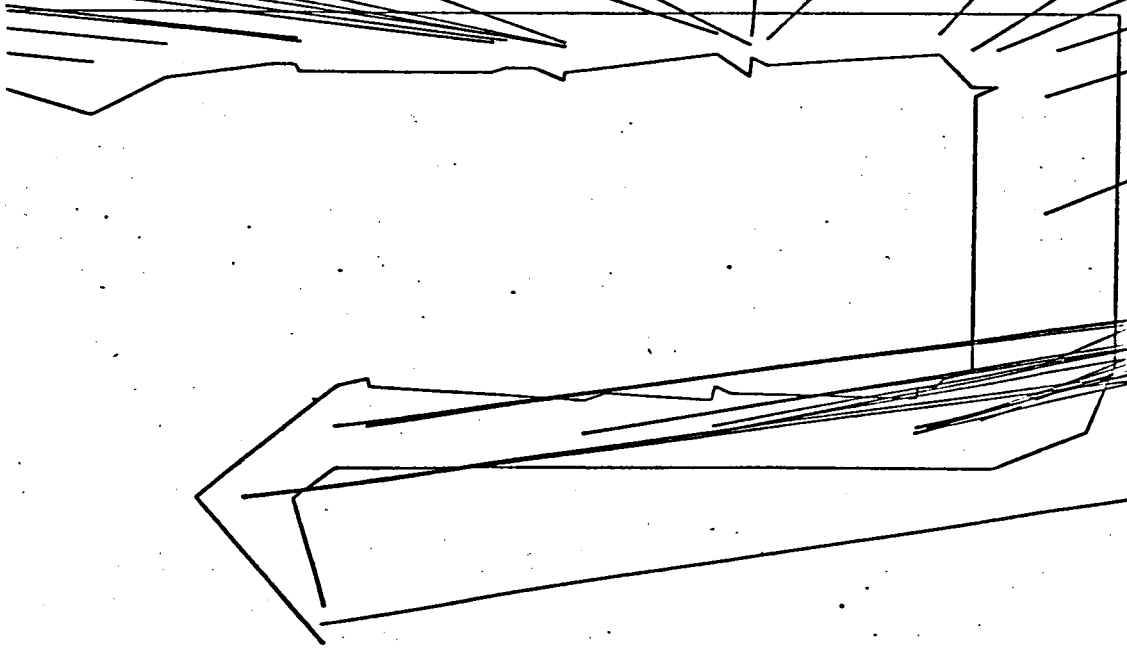

NOMENCLATURE

ORIFICE ELEMENT XX F = FIXED FLOW PERCENT
ORIFICE ELEMENT XX D = FIXED HOLE DIAMETER
ORIFICE ELEMENT XX B = BLEED FLOW EXTRACTED

W = AIR MASS FLOW RATE, LB/SEC
TT = TOTAL TEMPERATURE, R
PT = TOTAL PRESSURE, PSIA
PS = STATIC PRESSURE, PSIA
M = MACH NUMBER
SA = FLOW ANGLE, DEGREES FROM AXIAL
V = TOTAL FLOW VELOCITY, FPS
AV = AXIAL FLOW VELOCITY, FPS
TV = TANGENTIAL FLOW VELOCITY, FPS
DE = DENSITY, LB/CU FT
Q = DYNAMIC HEAD / PT LOCAL
WO = ORIFICE FLOW / INLET FLOW
NO = NUMBER OF ORIFICES
DO = ORIFICE DIAMETER, IN.
GA = STATION GEOMETRIC AREA, SQ. IN.
EA = STATION EFFECTIVE AREA, SQ. IN.
CD = ORIFICE DISCHARGE COEFFICIENT
JA = JET INJECTION ANGLE, DEGREES
JV = JET INJECTION VELOCITY, FPS

ORIFICE ELEM 36 F	ORIFICE ELEM 39	ORIFICE ELEM 42 F	ORIFICE ELEM 44 F
WO 0.02C0	WO 0.0757	WO 0.0200	WO 0.1053
NO 196	NO 36	NO 140	NO 36
DO 0.0447	DO 0.2020	DO 0.0525	DO 0.2364
GA 0.3C8	GA 1.154	GA 0.303	GA 1.581
EA 0.181	EA 0.687	EA 0.182	EA 0.957
CD 0.589	CD 0.595	CD 0.599	CD 0.606
JA 78.17	JA 80.12	JA 81.41	JA 84.56
JV 259.	JV 259.	JV 259.	JV 258.

ANNULUS ELEM 32	ANNULUS ELEM 33	ANNULUS ELEM 78	ANNULUS ELEM 34	ANNULUS ELEM 35	ANNULUS ELEM 37	ANNULUS ELEM 38	ANNULUS ELEM 40	ANNULUS ELEM 41	ANNULUS ELEM 43	ANNULUS ELEM 45	ANNULUS ELEM 46	ANNULUS ELEM 47	ANNULUS ELEM 48
W 2.163	W 2.163	W 2.163	W 2.163	W 2.163	W 2.003	W 2.003	W 1.398	W 1.398	W 1.238	W 0.395	W 0.395	W 0.395	W 0.395
TT 1300.	TT 1300.	TT 1300.	TT 1300.	TT 1300.	TT 1300.	TT 1300.	TT 1300.	TT 1299.	TT 1299.	TT 1299.	TT 1299.	TT 1299.	TT 1299.
PT 231.84	PT 231.73	PT 231.53	PT 231.52	PT 231.52	PT 231.52	PT 231.52	PT 231.51	PT 231.50	PT 231.50	PT 231.50	PT 231.49	PT 231.49	PT 231.49
PS 231.75	PS 231.63	PS 231.39	PS 231.38	PS 231.36	PS 231.37	PS 231.37	PS 231.40	PS 231.41	PS 231.43	PS 231.46	PS 231.47	PS 231.47	PS 231.48
M 0.025	M 0.026	M 0.029	M 0.030	M 0.031	M 0.030	M 0.030	M 0.026	M 0.023	M 0.021	M 0.015	M 0.012	M 0.011	M 0.007
SA 54.74	SA 53.32	SA 44.93	SA 42.04	SA 39.26	SA 40.79	SA 40.29	SA 45.78	SA 41.84	SA 45.45	SA 69.46	SA 65.52	SA 61.42	SA 51.66
V 43.	V 45.	V 51.	V 53.	V 55.	V 53.	V 52.	V 47.	V 41.	V 37.	V 27.	V 21.	V 20.	V 13.
AV 25.	AV 27.	AV 36.	AV 39.	AV 43.	AV 40.	AV 40.	AV 33.	AV 31.	AV 26.	AV 10.	AV 9.	AV 10.	AV 8.
TV 35.	TV 36.	TV 36.	TV 35.	TV 35.	TV 34.	TV 34.	TV 33.	TV 27.	TV 26.	TV 25.	TV 19.	TV 18.	TV 10.
DE 0.491	DE 0.491	DE 0.490	DE 0.490	DE 0.49C	DE 0.490	DE 0.490	DE 0.490	DE 0.490	DE 0.490	DE 0.490	DE 0.491	DE 0.491	DE 0.491
Q 0.0004	Q 0.0005	Q 0.0006	Q 0.0006	Q 0.0007	Q 0.0006	Q 0.0006	Q 0.0005	Q 0.0004	Q 0.0003	Q 0.0002	Q 0.0001	Q 0.0001	Q 0.0000

ORIFICE ELEM 50 F	
WO	0.0140
NO	140
DO	0.0436
GA	0.209
EA	0.127
CD	0.610
JA	87.65
JV	258.

ORIFICE ELEM 54 F	
WO	0.0200
NO	150
DO	0.0503
GA	0.298
EA	0.182
CD	0.611
JA	88.63
JV	258.

ORIFICE ELEM 56 F	
WO	0.0154
NO	150
DO	0.0441
GA	0.229
EA	0.140
CD	0.611
JA	89.07
JV	258.

ANNULUS ELEM 49	
W	0.395
TT	1299.
PT	231.49
PS	231.48
M	0.007
SA	51.36
V	12.
AV	8.
TV	10.
DE	0.491
Q	0.0000

ANNULUS ELEM 51	
W	0.283
TT	1299.
PT	231.49
PS	231.48
M	0.006
SA	57.67
V	10.
AV	6.
TV	9.
DE	0.491
Q	0.0000

ANNULUS ELEM 52	
W	0.283
TT	1299.
PT	231.49
PS	231.48
M	0.005
SA	54.86
V	9.
AV	5.
TV	7.
DE	0.491
Q	0.0000

ANNULUS ELEM 53	
W	0.283
TT	1299.
PT	231.49
PS	231.48
M	0.005
SA	54.28
V	9.
AV	5.
TV	7.
DE	0.491
Q	0.0000

ANNULUS ELEM 55	
W	0.123
TT	1299.
PT	231.49
PS	231.48
M	0.005
SA	31.42
V	8.
AV	7.
TV	4.
DE	0.491
Q	0.0000

APPENDIX II

APPENDIX II

AIRFLOW DISTRIBUTION, TRANSITION LINERS

(3 Pages)

GARRETT TURBINE ENGINE COMPANY
A DIVISION OF THE GARRETT CORPORATION
PHOENIX ARIZONA

XYXYXYXYXYXYXYXYXYXYXYXYXYXYXYXYXYXYXYXYXYXYXYXYXYXYXYXYXYXYXYXYXYXYXYXYXYXYXYXY
XYXYXYXYXYXYXYXYXYXYXYXYXYXYXYXYXYXYXYXYXYXYXYXYXYXYXYXYXYXYXYXYXYXYXYXYXYXYXYXY

COMBUSTOR NASA - TRANSITION LINER

INPUT DATA -

PICTURE WILL NOT BE PLOTTED (IPIC = 0)
OUTPUT PRINTING OCCURS AFTER FINAL SOLUTION ONLY (IDBUG = 0)

OVERALL PRESSURE DROP - .0249
ANNULUS EFFECTIVE AREA FACTOR - .8300
AIR RATIO OF SPECIFIC HEATS - 1.400
AIR GAS CONSTANT - 53.300
ANNULUS WALL ROUGHNESS FACTOR - -0.0000
TANGENT OF SEPARATION SPREAD ANGLE - .1000
DRAG COEFFICIENT FOR INSERTED BLOCKAGE - 1.2000
NUMBER OF POSITION ELEMENTS - 31

DIMEN. AT DOWNSTREAM END OF ELEMENT

ELEM NO.	ELEM TYPE	XO OUTER LENGTH	RO OUTER RADIUS	XI INNER LENGTH	RI INNER RADIUS	CL ELEMENT LENGTH	WALL TEMP, R	INSERT AREA FACTOR	INSERT DIAMETER IN.	HOLE DIAM IN.	NUMBER OF HOLES	HOLE TYPE	DISCH COEFF	ORIFICE FLOW / FLOW IN
1	L	0.000	8.000	0.000	7.680	-0.000	1290.0	1.000	1.000					
2	L	.500	8.000	.500	7.680	-0.000	1290.0	1.000	1.000					
3	L	1.000	8.000	1.000	7.560	-0.000	1290.0	1.000	1.000					
4	L	2.100	7.500	1.450	7.350	-0.000	1290.0	1.000	1.000					
5	L	2.100	7.400	1.450	7.250	-0.000	1290.0	1.000	1.000					
27	FF									-0.0000	192	3	*.0000	.2799
6	L	2.100	7.400	1.650	7.130	-0.000	1290.0	1.000	1.000					
7	L	2.100	7.400	1.800	7.050	-0.000	1290.0	1.000	1.000					
8	L	2.750	7.400	1.950	6.870	-0.000	1290.0	1.000	1.000					
9	L	2.750	6.500	2.200	6.500	-0.000	1290.0	1.000	1.000					
10	L	2.750	6.080	2.450	6.080	-0.000	1290.0	1.000	1.000					
11	L	2.750	6.050	2.350	6.050	-0.000	1290.0	1.000	1.000					
12	L	2.750	5.850	2.400	5.850	-0.000	1290.0	1.000	1.000					
13	L	2.750	5.750	2.500	5.750	-0.000	1290.0	1.000	1.000					
14	L	2.750	5.500	2.550	5.500	-0.000	1290.0	1.000	1.000					
15	L	2.750	4.800	2.500	4.800	-0.000	1290.0	1.000	1.000					
16	L	2.750	4.700	2.400	4.750	-0.000	1290.0	1.000	1.000					
28	FF									-0.0000	181	3	*.0000	.2544
29	FF									-0.0000	151	3	*.0000	.1654
17	L	2.750	4.400	2.330	4.400	-0.000	1290.0	1.000	1.000					
18	L	2.750	4.300	2.350	4.300	-0.000	1290.0	1.000	1.000					
19	L	2.750	4.000	2.200	4.000	-0.000	1290.0	1.000	1.000					
20	L	2.750	3.500	1.850	3.500	-0.000	1290.0	1.000	1.000					
21	L	2.750	2.960	1.700	3.500	-0.000	1290.0	1.000	1.000					
22	L	1.700	2.960	1.700	3.500	-0.000	1290.0	1.000	1.000					
23	L	1.500	2.960	1.500	3.300	-0.000	1290.0	1.000	1.000					
24	L	1.000	2.960	1.000	3.030	-0.000	1290.0	1.000	1.000					
25	L	.500	2.500	.500	2.850	-0.000	1290.0	1.000	1.000					
26	L	.495	2.500	.495	2.970	-0.000	1290.0	1.000	1.000					
30	FF									-0.0000	116	3	*.0000	.1730
31	FF									-0.0000	88	3	*.0000	.1272

START ITERATION NO. 1

COMBUSTOR NASA - TRANSITION LINER

OUTPUT RESULTS - PAGE 1

ELEM NO	ELEM TYPE	SWIRL ANGLE	FLOW RATE LB/S	MACH NO	FLOW VEL FPS	AXIAL VEL FPS	TANG VEL FPS	TOTAL TEMP, R	STATIC TEMP, R	TOTAL PRESS, PSIA	STATIC PRESS, PSIA	DENSITY LB/FT3	DYNAM HEAD, PSIA	DYN HD /PTOT --
1	L	30.00	.629	.0093	16.32	14.13	8.16	1290.0	1290.0	233.83	233.82	.4897	.014	.0001
2	L	23.96	.629	.0088	15.47	14.13	6.28	1290.0	1290.0	233.63	233.82	.4897	.013	.0001
3	L	21.90	.629	.0074	13.10	12.15	4.89	1290.0	1290.0	233.83	233.82	.4897	.009	.0000
4	L	20.71	.629	.0062	10.93	10.23	3.87	1290.0	1290.0	233.82	233.82	.4897	.006	.0000
5	L	20.71	.629	.0062	10.83	10.13	3.83	1290.0	1290.0	233.82	233.82	.4897	.006	.0000
27	FF	36.25	.453	.0037	6.48	5.23	3.83	1290.0	1290.0	233.82	233.82	.4897	.002	.0000
6	L	28.99	.453	.0044	7.66	6.70	3.71	1290.0	1290.0	233.82	233.82	.4897	.003	.0000
7	L	25.10	.453	.0048	8.47	7.67	3.59	1290.0	1290.0	233.82	233.81	.4897	.004	.0000
8	L	23.42	.453	.0044	7.70	7.07	3.06	1290.0	1290.0	233.82	233.81	.4897	.003	.0000
9	L	23.32	.453	.0044	7.78	7.14	3.08	1290.0	1290.0	233.81	233.81	.4897	.003	.0000
10	L	11.39	.453	.0081	14.28	14.00	2.82	1290.0	1290.0	233.81	233.80	.4897	.011	.0000
11	L	11.15	.453	.0080	14.06	13.79	2.72	1290.0	1290.0	233.81	233.80	.4897	.010	.0000
12	L	10.98	.453	.0077	13.62	13.37	2.60	1290.0	1290.0	233.81	233.80	.4897	.010	.0000
13	L	7.93	.453	.0102	17.93	17.76	2.47	1290.0	1290.0	233.81	233.79	.4897	.017	.0001
14	L	5.29	.453	.0132	23.31	23.21	2.15	1290.0	1290.0	233.81	233.78	.4896	.029	.0001
15	L	3.72	.453	.0121	21.32	21.28	1.38	1290.0	1290.0	233.80	233.78	.4896	.024	.0001
16	L	3.61	.453	.0119	20.91	20.86	1.32	1290.0	1290.0	233.80	233.78	.4896	.023	.0001
28	FF	7.59	.293	.0057	9.97	9.89	1.32	1290.0	1290.0	233.80	233.79	.4896	.005	.0000
29	FF	11.67	.189	.0037	6.51	6.37	1.32	1290.0	1290.0	233.80	233.80	.4897	.002	.0000
17	L	9.94	.189	.0036	6.35	6.26	1.10	1290.0	1290.0	233.80	233.80	.4897	.002	.0000
18	L	9.54	.189	.0036	6.32	6.24	1.05	1290.0	1290.0	233.80	233.80	.4897	.002	.0000
19	L	8.46	.189	.0036	6.28	6.21	.92	1290.0	1290.0	233.80	233.80	.4897	.002	.0000
20	L	7.84	.189	.0036	6.37	6.31	.87	1290.0	1290.0	233.80	233.80	.4897	.002	.0000
21	L	7.91	.189	.0037	6.52	6.46	.90	1290.0	1290.0	233.80	233.79	.4896	.002	.0000
22	L	7.87	.189	.0035	6.16	6.11	.84	1290.0	1290.0	233.78	233.77	.4896	.002	.0000
23	L	4.49	.189	.0057	10.04	10.01	.79	1290.0	1290.0	233.76	233.77	.4896	.005	.0000
24	L	.60	.189	.0289	50.83	50.83	.53	1290.0	1289.8	233.74	233.60	.4893	.136	.0006
25	L	.20	.189	.0175	30.80	30.80	.11	1290.0	1289.9	233.65	233.60	.4893	.050	.0002
26	L	.20	.189	.0164	28.78	28.78	.10	1290.0	1289.9	233.64	233.60	.4893	.044	.0002
30	FF	1.65	.080	.0020	3.52	3.51	.10	1290.0	1290.0	233.64	233.64	.4893	.001	.0000
31	FF	88.71	.000	.0001	.10	.00	.10	1290.0	1290.0	233.64	233.64	.4893	.000	.0000

COMBUSTOR NASA - TRANSITION LINER

OUTPUT RESULTS - PAGE 2

		/********** ANNULUS GEOMETRIC PARAMETERS ******** /							********** ORIFICE PARAMETERS ********** /								
ELEM NO.	ELEM TYPE	MEAN RADIUS IN.	CHANNEL WIDTH IN.	ANN AREA IN2	AN EFF ARLA IN2	WAKE AREA FACTOR	SEPAR AREA FACTOR	ATTCH LENGTH IN.	HOLE DIAM IN.	DISCH COEFF -	JET ANGLE DEG	ORIF GEOM AREA	ORIF EFF AREA	ORIF CUMUL EF AREA	JET VELOCITY FPS	ORIF FLOW /WIN	TOTAL COMBUSTION AIRFLOW %
1	L	7.840	.320	15.76	11.33	1.000	1.000	0.000									
2	L	7.840	.320	15.76	11.95	1.000	1.000	0.000									
3	L	7.780	.440	21.51	14.12	1.000	.853	0.000									
4	L	7.425	.667	31.12	16.91	1.000	.700	0.000									
5	L	7.325	.667	30.70	17.07	1.000	.716	0.000									
27	FF	7.325	.667	30.70	20.55	1.000	1.000	0.000	.0346	.8548	0.00	.181	.155	.155	334.62	.2799	2.2%
6	L	7.265	.525	23.96	17.39	1.000	1.000	0.000									
7	L	7.225	.461	20.93	15.73	1.000	1.000	0.000									
8	L	7.135	.960	43.02	17.28	1.000	.528	0.000									
9	L	6.500	.550	22.46	17.12	1.000	1.000	.401									
10	L	6.080	.300	11.46	9.32	1.000	1.000	0.000									
11	L	6.050	.400	15.21	9.47	1.000	.765	0.000									
12	L	5.850	.350	12.86	9.78	1.000	.933	0.000									
13	L	5.750	.250	9.03	7.42	1.000	1.000	0.000									
14	L	5.500	.200	6.91	5.71	1.000	1.000	0.000									
15	L	4.800	.250	7.54	6.24	1.000	1.000	.498									
16	L	4.725	.354	10.50	6.37	1.000	.733	0.000									
28	FF	4.725	.354	10.50	8.64	1.000	1.000	0.000	.0341	.8534	0.00	.165	.141	.296	333.96	.2544	1.99%
29	FF	4.725	.354	10.50	8.53	1.000	1.000	0.000	.0301	.8550	0.00	.107	.092	.387	333.96	.1654	1.30%
17	L	4.400	.420	11.61	8.75	1.000	.921	0.000									
18	L	4.300	.400	10.81	8.78	1.000	.993	0.000									
19	L	4.000	.550	13.82	8.84	1.000	.779	0.000									
20	L	3.500	.900	19.79	8.72	1.000	.536	0.000									
21	L	3.230	1.181	23.96	8.51	1.000	.432	0.000									
22	L	3.230	.540	10.96	9.01	1.000	1.000	.294									
23	L	3.130	.340	6.69	5.53	1.000	1.000	0.000									
24	L	2.995	.070	1.32	1.09	1.000	1.000	0.000									
25	L	2.675	.350	5.88	1.80	1.000	.370	0.000									
26	L	2.735	.470	8.08	1.93	1.000	.288	0.000									
30	FF	2.735	.470	8.08	6.70	1.000	1.000	0.000	.0354	.8523	0.00	.114	.097	.484	329.43	.1730	1.36%
31	FF	2.735	.470	8.08	.15	1.000	1.000	0.000	.0348	.8554	0.00	.084	.071	.555	329.44	.1272	1.00%

OVERALL FLOW COEFFICIENT = .8558
INLET CORRECTED FLOW, LB/S = .062
DISCHARGE PRESSURE, PSIA = 228.00
PRESSURE DROP / PT INLET = .0249
TOTAL GEOMETRIC AREA, IN2 = .651